

Copyright
by
Kyle Kurt Gabriel Smith
2014

The Dissertation Committee for Kyle Kurt Gabriel Smith
certifies that this is the approved version of the following dissertation:

**Approximate Quantum Dynamics Methods for Time
Correlation Functions**

Committee:

Peter J. Rossky, Supervisor

Arno Böhm

John F. Stanton

Dmitrii E. Makarov

Charles B. Mullins

**Approximate Quantum Dynamics Methods for Time
Correlation Functions**

by

Kyle Kurt Gabriel Smith, B.S.

DISSERTATION

Presented to the Faculty of the Graduate School of
The University of Texas at Austin
in Partial Fulfillment
of the Requirements
for the Degree of

DOCTOR OF PHILOSOPHY

THE UNIVERSITY OF TEXAS AT AUSTIN

May 2014

Dedicated to the Lord God Jesus Christ.

Acknowledgments

I would like to thank my advisor, Peter Rossky, for introducing me to the realm of approximate quantum time correlation function methods, which has resulted in this dissertation. In addition, Peter has been there to provide the guidance and mentorship necessary to complete this work. If it was not for his parent like advice, I probably would have dropped out of grad school due to the strong desire to get a real job and, what I would describe as, actually start my life. In addition, I would like to thank our collaborator in Sweden, Jens Poulsen. I was actually very blessed to have been able to work with Jens, and his bright ideas have been a huge contribution to this dissertation. Maybe one day I will make a trip to Sweden to thank him in person.

During my studies at UT, I have come to develop a friendship with a mathematical physicist, Prof. Arno Bohm, to whom I also owe thanks. Our friendship begun while taking his graduate level quantum mechanics course. One day after class, he told me that my homeworks were typically much better than the rest of the classes, and then asked what type of physics I was doing for my PhD work. Very much to his surprise, I told him that I was actually in the chemistry program doing theoretical chemistry. He then told me that he thought that I would make a *good* theoretical physicist, but now he thinks that I will make a *great* theoretical chemist! And this is where our friendship begun.

After that class I went on to take two more classes with Prof. Bohm, another quantum mechanics class and then a mathematical physics class. While I never had to worry about Gamow Vectors, Gel'fand Triplets, or the rigged Hilbert space formulation of quantum mechanics in my PhD work, the classes I took from Prof. Bohm really helped to develop my mathematical abilities/talent even further, which has contributed to a significant part of this dissertation.

In addition, I would like to thank my wife Megan, who has put up with, and supported me, during all of these years of school. During both undergraduate and grad school I have, unfortunately, become somewhat of a workaholic, which has resulted in a significant amount of isolation. Hopefully, I will be able to tune this down a bit and begin to experience more of a life outside of work in the near future. What fuels my workaholism is the extremely strong drive to complete my education in the minimum amount of time, such that I am then able to provide a better life for ourselves, as well as our families. Now that I have completed my PhD, hopefully we will soon begin reaping what I have so diligently sowed.

Most of all, I would like to thank the Lord God Jesus Christ. God has taken me, once hopeless and lost, and turned my life and circumstances completely around to give me a new hope and purpose in life, and I am very excited to experience the future He has for me!

Approximate Quantum Dynamics Methods for Time Correlation Functions

Publication No. _____

Kyle Kurt Gabriel Smith, Ph.D.
The University of Texas at Austin, 2014

Supervisor: Peter J. Rossky

The dynamic structure factor of liquid para-hydrogen and ortho-deuterium in corresponding thermodynamic states, ($T = 20.0\text{ K}, n = 21.24\text{ nm}^{-3}$) and ($T = 23.0\text{ K}, n = 24.61\text{ nm}^{-3}$) respectively, has been computed by both the Feynman-Kleinert linearized path-integral (FK-LPI) and Ring-Polymer Molecular Dynamics (RPMD) methods and compared with Inelastic X-ray Scattering spectra. The combined use of computational and experimental methods enables a reduction in experimental uncertainties for the determination of the true sample spectrum. Furthermore, the refined experimental spectrum of para-hydrogen and ortho-deuterium is consistently reproduced by both *FK – LPI* and *RPMD* at momentum transfers lower than 12.8 nm^{-1} . At larger momentum transfers the *FK – LPI* results agree with experiment much better for ortho-deuterium than for para-hydrogen. More specifically we

found that for $k \sim 20.0 \text{ nm}^{-1}$ para-hydrogen provides a test case for improved approximations to quantum dynamics.

We meet this demand for an improved approximate quantum dynamics method by developing two classes of quasi-classical dynamics that are shown to conserve the initial quantum ensemble when used in conjunction with the Feynman-Kleinert approximation of the density operator. As shown, both classes of dynamics are able to recover the exact classical and high temperature limits of the quantum time correlation function, while a subset is able to recover the exact harmonic limit. A comparison of the approximate quantum time correlation functions obtained from both classes of dynamics are made with the exact results for the challenging model problems of the quartic and double-well potentials. It is found that this new Feynman-Kleinert Quasi-Classical Wigner (FK-QCW) method provides a great improvement over the Feynman-Kleinert implementation of the classical Wigner approximation, also known as FK-LPI, in which purely classical dynamics are used. Furthermore, it is shown that the first class of dynamics reduces to Centroid Molecular Dynamics (CMD) when used within the framework of the classical Wigner approximation for the Kubo transformed time correlation function.

Finally, we apply the Feynman-Kleinert Quasi-Classical Wigner (FK-QCW) method to the same liquid para-hydrogen and ortho-deuterium system, previously studied using FK-LPI and RPMD. When applied to this challenging system, it is shown that this new FK-QCW method consistently reproduces the experimental dynamic structure factor for all momentum transfers considered.

This shows that FK-QCW provides a great improvement over FK-LPI for not only model problems, but also realistic systems. Furthermore, for small momentum transfers, where RPMD is applicable, it is shown that FK-QCW provides nearly the same results as RPMD, thus suggesting that FK-QCW provides a potentially more appealing algorithm than RPMD since one is not limited to correlation functions involving linear operators. This then suggests that the FK-QCW method is a top contender in the realm of approximate quantum dynamics methods which allow for the practical evaluation of time correlation functions.

Table of Contents

Acknowledgments	v
Abstract	vii
List of Tables	xiii
List of Figures	xiv
Chapter 1. Introduction	1
1.1 Introduction	1
Chapter 2. Refinement of the Experimental Dynamic Structure Factor for Liquid para-Hydrogen and ortho-Deuterium using Semi-classical Quantum Simulation	5
2.1 Introduction	5
2.2 Theory and Methodology	10
2.2.1 Inelastic Scattering	10
2.2.2 Classical Wigner	12
2.2.3 Feynman-Kleinert Linearized Path-Integral Method . . .	14
2.2.4 Ring-Polymer Molecular Dynamics	15
2.3 Results	19
2.3.1 Computational Details	19
2.3.2 Refinement of the Experimental Dynamic Structure Factor	22
2.3.3 Dynamic Structure Factor	26
2.4 Conclusions	34

Chapter 3. A New Class of Ensemble Conserving Algorithms for Approximate Quantum Dynamics: Theoretical Formulation and Model Problems	36
3.1 Introduction	36
3.2 Classical Wigner Approximation	39
3.3 Feynman-Kleinert density operator	41
3.4 The Feynman-Kleinert Quasi-Classical Wigner method: FK-QCW(1)	44
3.4.1 Harmonic limit	50
3.4.2 Classical and high temperature limits	51
3.4.3 Low temperature limit	52
3.5 An additional Feynman-Kleinert Quasi-Classical Wigner method: FK-QCW(2)	53
3.5.1 Harmonic limit	58
3.5.2 Classical and high temperature limits	59
3.5.3 Low temperature limit	60
3.6 Application to model problems	60
3.6.1 The double-well potential	63
3.6.2 The quartic potential	67
3.7 Conclusions	71
Chapter 4. Application of a New Ensemble Conserving Quantum Dynamics Simulation Algorithm to Liquid para-Hydrogen and ortho-Deuterium	73
4.1 Introduction	73
4.2 Theory and Methodology	77
4.2.1 Classical Wigner	77
4.2.2 Many-body Feynman-Kleinert density operator	78
4.2.3 FK-QCW in many dimensions	82
4.2.4 Inelastic Scattering	85
4.3 Results	89
4.3.1 Computational Details	89
4.3.2 The Experimental Dynamic Structure Factor	91
4.3.3 Dynamic Structure Factor	94
4.4 Conclusions	101

Appendices	103
Appendix A. Overview of the FK-LPI method	104
Appendix B. Time invariance of thermodynamic properties within the CW expression	108
Appendix C. Time-dependent dummy variable substitution	109
Appendix D. Liouville's theorem for the centroid distribution function	111
Appendix E. Determinant of the Jacobian matrix in terms of the dimensionless coordinates	115
Appendix F. Equivalence of FK-QCW and CMD for the Kubo-transformed time-correlation function of linear operators	117
Appendix G. FK-QCW Molecular Dynamics Algorithm	120
Bibliography	122
Vita	127

List of Tables

2.1	The simulation parameters used for the <i>FK – LPI</i> calculation of Eq. 2.17.	18
2.2	The simulation parameters used for the <i>RPMD</i> calculation of Eq. 2.30.	18
2.3	The fitting parameters used in Eq. 2.34 to refine the experimental dynamic structure factor using the <i>FK – LPI</i> results.	22
4.1	The simulation parameters used for the <i>FK-QCW</i> calculation of Eq. 4.37.	91
4.2	The fitting parameters used in Eq. 4.43 to refine the experimental dynamic structure factor using the <i>FK-QCW</i> results. Here the R^2 values are the coefficients of determination for the various fits.	93

List of Figures

2.1	The $FK - LPI$ (blue line) and $RPMD$ (magenta dashed line at low k 's) approximation to the intermediate scattering function for both ortho-deuterium (upper four panels) and para-hydrogen (lower four panels) for the different momentum transfers considered (as labeled). The real part of the correlation function is the upper curve while the negative imaginary part is the lower curve in each figure.	27
2.2	The refined experimental dynamic structure factors of Refs.[41] and [42], as obtained by using either $FK - LPI$ (black dots) or $RPMD$ (red dots) as the input (see text). The $FK - LPI$ (blue line) and $RPMD$ (dashed magenta line) dynamic structure factors are convoluted with the instrumental resolution function. The layout of the figure is the same as that in Fig. 2.1.	28
2.3	The static structure factors obtained from the the intermediate scattering function using the relation in Eq. 2.10 for both ortho-deuterium (left panel) and para-hydrogen (right panel) using $FK - LPI$ (blue circle), $RPMD$ (magenta cross), and the Classical simulation with the harmonic correction factor (black square).	31
2.4	The first moment of the dynamic structure factors obtained from the the intermediate scattering function using the relation in Eq. 2.11 for both ortho-deuterium (left panel) and para-hydrogen (right panel) using $FK - LPI$ (blue circle), $RPMD$ (magenta cross), and the Classical simulation with the harmonic correction factor (black square). These results are compared with the exact relation of Eq. 2.11 (black line).	32
3.1	A representative trajectory for the double well potential in Eq. 3.79 for $\beta = 8$. Black line: $x_c(t)$; Blue line: q_t from FK-LPI; Red line: q_t from FK-QCW(2) ($f = \Omega_t$). Both the FK-LPI and FK-QCW(2) dynamics were propagated from the same initial conditions.	64

3.2	The real part of the autocorrelation function for the double well potential in Eq. 3.79 for $\beta = 8$. Black points: exact; Green dot-dashed line: RPMD; Orange dot-dashed line: FK-CMD; Gold line: FK-LPI; Blue dashed line: FK-QCW(1) ($f = \Omega_t$); Magenta dashed line: FK-QCW(2) ($f = \Omega_t$). The exact results were taken from Ref. [15].	65
3.3	The real part of the autocorrelation function for the double well potential in Eq. 3.79 for $\beta = 8$. Black points: exact; Gold line: FK-LPI; Blue dashed line: FK-QCW(1) ($f = \Omega_t$); Magenta dashed line: FK-QCW(2) ($f = \Omega_t$); Red line: FK-QCW(2) with f given by Eq. 3.78. The exact results were taken from Ref. [24].	66
3.4	The real part of the autocorrelation function for the quartic potential in Eq. 3.80 for $\beta = 8$. Black points: exact; Green dot-dashed line: RPMD; Orange dot-dashed line: FK-CMD; Gold line: FK-LPI; Blue dashed line: FK-QCW(1) ($f = \Omega_t$); Magenta dashed line: FK-QCW(2) ($f = \Omega_t$). The exact results were taken from Ref. [15].	69
3.5	The real part of the autocorrelation function for the quartic potential in Eq. 3.80 for $\beta = 8$. Black points: exact; Gold line: FK-LPI; Blue dashed line: FK-QCW(1) ($f = \Omega_t$); Magenta dashed line: FK-QCW(2) ($f = \Omega_t$); Red line: FK-QCW(2) with f given by Eq. 3.78. The exact results were taken from Ref. [24].	70
4.1	The FK-QCW (black line with error bars), FK-LPI (blue line), and RPMD (magenta dashed line at low k 's) approximation to the intermediate scattering function for both ortho-deuterium (upper four panels) and para-hydrogen (lower four panels) for the different momentum transfers considered (as labeled). The real part of the correlation function is the upper curve while the negative imaginary part is the lower curve in each figure. Both the FK-LPI and RPMD results were taken from Ref. [1] (Ch. 2).	96
4.2	The refined experimental dynamic structure factors for para-hydrogen, as obtained using either FK-QCW (red dots) or FK-LPI (blue squares) as the input (see text). The FK-QCW (black dashed dot line), FK-LPI (blue line), and RPMD (magenta dashed line) dynamic structure factors are convoluted with the instrumental resolution function. The FK-LPI and RPMD results, as well as the experimental quantity obtained using FK-LPI as an input were taken from Ref. [1] (Ch. 2).	97

4.3	The refined experimental dynamic structure factors for ortho-deuterium, as obtained using either FK-QCW (red dots) or FK-LPI (blue squares) as the input (see text). The FK-QCW (black dashed dot line), FK-LPI (blue line), and RPMD (magenta dashed line) dynamic structure factors are convoluted with the instrumental resolution function. The FK-LPI and RPMD results, as well as the experimental quantity obtained using FK-LPI as an input were taken from Ref. [1] (Ch. 2). . .	98
4.4	The first moment of the dynamic structure factors obtained from the the intermediate scattering function using the relation in Eq. 4.34 for both ortho-deuterium (left panel) and parahydrogen (right panel) using FK-QCW (red circle), FK-LPI (blue circle), and RPMD (magenta cross). These results are compared with the exact relation of Eq. 4.34 (black line). . . .	99

Chapter 1

Introduction

1.1 Introduction

The main goal of quantum statistical mechanics is the evaluation of finite temperature expectation values of quantum mechanical operators, which in the canonical ensemble takes the general form

$$\langle \hat{B} \rangle = \frac{1}{Z} \text{Tr} \left(e^{-\beta \hat{H}} \hat{B} \right), \quad (1.1)$$

where Z is the partition function and β is the inverse temperature $1/k_b T$. The reason these quantities are so important is because one can know essentially any thermal equilibrium property of a quantum mechanical system if they are able to evaluate this expression exactly. In fact, Feynman said that

”This fundamental law is the summit of statistical mechanics, and the entire subject is either the slide-down from this summit, as the principle is applied to various cases, or the climb-up to where the fundamental law is derived and the concepts of thermal equilibrium and temperature T clarified.”

R. P. Feynman – Statistical Mechanics: A Set of Lectures

Of even more importance are finite temperature expectation values that involve a product of two operators, in which one of these operators is evolved

in time

$$\langle \hat{A}(0)\hat{B}(t) \rangle = \frac{1}{Z} \text{Tr} \left(e^{-\beta\hat{H}} \hat{A} e^{i\hat{H}t/\hbar} \hat{B} e^{-i\hat{H}t/\hbar} \right). \quad (1.2)$$

These time dependent expectation values are known as quantum time correlation functions and they provide extremely valuable dynamical information of a quantum system. That is because, for example, the dipole moment correlation function will yield absorption spectra, the flux correlation function will yield reaction rates, the velocity correlation function give the diffusion constant, and the list goes on. However, these quantities are extremely difficult if not impossible to evaluate exactly. This is because one is required either to compute a full real time path-integral or solve the corresponding time-dependent Schrodinger equation, which is not practical for realistic many-body systems due to the intense computational load. In order to overcome this difficulty, it is desirable to develop approximate quantum dynamics methods which are as accurate and efficient as possible, and enable the practical evaluation of Eq. 1.2.

Currently, there exists multiple approximation schemes including the Classical Wigner approximation (CW)[2, 17, 19], Centroid Molecular Dynamics (CMD) [15], as well as Ring-Polymer Molecular Dynamics (RPMD)[26] in which one uses a form of approximate dynamics to evaluate quantum time correlation functions approximately. While all of these methods provide relatively accurate and practical approximations to Eq. 1.2, each have their own downfalls. For example, while both CMD and RPMD have been shown to be exact in the harmonic, high temperature, and short time limits, both of these

methods begin to break down for correlation functions involving non-linear operators[15, 26, 28]. In addition, the intrinsic dynamics of the ring-polymer in RPMD can introduce artificial frequencies in the spectrum of the correlation function, which becomes especially important when simulating absorption spectra[32]. On the other hand, the CW approximation is also exact in the harmonic, high temperature, and short time limits, even for correlation functions involving non-linear operators[2, 20]. However, the CW approximation does not in general correctly produce time invariant thermodynamic properties of thermal equilibrium systems. Explicitly, for $\hat{A} = 1$ the exact quantum expression in Eq. 1.2 has the property that

$$\langle \hat{B}(t) \rangle = \langle \hat{B}(0) \rangle, \quad (1.3)$$

however this is generally not true for the CW approximation due to the classical dynamics used.

This dissertation begins in Ch. 2 by providing a benchmark comparison of two of these leading approximate methods. Specifically, I apply RPMD and the Feynman-Kleinert implementation of the CW approximation, known as the Feynman-Kleinert linearized path-integral (FK-LPI)[2] method, for the determination of the dynamic structure factor of low temperature liquid para-hydrogen and ortho-deuterium. This benchmark calculation establishes a challenging test case where both of these methods fail. In Ch. 3, I meet this demand for an improved approximate quantum dynamics method by developing two classes of quasi-classical dynamics that are shown to conserve

the initial quantum ensemble. In addition, I apply this new Feynman-Kleinert Quasi-Classical Wigner (FK-QCW) method in 1-D for the challenging model problems of the quartic and double-well potentials, and then compare these results with the exact quantum mechanical predictions, as well as that obtained by the three leading methods (FK-LPI, CMD, and RPMD). In Ch. 4, I apply the FK-QCW method to the same liquid para-hydrogen and ortho-deuterium system, previously studied using FK-LPI and RPMD. It is found that this new FK-QCW method performs excellent where RPMD and FK-LPI previously failed. This then suggests that the FK-QCW method is a top contender in the realm of approximate quantum dynamics methods which allow for the practical evaluation of time correlation functions.

Chapter 2

Refinement of the Experimental Dynamic Structure Factor for Liquid para-Hydrogen and ortho-Deuterium using Semi-classical Quantum Simulation

2.1 Introduction

In the last decades the study of quantum effects [47] in the dynamics and structure of liquids has greatly benefited from advances in both experimental techniques and computational methods investigating the so called mesoscopic regime, corresponding to distances and timescales respectively matching nearest neighbor separations and 'cage oscillation' periods. In fact, the quantum behavior of a fluid emerges only as far as the probed distance match both the mean free path of its microscopic components of a fluid and its quantum coherence length, i.e. the de Broglie wavelength $\lambda = h/\sqrt{(2\pi mk_B T)}$, with h , k_B , m , and T being the Planck and Boltzmann constants, molecular mass, and temperature. In moderately quantum fluids this occurs in a dynamic window lying by some decades beyond the range covered by Brillouin Visible Light Scattering and rather matching the domain of THz spectroscopic techniques such as Inelastic X Ray and Neutron Scattering (IXS and INS respectively). Although the behavior of the spectral lineshape is rather well understood in the

classical limit, to date no rigorous theoretical prediction is available to handle quantum deviations. This would hypothetically require a quantum mechanically exact theoretical expression for the quantum time correlation function, which, for a many-body system in the canonical ensemble takes the general form:

$$\langle \hat{A}(0)\hat{B}(t) \rangle = \frac{1}{Z} \text{Tr} \left(e^{-\beta\hat{H}} \hat{A} e^{i\hat{H}t/\hbar} \hat{B} e^{-i\hat{H}t/\hbar} \right), \quad (2.1)$$

Z being the partition function and β the inverse temperature $1/k_bT$. The time correlation functions defined by Eq. 2.1 is of pivotal interest since the spectrum measured by most spectroscopic techniques is proportional to it through linear response theory. In order to determine this quantity, one is, in principle, required either to compute a full real time path-integral for the many-body system or solve the corresponding time-dependent Schrodinger equation. This can, in principle, be achieved to arbitrary accuracy since the underlying laws of physics are known; however, such a calculation is not practical for realistic systems, even using the world's most advanced supercomputers. In order to overcome this difficulty, it is thus desirable to develop approximate quantum methods which are as accurate and efficient as possible, and enable the practical evaluation of Eq. 2.1. Two such approximation schemes are the Feynman-Kleinert linearized path-integral method (FK-LPI) [2], as well as Ring-Polymer Molecular Dynamics (RPMD)[26] in which one uses semi-classical methods to calculate quantum time correlation functions approximately.

The *FK – LPI* method is intimately related to the so-called classical

Wigner (CW) approximation[17], or equivalently the linearized semiclassical initial value representation (LSC-IVR)[19], which can be derived from multiple starting points. For example, the CW approximation can be shown to follow not only from a path linearization approximation implemented within the semiclassical initial value representation (SC-IVR) of the propagator, but also from a linearization of the action difference between the forward-backward time paths in the corresponding exact path-integral expression for a general time correlation function[2, 18].

The other approach (RPMD) exploits the isomorphism between the imaginary time-sliced path-integral expression of a many-body quantum partition function and the classical partition function of a system of ring-polymer molecules to evaluate the Kubo-transformed quantum time correlation function.

This method has been found to perform relatively well for realistic systems as long as the correlation function is not highly non-linear in position or momentum[27, 28]. In fact, as long as at least one of the operators in the correlation function is linear in either position or momentum, *RPMD* is exact in the limit that the number of beads n goes to infinity for a harmonic system, in the high-temperature limit, as well as when $t \rightarrow 0$ [26]. Furthermore, *RPMD* by construction gives the correct $t \rightarrow 0$ limit of the Kubo-transformed time correlation function for both linear and non-linear operators, provided that the $n \rightarrow \infty$ limit is taken[28]. In contrast, *FK - LPI* is not limited to linear operators and is exact in the harmonic and high temperature limit for

non-linear operators as well[2, 20].

The purpose of this chapter is to apply the methods of *FK – LPI* and *RPMD* to obtain the dynamic structure factor of low-temperature liquid para-Hydrogen and ortho-Deuterium in order to provide a comparison between the two methods as well as to the experimental dynamic structure factors from *IXS* data. The low-temperature liquid para-hydrogen and ortho-deuterium system has been chosen because they have become a standard benchmark in the development of semi-classical quantum nuclear dynamics methods[3, 14, 21, 27, 29, 35, 40]. This is due to pronounced nuclear quantum effects being exhibited in their dynamical properties, which is a direct consequence of their low molecular mass which in turn causes their thermal de Broglie wavelength to be comparable to the intermolecular distance. Luckily however, this quantum delocalization is not significant enough that one must worry about the quantum statistics of molecular indistinguishability, which greatly simplifies matters. Thus low-temperature liquid para-Hydrogen and ortho-Deuterium are very well suited benchmark systems for semi-classical quantum nuclear dynamics methods, such as *FK – LPI* and *RPMD*. At the same time, *IXS* provides an unambiguous result with which to compare the performance of such methods.

We note at the outset that there are uncertainties in the experimental data, discussed further below, as well as in the approximate quantum dynamics theory used. Hence, a level of uncertainty that cannot currently be quantified will necessarily remain in the data after refinement by the combined analysis.

Nevertheless, the data refinement using these currently best available methods will lead to what we believe are the best available estimates of the true dynamic structure factors. At the same time, an inability to bring the experimental data and calculations into agreement will certainly indicate a limitation of the theory, and hence establish a test case for improved methods.

We finally remark that within the low k range considered here ($k \leq 12.8 \text{ nm}^{-1}$) the *RPMD* method can be safely applied based on the linearization of $e^{-ik\hat{x}} \approx 1 - ik\hat{x}$ (x being the space coordinate). This approximation is consistent with the previous findings of Ref. [27] suggesting that the non-linearity of the correlation function does not influence *RPMD* results so long as $k \leq 15 \text{ nm}^{-1}$. As will be shown in Section III, this accuracy is consistent with present data.

This chapter is organized as follows: A brief overview of the basic theory of inelastic scattering, the *FK - LPI* methodology, and *RPMD* is presented in Section II. In Section III we begin by discussing the computational details of our simulations, as well as an overview of the method used to refine the experimental dynamic structure factor from the raw *IXS* data of Cunsolo and coworkers[41, 42]. This is followed by a comparison of the refined quantity with the theoretical predictions of *FK - LPI* and *RPMD*. Lastly, we compare the *FK - LPI* and *RPMD* dynamic structure factors. The conclusions are presented in Section IV.

2.2 Theory and Methodology

2.2.1 Inelastic Scattering

The dynamic variable of interest in this chapter is the dynamic structure factor, which is accessible through inelastic neutron or X-ray scattering. In such an experiment, what one measures is the inelastic scattering cross-section of the sample as a function of the change in energy and momentum of the scattered particle, which is a measurement of the probability that a neutron or photon transfers momentum $\hbar(\vec{k}_f - \vec{k}_i)$ and energy $\hbar(\omega_f - \omega_i)$ to the sample. In this work, using IXS rather than neutrons, we will assume that the incoherent part of the scattering is negligible and the measured intensity is proportional to the dynamic structure factor[11]. Under this reasonable assumption, a straightforward comparison can be achieved between the outcomes of computational and experimental results. Van-Hove[13] showed that within the first Born approximation, the inelastic scattering cross-section is proportional to the dynamic structure factor, $S(\vec{k}, \omega)$, which is defined as the Fourier transform over space and time of the time-dependent pair distribution function $G(\vec{r}, t)$.

$$S(\vec{k}, \omega) = \frac{1}{2\pi} \int d^3\vec{r} dt e^{i(\vec{k}\cdot\vec{r}-\omega t)} G(\vec{r}, t) \quad (2.2)$$

where $G(\vec{r}, t)$ for a system of N particles is defined as

$$G(\vec{r}, t) = \frac{1}{N} \sum_{i,j=1}^N \left\langle \int d^3\vec{r}' \delta(\vec{r} + \hat{r}_i(0) - \vec{r}') \delta(\vec{r}' - \hat{r}_j(t)) \right\rangle. \quad (2.3)$$

Here, $\langle \dots \rangle$ denotes a canonical ensemble average, and $\hat{r}_i(t)$ is the time-dependent position operator of the i -th particle, which, in the Heisenberg formalism is given by $\hat{r}_i(t) = e^{i\hat{H}t/\hbar} \hat{r}_i e^{-i\hat{H}t/\hbar}$. By working in the basis of energy eigenstates, one can also show that the dynamic structure factor obeys the principle of detailed balance

$$S(\vec{k}, \omega) = e^{\beta\hbar\omega} S(\vec{k}, -\omega). \quad (2.4)$$

It is convenient to define the intermediate scattering function $F(\vec{k}, t)$ as the spatial Fourier transform of $G(\vec{r}, t)$ so that

$$S(\vec{k}, \omega) = \frac{1}{2\pi} \int_{-\infty}^{\infty} dt e^{-i\omega t} F(\vec{k}, t), \quad (2.5)$$

where

$$F(\vec{k}, t) \equiv \int d^3\vec{r} e^{i\vec{k}\cdot\vec{r}} G(\vec{r}, t) = \frac{1}{N} \sum_{i,j=1}^N \left\langle e^{-i\vec{k}\cdot\hat{r}_i(0)} e^{i\vec{k}\cdot\hat{r}_j(t)} \right\rangle. \quad (2.6)$$

By defining the density fluctuation operator[12]

$$\hat{\rho}(\vec{k}, t) \equiv \sum_{i=1}^N e^{-i\vec{k}\cdot\hat{r}_i(t)}, \quad (2.7)$$

the intermediate scattering function takes the compact form

$$F(\vec{k}, t) = \frac{1}{N} \left\langle \hat{\rho}(\vec{k}, 0) \hat{\rho}^\dagger(\vec{k}, t) \right\rangle. \quad (2.8)$$

From the relation in Eq. 2.5, one sees that the dynamic structure factor gives the spectrum of density fluctuations. For an isotropic system as a fluid, the intermediate scattering function does not depend on the direction of \vec{k} , but only on its amplitude k such that $F(\vec{k}, t) = F(k, t)$ and, of course, $S(\vec{k}, \omega) = S(k, \omega)$.

The shape of the dynamic structure factor is defined by its n -order spectral moments

$$\langle \omega^n \rangle \equiv \int_{-\infty}^{\infty} d\omega \omega^n S(k, \omega) = i^{-n} \left[\frac{\partial^n F(k, t)}{\partial t^n} \right]_{t=0}. \quad (2.9)$$

The comparison between measured and computed values of the spectral moments can be used as a metric to judge the quality of a theoretical simulation. The zeroth moment is the static structure factor[11], $S(\vec{k})$, which is related to the spatial Fourier transform of the pair distribution function by

$$S(\vec{k}) \equiv \langle \omega^0 \rangle = 1 + \int_{-\infty}^{\infty} d^3\vec{r} e^{i\vec{k}\cdot\vec{r}} g(\vec{r}). \quad (2.10)$$

The first moment of $S(\vec{k}, \omega)$ is of special interest since for a system which interacts through a momentum-independent potential [12], the first moment of the dynamic structure factor can be rigorously expressed as

$$\langle \omega \rangle \equiv \int_{-\infty}^{\infty} d\omega \omega S(\vec{k}, \omega) = \frac{\hbar k^2}{2m}. \quad (2.11)$$

It has been shown that the *FK-LPI* approximation to the dynamic structure factor obeys this sum rule exactly[4].

2.2.2 Classical Wigner

The CW[2, 17, 19] expression for a general quantum time correlation function of a system of N particles in three dimensions is given by

$$\begin{aligned} \langle \hat{A}(0)\hat{B}(t) \rangle &\approx \frac{1}{Z (2\pi\hbar)^{3N}} \int_{-\infty}^{\infty} d\vec{p}_0^N d\vec{q}_0^N [e^{-\beta\hat{H}} \hat{A}]_W(\vec{q}_0^N, \vec{p}_0^N) \\ &\quad \times [\hat{B}]_W(\vec{q}_t^N, \vec{p}_t^N) \end{aligned} \quad (2.12)$$

where $\vec{q}_t^N = \{\vec{q}_j(t)\}_{j=1}^N$ and $\vec{p}_t^N = \{\vec{p}_j(t)\}_{j=1}^N$ is the classically evolved quantum phase space, $(\vec{q}_0^N, \vec{p}_0^N)$ being the initial quantum distribution, and the Wigner transform of a general operator \hat{C} is given by

$$[\hat{C}]_W(\vec{q}^N, \vec{p}^N) \equiv \int_{-\infty}^{\infty} \prod_{j=1}^N [d^3\vec{\eta}_j e^{-i\vec{p}_j \cdot \vec{\eta}_j / \hbar}] \times \left\langle \vec{q}^N + \frac{\vec{\eta}^N}{2} \left| \hat{C} \right| \vec{q}^N - \frac{\vec{\eta}^N}{2} \right\rangle \quad (2.13)$$

where $|\vec{x}^N\rangle \equiv |\vec{x}_1\rangle \otimes |\vec{x}_2\rangle \cdots \otimes |\vec{x}_N\rangle$ is the direct product of the single particle position kets $|\vec{x}_j\rangle$.

The CW approximation can be conjectured from the exact Wigner representation of the quantum time correlation function given by

$$\begin{aligned} \langle \hat{A}(0)\hat{B}(t) \rangle &= \frac{1}{Z (2\pi\hbar)^{3N}} \int_{-\infty}^{\infty} d\vec{p}^N d\vec{q}^N [e^{-\beta\hat{H}} \hat{A}]_W(\vec{q}^N, \vec{p}^N) \\ &\quad \times [\hat{B}(t)]_W(\vec{q}^N, \vec{p}^N), \end{aligned} \quad (2.14)$$

since the CW approximation simply amounts to replacing the exact quantum evolution of $\hat{B}(t) = e^{i\hat{H}t/\hbar} \hat{B} e^{-i\hat{H}t/\hbar}$ with the classical evolution of the quantum phase-space such that

$$[\hat{B}(t)]_W(\vec{q}^N, \vec{p}^N) \rightarrow [\hat{B}]_W(\vec{q}_t^N, \vec{p}_t^N). \quad (2.15)$$

It is worth noting that for an operator \hat{B} which is a function of only the system's momentum or position operators, the analytical evaluation of $[\hat{B}]_W(\vec{q}_t^N, \vec{p}_t^N)$ is readily performed and is given by the corresponding classical expression

$$\begin{aligned}
[\hat{B}(\{\hat{x}_j\}_{j=1}^N)]_W(\vec{q}_t^N, \vec{p}_t^N) &= B(\vec{q}_t^N) \\
[\hat{B}(\{\hat{p}_j\}_{j=1}^N)]_W(\vec{q}_t^N, \vec{p}_t^N) &= B(\vec{p}_t^N)
\end{aligned} \tag{2.16}$$

2.2.3 Feynman-Kleinert Linearized Path-Integral Method

As seen in Eq. 2.12, the Wigner transform of $e^{-\beta\hat{H}}\hat{A}$ needs to be performed in order to implement the CW approximation. Hence, for a realistic many-body system one must invoke an approximation to $e^{-\beta\hat{H}}$ that allows for an efficient numerical evaluation of $[e^{-\beta\hat{H}}\hat{A}]_W(\vec{q}_0^N, \vec{p}_0^N)$. The *FK – LPI* method accomplishes this by casting $e^{-\beta\hat{H}}$ into a harmonic form using the effective frequency variational theory of Feynman[8] and Kleinert[9] along with the quasidensity operator formalism of Jang and Voth[16]. The harmonic form of the density operator allows for an analytical expression of $[e^{-\beta\hat{H}}\hat{A}]_W(\vec{q}_0^N, \vec{p}_0^N)$ to be obtained since only gaussian integrals are required. The details of the method are described in Refs. [2], [4] and [5] and a brief summary is provided in Appendix A.

Choosing \vec{k} to be parallel to the x-axis, the *FK – LPI* approximation to the intermediate scattering function takes the form

$$\begin{aligned}
F(\vec{k}, t) &\approx \frac{1}{Z(2\pi\hbar)^{3N}} \frac{1}{N} \sum_{i,j=1}^N \int_{-\infty}^{\infty} \prod_{j=1}^N [d^3\vec{p}_0^{(j)} d^3\vec{q}_0^{(j)}] \\
&\times [e^{-\beta\hat{H}} e^{-ik\hat{x}_i}]_W(\vec{q}_0^N, \vec{p}_0^N) [e^{ik\hat{x}_j}]_W(\vec{q}_t^N, \vec{p}_t^N)
\end{aligned} \tag{2.17}$$

where

$$[e^{ik\hat{x}_j}]_W(\vec{q}_t^N, \vec{p}_t^N) = e^{ikx_j(t)}. \tag{2.18}$$

The rather lengthy expression of $[e^{-\beta\hat{H}}e^{-ik\hat{x}_i}]_W(\vec{q}_0^N, \vec{p}_0^N)$ is derived in Ref. [4] (see Eq. 18 therein). The *FK – LPI* approximation to the dynamic structure factor can be obtained from the *FK – LPI* approximation of the intermediate scattering function by a simple Fourier transform as prescribed by Eq. 2.5.

2.2.4 Ring-Polymer Molecular Dynamics

As previously mentioned, Ring-Polymer Molecular Dynamics is a semi-classical method which allows one to calculate the Kubo-transformed quantum time correlation function of a many-body system, defined as

$$\langle \hat{A}(0)\hat{B}(t) \rangle_{Kubo} \equiv \frac{1}{\beta Z} \int_0^\beta d\lambda \text{Tr} \left(e^{-(\beta-\lambda)\hat{H}} \hat{A}(0) e^{-\lambda\hat{H}} \hat{B}(t) \right). \quad (2.19)$$

Its Fourier transform

$$\tilde{C}_{AB}(\omega) \equiv \int_{-\infty}^{\infty} dt e^{-i\omega t} \langle \hat{A}(0)\hat{B}(t) \rangle_{Kubo}, \quad (2.20)$$

is related to its standard quantum counterpart, $C_{AB}(\omega)$, through:

$$C_{AB}(\omega) = \frac{\beta\hbar\omega}{1 - e^{-\beta\hbar\omega}} \tilde{C}_{AB}(\omega). \quad (2.21)$$

In RPMD, the N particle quantum many-body system with a Hamiltonian of the form

$$\hat{H} = \sum_{i=1}^N \frac{\hat{p}_i^2}{2m} + V(\{\hat{q}_j\}_{j=1}^N) \quad (2.22)$$

is mapped onto a classical system of N ring-polymer necklaces with n beads and described by a Hamiltonian

$$\begin{aligned}
H_n(\{\vec{q}_i^{(k)}\}, \{\vec{p}_i^{(k)}\}) = & \\
& \sum_{i=1}^N \sum_{k=1}^n \left[\frac{(\vec{p}_i^{(k)})^2}{2m} + \frac{m}{2\beta_n^2 \hbar^2} (\vec{q}_i^{(k)} - \vec{q}_i^{(k-1)})^2 \right] \\
& + \sum_{k=1}^n V(\{\vec{q}_j^{(k)}\}_{j=1}^N)
\end{aligned} \tag{2.23}$$

where $(\vec{q}_i^{(k)}, \vec{p}_i^{(k)})$ is the position and momentum of the k -th bead on the i -th ring, $\beta_n \equiv \beta/n$, and $\vec{q}_i^{(0)} \equiv \vec{q}_i^{(n)}$. It is worth noting that in the ring-polymer Hamiltonian, bead k on ring i interacts with bead k on ring j through the systems original potential, while bead k and bead $k+1$ on the same ring interact through a harmonic potential.

Within the *RPMD* approximation, the Kubo-transformed time correlation function takes the form

$$\begin{aligned}
\langle \hat{A}(0) \hat{B}(t) \rangle_{Kubo} &\approx \frac{1}{Z_n (2\pi\hbar)^{3Nn}} \\
&\times \int_{-\infty}^{\infty} \prod_{i=1}^N \prod_{k=1}^n [d^3 \vec{q}_i^{(k)} d^3 \vec{p}_i^{(k)}] e^{-\beta_n H_n} A_n(0) B_n(t)
\end{aligned} \tag{2.24}$$

where

$$Z_n = \frac{1}{(2\pi\hbar)^{3Nn}} \int_{-\infty}^{\infty} \prod_{i=1}^N \prod_{k=1}^n [d^3 \vec{q}_i^{(k)} d^3 \vec{p}_i^{(k)}] e^{-\beta_n H_n} \tag{2.25}$$

and

$$A_n(0) = \frac{1}{n} \sum_{k=1}^n A(\{\vec{q}_j^{(k)}, \vec{p}_i^{(k)}\}_{j=1}^N), \tag{2.26}$$

$$B_n(t) = \frac{1}{n} \sum_{k=1}^n B(\{\vec{q}_j^{(k)}(t), \vec{p}_i^{(k)}(t)\}_{j=1}^N). \tag{2.27}$$

The equations of motion propagating classically the positions and momenta of the ring-polymer from the initial phase space point $(\vec{q}_i^{(k)}, \vec{p}_i^{(k)})$ to the the space point $(\vec{q}_i^{(k)}(t), \vec{p}_i^{(k)}(t))$ are generated from the Hamiltonian in Eq. 2.23 and explicitly read

$$\begin{aligned} \frac{d}{dt} \vec{p}_i^{(k)} = & -\frac{m}{\beta_n^2 \hbar^2} \left(2\vec{q}_i^{(k)} - \vec{q}_i^{(k-1)} - \vec{q}_i^{(k+1)} \right) \\ & - \vec{\nabla}_i^{(k)} V(\{\vec{q}_j^{(k)}\}_{j=1}^N), \end{aligned} \quad (2.28)$$

$$\frac{d}{dt} \vec{q}_i^{(k)} = \frac{\vec{p}_i^{(k)}}{m}. \quad (2.29)$$

In a *RPMD* simulation, evaluation of the Kubo-transformed time correlation function in Eq. 2.24 is performed by using the standard methods of a molecular dynamics simulation in which one uses the classical dynamics in Eqs. 2.28 and 2.29 to not only explore the configuration space of the ring-polymer system, but also for the explicit evaluation of $B_n(t)$.

The *RPMD* approximation to the Kubo-transformed intermediate scattering function takes the following form

$$\begin{aligned} \tilde{F}(\vec{k}, t) \approx & \frac{1}{Z_n (2\pi\hbar)^{3Nn}} \int_{-\infty}^{\infty} \prod_{i=1}^N \prod_{k=1}^n \left[d^3 \vec{q}_i^{(k)} d^3 \vec{p}_i^{(k)} \right] \\ & \times e^{-\beta_n H_n} \frac{1}{N} \rho_n(\vec{k}, 0) \rho_n^*(\vec{k}, t), \end{aligned} \quad (2.30)$$

where in analogy to Eq. 2.7 we have defined

$$\rho_n(\vec{k}, t) \equiv \frac{1}{n} \sum_{i=1}^N \sum_{k=1}^n e^{-ikx_i^{(k)}(t)}. \quad (2.31)$$

Table 2.1: The simulation parameters used for the $FK - LPI$ calculation of Eq. 2.17.

D_2					
$k (nm^{-1})$	N	$l (bohr)$	$\rho (nm^{-3})$	MC steps	acc %
5.5	37	21.65	24.61	3.2×10^6	60%
12.8	78	27.76	24.61	1.5×10^6	59%
15.3	109	31.03	24.61	1.5×10^6	53%
20.0	95	29.64	24.61	1.5×10^6	56%
H_2					
$k (nm^{-1})$	N	$l (bohr)$	$\rho (nm^{-3})$	MC steps	acc %
5.5	32	21.66	21.24	3.2×10^6	62%
12.8	68	27.85	21.24	1.6×10^6	60%
15.3	94	31.03	21.24	1.5×10^6	61%
20.0	82	29.65	21.24	1.5×10^6	56%

Table 2.2: The simulation parameters used for the $RPMD$ calculation of Eq. 2.30.

D_2				H_2		
$k (nm^{-1})$	N	$l (bohr)$	$\rho (nm^{-3})$	N	$l (bohr)$	$\rho (nm^{-3})$
5.5	37	21.65	24.61	32	21.66	21.24
12.8	79	27.88	24.61	68	27.85	21.24

in which, once again, \vec{k} is taken parallel to the x-axis. The $RPMD$ approximation to the dynamic structure factor can be obtained from the Kubo-transform of the intermediate scattering function by using Eq. 2.21 and is given by

$$S(\vec{k}, \omega) = \frac{\beta \hbar \omega}{1 - e^{-\beta \hbar \omega}} \tilde{S}(\vec{k}, \omega) \quad (2.32)$$

where

$$\tilde{S}(\vec{k}, \omega) \equiv \frac{1}{2\pi} \int_{-\infty}^{\infty} dt e^{-i\omega t} \tilde{F}(\vec{k}, t). \quad (2.33)$$

2.3 Results

2.3.1 Computational Details

In order to obtain the dynamic structure factor for liquid para-hydrogen and ortho-deuterium at a state point of $(T = 20.0 \text{ K}, n = 21.24 \text{ nm}^{-3})$ and $(T = 23.0 \text{ K}, n = 24.61 \text{ nm}^{-3})$ respectively, the *FK – LPI* approximation to the intermediate scattering function in Eq. 2.17 as well as the *RPMD* approximation to the Kubo-transformed intermediate scattering function in Eq. 2.30 were evaluated by using the Silvera-Goldman (SG) potential[7]. The SG potential has been used in a number of previous studies[14, 20, 21, 27, 29, 35] and has been shown to provide very accurate descriptions of the fluid and solid thermodynamics, except at extremely high pressure[36, 37]. This semi-empirical isotropic pair potential, applicable to both para-hydrogen and ortho-deuterium, treats each molecule as a spherical particle which is justifiable at low temperatures since only the $J=0$ rotational state is populated in each isotope. When performing the *FK – LPI* simulation, to expedite the determination of the FK centroid potential we represented the SG potential as a sum over four Gaussian functions whose parameters can be found in Table II of Ref. [3].

Both the *FK – LPI* and *RPMD* simulations were performed by employing cubic periodic boundary conditions with the minimum image convention and a spherical cutoff at half box length. It should be noted that in the *RPMD* simulations the truncation of the interaction was determined by the centroid-to-centroid distance. Furthermore, due to the isotropic nature of

the SG potential, in both simulations, the momentum transfer \vec{k} was chosen, without loss of generality, to be in the x -direction. In order to fulfill the Laue condition [10] $k = 2\pi n/l$ where l is the length of the simulation cell and n is an integer, the number of particles N treated in the simulation had to be varied for each momentum transfer and these, as well as the simulation box size used, for each k are listed in Tables. I and II for the *FK – LPI* and *RPMD* simulations, respectively. It should be noted that for a momentum transfer of $k = 5.5 \text{ nm}^{-1}$, the only choice for the number of particles was either $N = 32$ ($N = 37$) or $N = 253$ ($N = 294$) for the para-hydrogen (ortho-deuterium) system. Therefore, due to the computational load involved with obtaining the variational effective frequency in the *FK – LPI* method, we chose a system size of $N = 32$ ($N = 37$) for the para-hydrogen (ortho-deuterium) system. However, in order to make sure that a system size of $N = 32$ ($N = 37$) can faithfully describe the para-hydrogen (ortho-deuterium) system, we evaluated system size dependence using *RPMD* and found no significant dependence.

In the *FK – LPI* simulation, centroid positions were generated by performing a Monte Carlo (MC) walk using the multidimensional generalization of the centroid phase-space density in Ref. [5]. At every 30th MC step, 10 phase-space points $(\vec{q}_0^N, \vec{p}_0^N)$ were generated from the corresponding weight factor defined in Eq. 25 of Ref. [4]. These phase-space points were then propagated classically to $(\vec{q}_t^N, \vec{p}_t^N)$ for 5.9 ps using the velocity Verlet algorithm with a time step of 2.9 fs . The *FK – LPI* intermediate scattering function was then constructed using Eq. 2.17. In order to obtain statistical uncertain-

ties, two independent initial configurations were equilibrated. From these two initial configurations, two intermediate scattering function calculations were performed employing a minimum of 1.5 million MC steps each. The standard deviation was then obtained by first obtaining averages of the two results over a minimum of 300,000 MC step blocks, and then calculating the standard deviation between the different block averages. For the exact number of MC steps employed for each k as well as the MC acceptance ratios see Table. I. The $FK - LPI$ approximation to the dynamic structure factor was obtained from the intermediate scattering function by invoking the relation in Eq. 2.5.

The $RPMD$ simulation was performed by first generating initial ring-polymer configurations of $n = 48$ beads from an equilibrated PIMD simulation in which we invoked the symplectic integration algorithm as well as the path-integral Langevin equation (PILE) thermostat of Ref. [45]. From an equilibrated configuration, the Kubo-transformed intermediate scattering function in Eq. 2.30 was obtained by averaging over 1000 consecutive $3 ps$ trajectories in which we employed the symplectic integration algorithm of Ref. [45] with a time step of $1 fs$. To ensure a canonical ensemble average, before each trajectory, we resampled the ring-polymer momentum from the boltzmann distribution at inverse temperature β_n . In order to obtain statistical uncertainties, this entire process was repeated six times. After the Kubo-transformed intermediate scattering function was obtained, the corresponding $RPMD$ approximation to the dynamic structure factor was computed by invoking the relation in Eq. 2.32.

Table 2.3: The fitting parameters used in Eq. 2.34 to refine the experimental dynamic structure factor using the *FK – LPI* results.

D_2						
$k (nm^{-1})$	$\alpha(\vec{k})$	$T(\vec{k})$	$\delta (meV)$	$\theta (meV)$	$ \delta - \theta $	R^2
5.5	7.49×10^4	0.897	-0.564	-0.380	0.184	0.96
12.8	1.46×10^5	0.896	0.109	0.372	0.263	0.99
15.3	2.15×10^5	0.895	-0.329	-0.128	0.201	0.98
20.0	3.48×10^5	0.893	-0.812	-0.241	0.571	0.96
H_2						
$k (nm^{-1})$	$\alpha(\vec{k})$	$T(\vec{k})$	$\delta (meV)$	$\theta (meV)$	$ \delta - \theta $	R^2
5.5	5.39×10^4	0.731	0.048	0.578	0.530	0.99
12.8	1.87×10^5	0.954	0.486	0.833	0.347	0.97
15.3	1.54×10^5	0.740	0.019	0.655	0.636	0.98
20.0	3.53×10^5	0.952	-1.060	-0.936	0.124	0.89

2.3.2 Refinement of the Experimental Dynamic Structure Factor

When performing an inelastic scattering experiment on a liquid, one must cope with the spurious scattering from the container which must be carefully subtracted from the raw intensity. However, for the present measurements such a subtraction is not completely straightforward due to a random uncertainty in the zero of energy transfer ($\omega = 0$) between the sample+container and empty container scattering measurements, which is caused by random temperature drifts in the analyzer crystal [39]. Owing to the rather intense empty container scattering, neglecting such a small relative shift can nonetheless cause significant distortions of the corrected spectral shape.

Taking into account this unknown shift in ω , the experimentally mea-

sured dynamic structure factor $S_{exp}(\vec{k}, \omega)$ of the sample can be expressed as

$$S_{exp}(\vec{k}, \omega) = \alpha(\vec{k}) \left(I_{raw}(\vec{k}, \omega - \delta) - T(\vec{k}) I_{EC}(\vec{k}, \omega - \theta) \right), \quad (2.34)$$

where $I_{raw}(\vec{k}, \omega)$ and $I_{EC}(\vec{k}, \omega)$ are the measured intensities scattered by the sample+container system and by the empty container, respectively. It should be noted that, due to the finite resolution of the experiment, the experimental dynamic structure factor is related to the sample's true dynamic structure factor, $S(\vec{k}, \omega)$, through a convolution with the instrument resolution function, $R(\omega)$, such that

$$S_{exp}(\vec{k}, \omega) = S(\vec{k}, \omega) \otimes R(\omega) = \int_{-\infty}^{\infty} d\omega' S(\vec{k}, \omega') R(\omega - \omega'). \quad (2.35)$$

The parameter $\alpha(\vec{k})$ in Eq. 2.34 is the \vec{k} dependent proportionality factor that relates the dynamic structure factor to the inelastic scattering cross-section, and $|\delta - \theta|$ is the sought after random shift in the zero of energy transfer. Assuming that $I_{raw}(\vec{k}, \omega)$ and $I_{EC}(\vec{k}, \omega)$ are normalized to the incident flux, $T(\vec{k})$ is the transmission coefficient of the sample which can be determined by the following relation

$$T(k) = e^{-d(\theta)/\lambda}, \quad (2.36)$$

where

$$d(\theta) = \frac{l}{2} \left(1 + \frac{1}{\cos(\theta)} \right) \quad (2.37)$$

is the effective sample length at a given scattering angle θ , l being the actual thickness of the sample slab (here $l = 10mm$), and λ is the absorption length [46] of the sample.

The determination of the experimental dynamic structure factor has previously been accomplished by performing a fit to a model function derived from the classical viscoelastic theory of liquids multiplied by a quantum correction factor, which ensures both the detailed balance and first moment sum rule fulfillment [41, 42]. The dynamic structure factor obtained by the *FK – LPI* method has been shown to obey the detailed balance condition as well as the first moment sum rule [4, 6] and it can be used to fix the unknown spectral shift $|\delta - \theta|$. Here the outcome of the *FK – LPI* computation has been used as an input to refine the spectral line-shapes reported in Refs. [41] and [42], by performing a least squares fit of Eq. 2.34 to the *FK – LPI* results. We have opted to use the *FK – LPI* rather than the *RPMD* results, since the latter do not rigorously obey the first moment sum rule and cannot access high k . During the fit of Eq. 2.34 to the *FK – LPI* results, for each (δ, θ) we determined $\alpha(\vec{k})$ through the following relation

$$\alpha(\vec{k}) = \frac{\int_{-\infty}^{\infty} d\omega \omega S_{FK}(\vec{k}, \omega) \otimes R(\omega)}{\int_{-\infty}^{\infty} d\omega \omega \left(I_{raw}(\vec{k}, \omega - \delta) - T(\vec{k}) I_{EC}(\vec{k}, \omega - \theta) \right)}, \quad (2.38)$$

where $S_{FK}(\vec{k}, \omega) \otimes R(\omega)$ is the convolution of the *FK – LPI* dynamic structure factor with the instrumental resolution function. This form for $\alpha(\vec{k})$ can be derived from Eqs. 2.34 and 2.35 by superimposing the fulfillment of the first moment sum rule

$$\begin{aligned}
\int_{-\infty}^{\infty} d\omega \omega S_{exp}(\vec{k}, \omega) &= \int_{-\infty}^{\infty} d\omega \omega S(\vec{k}, \omega) \otimes R(\omega) \\
&= \frac{\hbar k^2}{2m} \int_{-\infty}^{\infty} d\omega R(\omega) + S(\vec{k}) \int_{-\infty}^{\infty} d\omega R(\omega) \omega,
\end{aligned} \tag{2.39}$$

and furthermore assuming that the *FK – LPI* method provides an exact determination of the static structure factor. This assumption is justified since the CW approach is exact for $t = 0$, where one has $F(k, 0) = S(k)$. The only approximation the *FK – LPI* method relies on, when deriving $S(k)$ for this quantity is the local harmonic approximation (FK approximation) of the density operator. The parameters obtained by using this method to refine the experimental dynamic structure factor from the raw inelastic x-ray scattering data of Cunsolo et al. [41, 42] are shown in Table III [48].

Although the *RPMD* results do not fulfill the first moment sum rule, we also performed a separate set of refinements using the *RPMD* results, in order to establish that the fit of Eq. 2.34 to the *FK – LPI* results does not skew the refined experimental dynamic structure factor. The non-compliance of *RPMD* with this sum rule was circumvented by invoking the following relation for $\alpha(\vec{k})$ (see Eq. 2.38)

$$\alpha(\vec{k}) = \frac{\frac{\hbar k^2}{2m} \int_{-\infty}^{\infty} d\omega R(\omega) + S(\vec{k}) \int_{-\infty}^{\infty} d\omega R(\omega) \omega}{\int_{-\infty}^{\infty} d\omega \omega \left(I_{raw}(\vec{k}, \omega - \delta) - T(\vec{k}) I_{EC}(\vec{k}, \omega - \theta) \right)}, \tag{2.40}$$

which takes advantage of the appearance of the exact first moment in Eq. 2.40 and also makes explicit use of the *RPMD* static structure factor.

2.3.3 Dynamic Structure Factor

The *FK – LPI* and *RPMD* results for the intermediate scattering function are shown in Fig. 2.1. The *RPMD* results were obtained from the Kubo-transformed intermediate scattering function by first computing the dynamic structure factor using Eq. 2.32 and then inverse Fourier transforming this quantity. As readily noticed, both theoretical methods predict a significant imaginary contribution to the intermediate scattering function in all cases. Further, the imaginary part of the intermediate scattering function of para-hydrogen is systematically larger for all k values, consistent with expectations that quantum effects are more relevant for para-hydrogen, which exhibits larger quantum effects. In fact, the amplitude of the imaginary component vanishes classically (i.e. for small de Broglie wavelength) and provides a measure of the quantum deviations. Although the *FK – LPI* and *RPMD* results are qualitatively similar, they tend to show the most significant differences after about 0.3ps . The agreement between the *FK – LPI* and *RPMD* results for short times is consistent with the expectation that both methods should be accurate mainly for times up to $\sim \beta \hbar$, i.e. 0.38ps and 0.33ps for para-hydrogen and ortho-deuterium respectively.

In Fig. 2.2 the *FK – LPI* and *RPMD* dynamic structure factor is compared with the experimental dynamic structure factor of Ref. [41] and [42] refined using *FK – LPI* as the input as described in the previous section. The analogous spectral shapes refined using *RPMD* as the input along with the variable $\alpha(\vec{k})$ in Eq. 2.40 are also shown in Fig. 2.2 for comparison. As

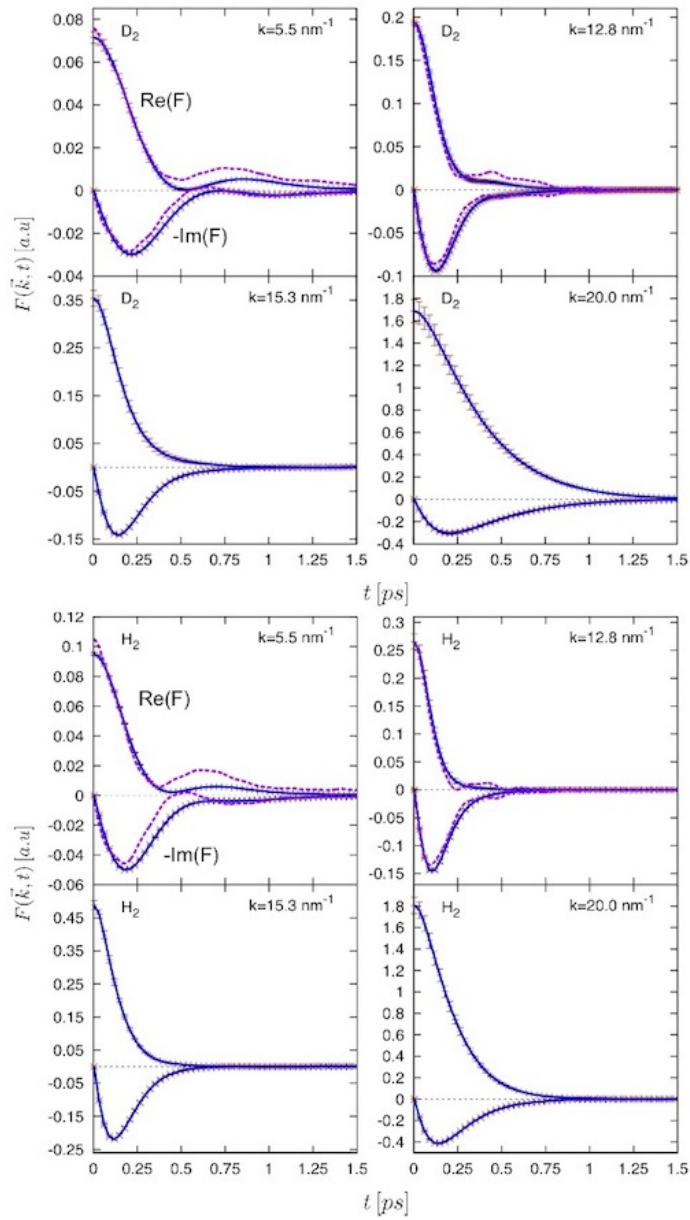


Figure 2.1: The $FK-LPI$ (blue line) and $RPMD$ (magenta dashed line at low k 's) approximation to the intermediate scattering function for both ortho-deuterium (upper four panels) and para-hydrogen (lower four panels) for the different momentum transfers considered (as labeled). The real part of the correlation function is the upper curve while the negative imaginary part is the lower curve in each figure.

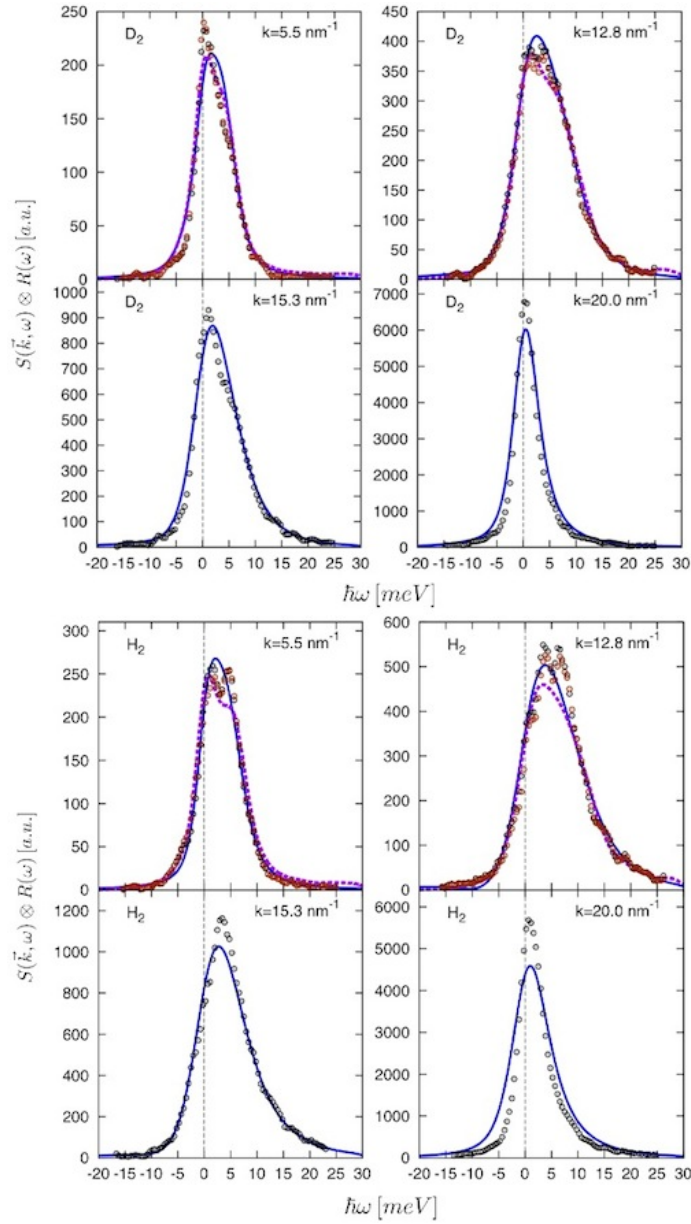


Figure 2.2: The refined experimental dynamic structure factors of Refs.[41] and [42], as obtained by using either *FK – LPI* (black dots) or *RPMD* (red dots) as the input (see text). The *FK – LPI* (blue line) and *RPMD* (dashed magenta line) dynamic structure factors are convoluted with the instrumental resolution function. The layout of the figure is the same as that in Fig. 2.1.

readily noticed, the difference between the experimental line-shapes refined using either theoretical method as an input is negligible. The *FK – LPI* and *RPMD* dynamic structure factors have both been convoluted with the instrument resolution function in order to provide a meaningful comparison with the experimental results. As seen in Fig. 2.2, the more sharply resolved frequency spectrum of *RPMD* appears to somewhat better reproduce the refined experimental dynamic structure factors for a momentum transfer of 5.5 nm^{-1} as compared to the broader spectrum of *FK-LPI*, although a preference is unclear at 12.8 nm^{-1} . This discrepancy between the *FK – LPI* and *RPMD* results is plausibly linked to the differences in the long time behavior of the corresponding intermediate scattering functions and, specifically, to the more pronounced oscillations of the *RPMD* profiles.

For the two largest k values, *RPMD* is not applicable due to the increased non-linearity of the associated correlation function. One can recognize an overall increase in the decay time of the *FK – LPI* intermediate scattering function (see Fig. 2.1) for both para-hydrogen and ortho-deuterium, with that of 20.0 nm^{-1} showing the slowest decay. The decay time of the ortho-deuterium intermediate scattering function is longer than that of para-hydrogen for the two highest k values. One should expect that *FK – LPI* will perform better for ortho-deuterium than for para-hydrogen, since the latter exhibits a more pronounced quantum behavior, while the *FK – LPI* approach mainly relies upon classical dynamics. This should become particularly evident when the long-time behavior of the correlation function becomes relevant. This expect-

tation is apparently confirmed by the data in Fig. 2.2, where it is evident that $FK - LPI$ agrees more closely with the ortho-deuterium experimental data than that of para-hydrogen. This is most evident at the highest momentum transfer (20.0 nm^{-1}) where $FK - LPI$ closely reproduces the experimental spectra of ortho-deuterium, while for para-hydrogen it consistently underestimates the intensity and overestimates the width of the spectrum. This allows us to roughly identify $k = 20.0 \text{ nm}^{-1}$ as a k -threshold to perform a challenging test for semi-classical simulations in para-hydrogen. In fact, for $k \sim 20.0 \text{ nm}^{-1}$ the classical propagation inherent to $FK - LPI$ evidently does not correctly account for the quantum behavior of the correlation function.

The static structure factor obtained from the $FK - LPI$ and $RPMD$ methods are shown in Fig. 2.3. Also shown in the figure are the results from a classical simulation for ortho-deuterium, which was performed identically to that of $RPMD$, the only difference being that we set the number of beads n equal to 1, which limit reduces to the classical time correlation function. Classical simulations were not performed for para-hydrogen due to the similarity of our para-hydrogen state points with those in Ref. [43] in which they found that for para-hydrogen, the state points ($T = 25 \text{ K}, n = 19.0 \text{ nm}^{-3}$) and ($T = 14 \text{ K}, n = 23.5 \text{ nm}^{-3}$) lie in the liquid-vapor coexistence region of the classical phase diagram. The $FK - LPI$ static structure factor was obtained by simply taking the $t = 0$ value of the intermediate scattering function, while the $RPMD$ and classical static structure factors were obtained by first computing the dynamic structure factor using the relation in Eq. 2.21, and then integrat-

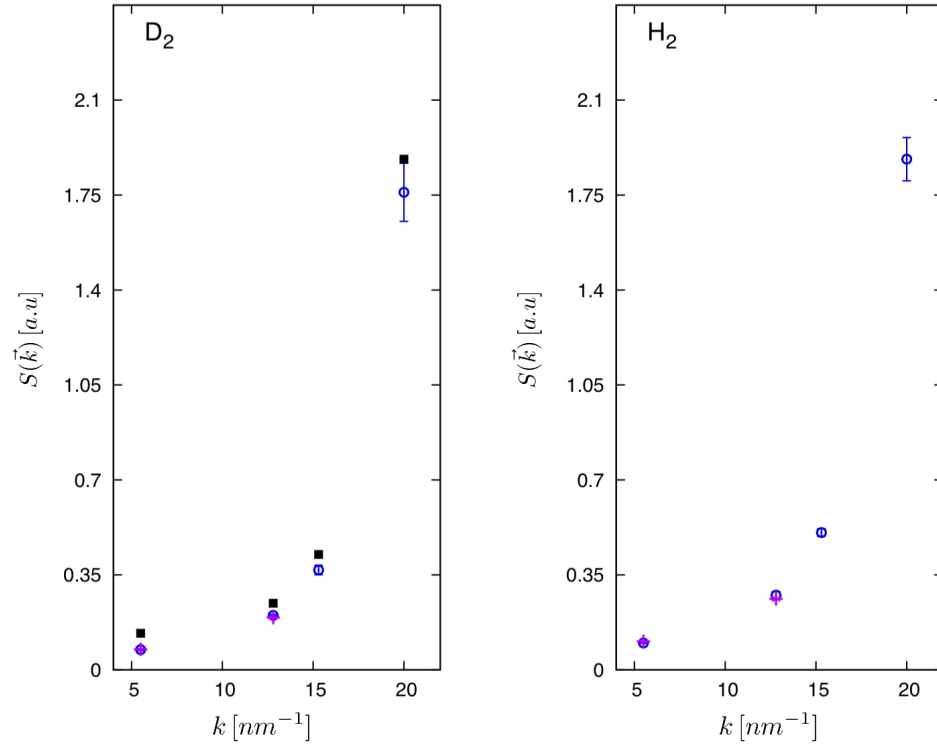


Figure 2.3: The static structure factors obtained from the the intermediate scattering function using the relation in Eq. 2.10 for both ortho-deuterium (left panel) and para-hydrogen (right panel) using $FK-LPI$ (blue circle), $RPMD$ (magenta cross), and the Classical simulation with the harmonic correction factor (black square).

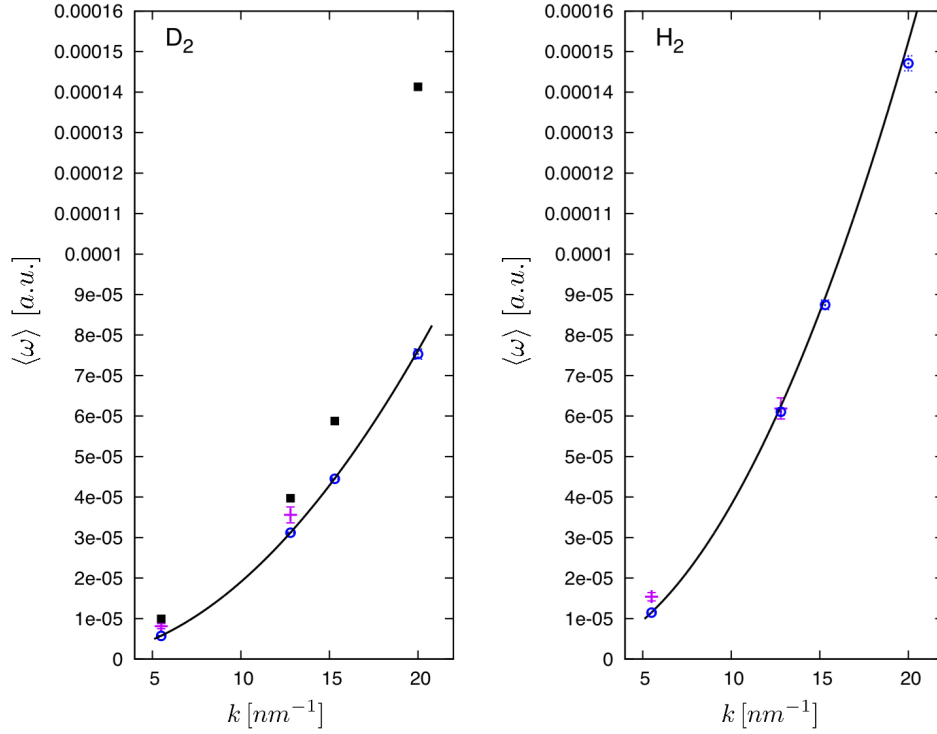


Figure 2.4: The first moment of the dynamic structure factors obtained from the the intermediate scattering function using the relation in Eq. 2.11 for both ortho-deuterium (left panel) and para-hydrogen (right panel) using $FK - LPI$ (blue circle), $RPMD$ (magenta cross), and the Classical simulation with the harmonic correction factor (black square). These results are compared with the exact relation of Eq. 2.11 (black line).

ing this quantity over ω , as in Eq. 2.10. It should be noted that by computing the classical quantity this way, we are actually applying the well known harmonic quantum correction factor[44]. One finds in Fig. 2.3 that both the *FK – LPI* and *RPMD* methods reproduce the experimental static structure factors of ortho-deuterium and para-hydrogen published in Ref. [42] to within the combined uncertainty of the experiment and simulation, while the classical quantity with the harmonic correction factor consistently overestimates this quantity for ortho-deuterium. The agreement between the *FK – LPI* and experimental static structure factors validates *a posteriori* the assumption, made in Eq. 2.38, that *FK – LPI* provides an exact result for $S(k)$, thus also demonstrating the accuracy of the FK local harmonic approximation for the density operator. Furthermore, the fact that the classical quantity with the harmonic correction factor consistently overestimates the static structure factor for ortho-deuterium shows that this quantity could not be used as an input to refine the experimental quantity, since the resulting refined quantity would have an incorrect static structure factor. This is due to the fact that while the refinement process guarantees the experimental quantity to have the correct first moment, there are no constraints imposed on the zeroth moment (static structure factor).

Upon comparison of the first moment of the dynamic structure factor in Fig. 2.4 obtained from the *FK – LPI* and *RPMD* methods with the exact relation in Eq. 2.11, one clearly sees that *RPMD* gives a relatively good estimate for this quantity at the k values where it can be applied. This

fact shows that the non-linearity of the correlation function does not degrade the quality of the *RPMD* results in this range of momentum transfers, in agreement with the findings of Ref. [27].

2.4 Conclusions

We have provided a benchmark comparison between *FK – LPI* and *RPMD* simulated dynamic structure factors and the one measured by Inelastic X-ray Scattering in low-temperature para-hydrogen and ortho-deuterium. As a result, we have proposed a successful method to cope with spurious experimental effects by using either of the computational methods as an input, while using a best fit approach. The consistency between the experimental line-shapes refined by either computational method indicates that the used procedure provides the best available estimate for the true dynamic structure factor of the samples.

Furthermore, we observed that *FK – LPI* is able to reproduce the refined experimental spectrum of ortho-deuterium and para-hydrogen relatively well at low momentum transfers. Small differences between *RPMD* and *FK – LPI* low- k results may reflect the higher accuracy of the former computational method, even though results were not completely systematic in this regard.

At higher k , *FK – LPI* provides an overall better agreement with the experimental spectra of ortho-deuterium, compared to para-hydrogen. This is ascribed to the less pronounced quantum behavior of ortho-deuterium, conse-

quent to its higher molecular mass, which makes more accurate the classical approximation inherent to the $FK - LPI$ approach. Conversely, the substantial disagreement between $FK - LPI$ and the experimental spectrum of para-hydrogen at $k = 20.0 \text{ nm}^{-1}$ strongly suggests that we have identified a challenging test system which can serve as a benchmark for new method development.

Overall, both $FK - LPI$ and $RPMD$ consistently showed residual differences in the small energy transfer region when compared to experimental data. While this is most likely due to the classical dynamic propagation used by both of these methods, which does not properly account for the long time behavior of the quantum time correlation function, the use of a semi-empirical potential to model the para-hydrogen and ortho-deuterium system cannot be ruled out as an error source.

Chapter 3

A New Class of Ensemble Conserving Algorithms for Approximate Quantum Dynamics: Theoretical Formulation and Model Problems

3.1 Introduction

One of the main goals in quantum statistical mechanics is the calculation of quantum time correlation functions, which in the canonical ensemble takes the general form

$$\langle \hat{A}(0)\hat{B}(t) \rangle = \frac{1}{Z} \text{Tr} \left(e^{-\beta\hat{H}} \hat{A} e^{i\hat{H}t/\hbar} \hat{B} e^{-i\hat{H}t/\hbar} \right), \quad (3.1)$$

Z being the partition function and β the inverse temperature $1/k_bT$. The time correlation functions defined by Eq. 3.1 are of pivotal interest since they are accessible by most experimental spectroscopic techniques. For example, the dynamic structure factor, which is measured by either Inelastic X Ray or Neutron Scattering, the diffusion constant, and absorption spectra are just some of the quantities that can be related to quantum time correlation functions of the form of Eq. 3.1. Unfortunately, in order to compute these quantities exactly, one is required either to compute a full real time path-integral or solve the corresponding time-dependent Schrodinger equation, which is not

practical for realistic systems due to the intense computational load. In order to overcome this difficulty, it is desirable to develop approximate quantum methods which are as accurate and efficient as possible, and therefore enable the practical evaluation of Eq. 3.1. To date, there exists multiple approximation schemes including the Classical Wigner approximation (CW)[2, 17, 19], Centroid Molecular Dynamics (CMD) [15], as well as Ring-Polymer Molecular Dynamics (RPMD)[26] in which one uses semi-classical methods to calculate quantum time correlation functions approximately.

While all of these methods provide relatively accurate and practical approximations to Eq. 3.1, each have their own downfalls. For example, while both CMD and RPMD have been shown to be exact in the harmonic, high temperature, and short time limits, both of these methods begin to break down for correlation functions involving non-linear operators[15, 26, 28]. In addition, the intrinsic dynamics of the ring-polymer in RPMD can introduce artificial frequencies in the spectrum of the correlation function, which becomes especially important when simulating absorption spectra[32]. On the other hand, the CW approximation is also exact in the harmonic, high temperature, and short time limits, even for correlation functions involving non-linear operators[2, 20]. However, the CW approximation does not in general correctly produce time invariant thermodynamic properties of thermal equilibrium systems. Explicitly, for $\hat{A} = 1$ the exact quantum expression in Eq. 3.1 has the property that

$$\langle \hat{B}(t) \rangle = \langle \hat{B}(0) \rangle, \quad (3.2)$$

however this is generally not true for the CW approximation due to the classical dynamics used. While both CMD and RPMD also use a form of classical dynamics, these methods are able to retain the desirable property in Eq. 3.2 of the exact quantum time correlation function because the form of classical dynamics used in these methods conserves the initial quantum ensemble, while the purely classical dynamics used in the CW approximation do not. Recently, Liu and Miller[20, 22, 24] have proposed a route to remedy this downfall of the CW approximation by replacing the classical propagation of the initial phase space distribution with a form of dynamics that conserves the initial quantum ensemble. Similarly, we set out to present a simple form of dynamics which conserve the ensemble and can be used to improve upon the Feynman-Kleinert implementation of the CW approximation, known as the Feynman-Kleinert linearized path-integral (FK-LPI)[2] method.

This chapter is organized as follows: An introduction to the CW approximation and the Feynman-Kleinert (FK) approximation of the density operator is presented in Section II and III. Based upon the FK approximation of the density operator, we then present two different classes of ensemble conserving dynamics in Section IV and V. In Section VI, we apply these dynamics within the CW approximation for both the quartic and double-well potentials, and a comparison with the exact quantum time correlation function, as well as RPMD, CMD, and FK-LPI is made. The conclusions are presented in Section VII.

3.2 Classical Wigner Approximation

The CW[2, 17, 19] expression for a general quantum time correlation function of a system in one dimension is given by

$$\langle \hat{A}(0)\hat{B}(t) \rangle \approx \frac{1}{Z} \frac{1}{2\pi\hbar} \int_{-\infty}^{\infty} dpdq [e^{-\beta\hat{H}} \hat{A}]_W(q, p) [\hat{B}]_W(q_t, p_t) \quad (3.3)$$

where (q_t, p_t) is the classically evolved quantum phase space, (q, p) being the initial quantum distribution, and the Wigner transform of a general operator \hat{C} is given by

$$[\hat{C}]_W(q, p) \equiv \int_{-\infty}^{\infty} d\eta e^{-ip\eta/\hbar} \left\langle q + \frac{\eta}{2} \left| \hat{C} \right| q - \frac{\eta}{2} \right\rangle. \quad (3.4)$$

The CW approximation can be shown to follow not only from a path linearization approximation implemented within the semiclassical initial value representation (SC-IVR) of the propagator[19], but also from a linearization of the action difference between the forward-backward time paths in the corresponding exact path-integral expression for a general time correlation function[2, 18]. Furthermore, the CW approximation is exact in the limit that $t \rightarrow 0$ since in this limit Eq. 3.3 reduces to the Wigner representation of $\langle \hat{A}\hat{B} \rangle$.

In fact, the CW approximation can be conjectured from the exact Wigner representation of the quantum time correlation function given by

$$\langle \hat{A}(0)\hat{B}(t) \rangle = \frac{1}{Z} \frac{1}{2\pi\hbar} \int_{-\infty}^{\infty} dpdq [e^{-\beta\hat{H}} \hat{A}]_W(q, p) [\hat{B}(t)]_W(q, p) \quad (3.5)$$

since this approximation simply amounts to replacing the exact quantum evolution of $\hat{B}(t) = e^{i\hat{H}t/\hbar} \hat{B} e^{-i\hat{H}t/\hbar}$ with the classical evolution of the quantum phase space such that

$$[\hat{B}(t)]_W(q, p) \rightarrow [\hat{B}]_W(q_t, p_t). \quad (3.6)$$

However, the classical evolution of the quantum phase space does not, in general, conserve the initial quantum phase space distribution, which results in thermodynamic properties of equilibrium systems being, incorrectly, time dependent. Liu and Miller[20, 22, 24] have proposed a route to remedy this downfall of the CW approximation by replacing the classical propagation of the initial phase space distribution with a form of dynamics that preserves the time invariance of thermodynamic properties, such that $\langle \hat{B}(t) \rangle = \langle \hat{B}(0) \rangle$ in accord with the exact correlation function. As we show in Appendix B, the CW expression in Eq. 3.3 can be made to share this property so long as the dynamics fulfil

$$dqdp[e^{-\beta\hat{H}}]_W(q, p) = dq_t dp_t[e^{-\beta\hat{H}}]_W(q_t, p_t), \quad (3.7)$$

such that they conserve the initial quantum phase space probability within the infinitesimal phase space volume along the trajectory, which is equivalent to the initial quantum ensemble being conserved. As we will show in Sec. IV and V, we are able to find two classes of dynamics that preserve this property and can therefore be used to improve the CW approximation.

3.3 Feynman-Kleinert density operator

Regardless of the dynamics used, the first step in invoking the CW approximation is obtaining the corresponding density matrix, since the Wigner transform of $e^{-\beta\hat{H}}\hat{A}$ is required. As in the FK-LPI method, we accomplish this by combining the effective frequency variational theory of Feynman[8] and Kleinert[9] (FK) with the quasidensity operator formalism of Jang and Voth[16]. This FK approximation to the density operator enables one to obtain an analytical expression for the Wigner transform of $e^{-\beta\hat{H}}\hat{A}$ which in turn allows for an efficient numerical evaluation of the CW approximation. The FK approximation of the density operator is exact in the harmonic and high temperature limits. Furthermore, the FK approximation to $e^{-\beta\hat{H}}$ gives the best local harmonic approximation to the systems free energy and has been shown to be very accurate[1–6].

The *FK* approximation for $e^{-\beta\hat{H}}$ in one dimension is given by

$$e^{-\beta\hat{H}} \approx \int_{-\infty}^{\infty} dx_c dp_c \rho_{FK}(x_c, p_c) \hat{\delta}_{FK}(x_c, p_c) \quad (3.8)$$

where (x_c, p_c) are the classical centroid phase space variables describing the average position and momentum of a particle during thermal time $\beta\hbar$ and are defined as

$$x_c \equiv \frac{1}{\beta\hbar} \int_0^{\beta\hbar} d\tau x(\tau) \quad p_c \equiv \frac{1}{\beta\hbar} \int_0^{\beta\hbar} d\tau p(\tau). \quad (3.9)$$

The FK approximation to the centroid phase space density $\rho_{FK}(x_c, p_c)$ is given by

$$\rho_{FK}(x_c, p_c) \equiv \frac{1}{2\pi\hbar} \exp \left\{ -\beta \left(\frac{p_c^2}{2m} + W_1(x_c) \right) \right\}, \quad (3.10)$$

$W_1(x_c)$ being the FK approximation to the centroid potential. The effective frequency quasidensity operator $\hat{\delta}_{FK}(x_c, p_c)$ is defined as

$$\begin{aligned} \hat{\delta}_{FK}(x_c, p_c) &\equiv \sqrt{\frac{m\Omega(x_c)}{\pi\hbar\alpha(x_c)}} \int_{-\infty}^{\infty} dx dx' |x'\rangle \langle x| \\ &\times \exp \left\{ i\frac{p_c}{\hbar} (x' - x) - \frac{m\Omega(x_c)}{\hbar\alpha(x_c)} \left(\frac{x' + x}{2} - x_c \right)^2 \right\} \\ &\times \exp \left\{ -\frac{m\Omega(x_c)\alpha(x_c)}{4\hbar} (x' - x)^2 \right\}, \end{aligned} \quad (3.11)$$

where the centroid dependent variational effective frequency $\Omega(x_c)$ is determined from the local curvature of the systems Gaussian smeared potential, and is given by

$$\Omega^2(x_c) = \frac{1}{m} \left[\frac{\partial^2 V_{a^2}(x_c)}{\partial x_c^2} \right]_{a^2=a^2(x_c)}. \quad (3.12)$$

The smeared potential, $V_{a^2}(x_c)$, which accounts for quantum-statistical path fluctuations is defined as

$$V_{a^2}(x_c) \equiv \sqrt{\frac{1}{2\pi a^2}} \int_{-\infty}^{\infty} dy V(y) \exp \left\{ -\frac{(y - x_c)^2}{2a^2} \right\}, \quad (3.13)$$

the smearing width $a^2(x_c)$ being

$$a^2(x_c) = \frac{1}{m\beta\Omega^2(x_c)} \left(\frac{\beta\hbar\Omega(x_c)}{2} \coth \left(\frac{\beta\hbar\Omega(x_c)}{2} \right) - 1 \right) \quad (3.14)$$

which measures the importance of quantum fluctuations around the classical-like position x_c . In Eq. 3.11, $\alpha(x_c)$ is related to the smearing width $a^2(x_c)$ by

$$\alpha(x_c) = \frac{2m\Omega(x_c)a^2(x_c)}{\hbar} = \coth \left(\frac{\beta\hbar\Omega(x_c)}{2} \right) - \frac{2}{\beta\hbar\Omega(x_c)}. \quad (3.15)$$

Note that when using Eq. 3.12 to determine the effective frequency $\Omega(x_c)$, the derivative is taken while treating $a^2(x_c)$ as a constant. Furthermore, by using Eq. 3.12 and 3.13 one can write the explicit form that $\Omega^2(x_c)$ takes in terms of $a^2(x_c)$, and it is given by

$$\Omega^2(x_c) = \frac{1}{m} \sqrt{\frac{1}{2\pi a^2(x_c)}} \int_{-\infty}^{\infty} dy \frac{\partial^2 V(y + x_c)}{\partial x_c^2} \times \exp \left\{ -\frac{y^2}{2a^2(x_c)} \right\}. \quad (3.16)$$

Once $\Omega(x_c)$ is determined by solving Eq. 3.14 and 3.16 iteratively, the FK approximation to the centroid potential $W_1(x_c)$ is given by

$$W_1(x_c) = \frac{1}{\beta} \ln \left\{ \frac{\sinh \left(\frac{\beta \hbar \Omega(x_c)}{2} \right)}{\frac{\beta \hbar \Omega(x_c)}{2}} \right\} + V_{a^2}(x_c) - \frac{1}{2} m \Omega^2(x_c) a^2(x_c). \quad (3.17)$$

Using this *FK* approximation of the density operator, the Wigner distribution function, $[e^{-\beta \hat{H}}]_W(q, p)$, takes the form

$$[e^{-\beta \hat{H}}]_W(q, p) = \int dx_c dp_c \rho_{FK}(x_c, p_c) [\hat{\delta}_{FK}]_W(q, p), \quad (3.18)$$

where the Wigner transform of the QDO is written explicitly as

$$[\hat{\delta}_{FK}]_W(q, p) = \frac{2}{\alpha} \exp \left\{ -\frac{m\Omega}{\hbar\alpha} (q - x_c)^2 - \frac{(p - p_c)^2}{m\hbar\Omega\alpha} \right\}. \quad (3.19)$$

3.4 The Feynman-Kleinert Quasi-Classical Wigner method: FK-QCW(1)

As it turns out, there are multiple ways of generating dynamics that conserve the initial quantum ensemble and can be used to evaluate the CW approximation. For example, Liu and Miller[22] proposed a clever way of generating ensemble conserving dynamics by making an analogy to Liouville's theorem in classical mechanics and set

$$\frac{d}{dt}[e^{-\beta\hat{H}}]_W(q_t, p_t) = 0, \quad (3.20)$$

and then proceed to generate the dynamics from this relation by choosing

$$\dot{q}_t = \frac{p_t}{m} \quad (3.21)$$

from which it will follow that the effective force will be given by

$$\begin{aligned} \dot{p}_t &= -\frac{\partial V_{eff}(q_t, p_t)}{\partial q_t} \\ &= -\frac{p_t}{m} \frac{\partial}{\partial q_t} [e^{-\beta\hat{H}}]_W(q_t, p_t) / \frac{\partial}{\partial p_t} [e^{-\beta\hat{H}}]_W(q_t, p_t). \end{aligned} \quad (3.22)$$

However, if one takes this Equilibrium Liouville Dynamics[22] route for the FK approximation of the Wigner distribution function then, as shown in Ref. [23], the dynamics involve an integration over the centroid distribution at each time step, which adds a significant computational load.

However, within the FK approximation to the density operator, one can find another set of dynamics that conserves the ensemble and avoids this complication. This is accomplished by first casting the FK Wigner distribution

function into another form by making a dummy variable substitution of the integration variables in Eq. 3.18 from $(x_c, p_c) \rightarrow (x_c(t), p_c(t))$ (see Appendix C for a rigorous proof) such that this function evaluated at a point (q_t, p_t) takes the form

$$[e^{-\beta\hat{H}}]_W(q_t, p_t) = \int dx_c(t) dp_c(t) \rho_{FK}(x_c(t), p_c(t)) \times [\hat{\delta}_{FK}(t)]_W(q_t, p_t), \quad (3.23)$$

where $\hat{\delta}_{FK}(t) \equiv \hat{\delta}_{FK}(x_c(t), p_c(t))$ and the centroid variables evolve according to the classical like equations

$$\begin{aligned} \dot{x}_c(t) &= \frac{p_c(t)}{m} \\ \dot{p}_c(t) &= - \left[\frac{\partial V_{a^2}(x_c(t))}{\partial x_c(t)} \right]_{a^2=a^2(x_c(t))}. \end{aligned} \quad (3.24)$$

However, as we show in Appendix D, the centroid distribution fulfills Liouville's theorem such that

$$dx_c dp_c \rho_{FK}(x_c, p_c) = dx_c(t) dp_c(t) \rho_{FK}(x_c(t), p_c(t)), \quad (3.25)$$

and using this identity in Eq. 3.23 we have that

$$[e^{-\beta\hat{H}}]_W(q_t, p_t) = \int dx_c dp_c \rho_{FK}(x_c, p_c) [\hat{\delta}_{FK}(t)]_W(q_t, p_t). \quad (3.26)$$

Thus, using this form of the FK Wigner distribution function, in order for

$$dq_t dp_t [e^{-\beta\hat{H}}]_W(q_t, p_t) = dq dp [e^{-\beta\hat{H}}]_W(q, p) \quad (3.27)$$

such that the ensemble is conserved, the dynamics must fulfil

$$\int dx_c dp_c \rho_{FK}(x_c, p_c) \left(dq_t dp_t [\hat{\delta}_{FK}(t)]_W(q_t, p_t) - dq dp [\hat{\delta}_{FK}(0)]_W(q, p) \right) = 0 \quad (3.28)$$

which we see can be satisfied independent of the centroid distribution function if the dynamics fulfill the less restrictive condition

$$dq_t dp_t [\hat{\delta}_{FK}(t)]_W(q_t, p_t) = dq dp [\hat{\delta}_{FK}(0)]_W(q, p). \quad (3.29)$$

Furthermore, the phase space volume element at time t is related to the initial volume element through

$$dq_t dp_t = \det(J(t)) dq dp \quad (3.30)$$

where $\det(J(t))$ is the determinant of the Jacobian matrix and explicitly given by[22]

$$\det(J(t)) = \exp\left(\int_0^t \frac{\partial \dot{q}_t}{\partial q_t} + \frac{\partial \dot{p}_t}{\partial p_t} dt\right), \quad (3.31)$$

such that Eq. 3.29 is equivalent to

$$\det(J(t)) [\hat{\delta}_{FK}(t)]_W(q_t, p_t) = [\hat{\delta}_{FK}(0)]_W(q, p). \quad (3.32)$$

As we now show, we are able to easily find a set of dynamics that fulfill this relation and therefore are guaranteed to conserve the ensemble. This is accomplished by working in terms of the dimensionless relative coordinates

$$\begin{aligned} \tilde{q}(t) &\equiv \sqrt{\frac{m\Omega_t}{\hbar\alpha_t}} (q_t - x_c(t)) \\ \tilde{p}(t) &\equiv \sqrt{\frac{1}{m\hbar\Omega_t\alpha_t}} (p_t - p_c(t)) \end{aligned} \quad (3.33)$$

in which the Wigner transformed QDO takes the simple form

$$[\hat{\delta}_{FK}(t)]_W(q_t, p_t) = \frac{2}{\alpha_t} \exp(-\tilde{q}(t)^2 - \tilde{p}(t)^2), \quad (3.34)$$

and, as shown in Appendix E, the determinant of the Jacobian matrix in Eq. 3.31 takes the form

$$\begin{aligned} \det(J(t)) &= \exp\left(\int_0^t \frac{\partial \dot{q}_t}{\partial q_t} + \frac{\partial \dot{p}_t}{\partial p_t} dt\right) \\ &= \exp\left(\int_0^t \frac{\partial \dot{\tilde{q}}(t)}{\partial \tilde{q}(t)} + \frac{\partial \dot{\tilde{p}}(t)}{\partial \tilde{p}(t)} dt\right) \frac{\alpha_t}{\alpha_0}. \end{aligned} \quad (3.35)$$

Thus, using these relations in Eq. 3.32, we have that the ensemble will be conserved as long as the dynamics fulfil

$$\begin{aligned} \exp\left(\int_0^t \frac{\partial \dot{\tilde{q}}(t)}{\partial \tilde{q}(t)} + \frac{\partial \dot{\tilde{p}}(t)}{\partial \tilde{p}(t)} dt\right) \exp(-\tilde{q}(t)^2 - \tilde{p}(t)^2) \\ = \exp(-\tilde{q}(0)^2 - \tilde{p}(0)^2). \end{aligned} \quad (3.36)$$

Therefore, if we require the dynamics to satisfy

$$\exp(-\tilde{q}(t)^2 - \tilde{p}(t)^2) = \exp(-\tilde{q}(0)^2 - \tilde{p}(0)^2), \quad (3.37)$$

or equivalently

$$\tilde{q}(t) \dot{\tilde{q}}(t) + \tilde{p}(t) \dot{\tilde{p}}(t) = 0, \quad (3.38)$$

and furthermore require

$$\frac{\partial \dot{\tilde{q}}(t)}{\partial \tilde{q}(t)} + \frac{\partial \dot{\tilde{p}}(t)}{\partial \tilde{p}(t)} = 0, \quad (3.39)$$

then the ensemble will be conserved.

This then gives us two conditions that must be met, however, it does not give us a way to generate dynamics without first assuming a form for either

$\dot{\tilde{q}}(t)$ or $\dot{\tilde{p}}(t)$. Therefore, to guide us in this matter, we look to the harmonic limit in which Ω is constant and the exact dynamics of the centroid and quantum phase space variables are given by their corresponding classical equations. In this limit, it is straightforward to show that the exact relation for $\dot{\tilde{q}}(t)$ is

$$\dot{\tilde{q}}(t) = \Omega \tilde{p}(t). \quad (3.40)$$

Thus, assuming this harmonic form and furthermore introducing an arbitrary frequency function f such that for a general potential $\dot{\tilde{q}}(t)$ takes the form

$$\dot{\tilde{q}}(t) = f \tilde{p}(t), \quad (3.41)$$

then from the condition in Eq. 3.38 we have that

$$\dot{\tilde{p}}(t) = -f \tilde{q}(t). \quad (3.42)$$

Furthermore, the second condition in Eq. 3.39 that must be met for these dynamics to conserve the ensemble is

$$\frac{\partial \dot{\tilde{q}}(t)}{\partial \tilde{q}(t)} + \frac{\partial \dot{\tilde{p}}(t)}{\partial \tilde{p}(t)} = \frac{\partial f}{\partial \tilde{q}(t)} \tilde{p}(t) - \frac{\partial f}{\partial \tilde{p}(t)} \tilde{q}(t) = 0. \quad (3.43)$$

However, by using Eq. 3.33 we can make a change of variables for the partial derivatives and this condition can be equivalently written as

$$\sqrt{\frac{\hbar \alpha_t}{m \Omega_t}} \frac{\partial f}{\partial q_t} \tilde{p}(t) - \sqrt{m \hbar \Omega_t \alpha_t} \frac{\partial f}{\partial p_t} \tilde{q}(t) = 0, \quad (3.44)$$

which we recognize is always satisfied as long as our arbitrary function f does not depend on q_t or p_t . Therefore, the dynamics of the general form

$$\begin{aligned}
\dot{\tilde{q}}(t) &= f(x_c(t), p_c(t)) \tilde{p}(t) \\
\dot{\tilde{p}}(t) &= -f(x_c(t), p_c(t)) \tilde{q}(t)
\end{aligned} \tag{3.45}$$

are guaranteed to conserve the ensemble since they fulfill the relation in Eq. 3.36 and therefore Eq. 3.27. Furthermore, using Eq. 3.33 these dynamics can be written explicitly in terms of the quantum phase space variables as

$$\begin{aligned}
\dot{q}_t &= \dot{x}_c(t) + \frac{f}{m\Omega_t} (p_t - p_c(t)) - \frac{1}{2} \frac{d}{dt} \ln \left(\frac{\Omega_t}{\alpha_t} \right) (q_t - x_c(t)) \\
\dot{p}_t &= \dot{p}_c(t) - fm\Omega_t (q_t - x_c(t)) + \frac{1}{2} \frac{d}{dt} \ln (\Omega_t \alpha_t) (p_t - p_c(t))
\end{aligned} \tag{3.46}$$

from which one can show that the determinant of the Jacobian matrix is given by

$$\det(J(t)) = \frac{\alpha_t}{\alpha_0}. \tag{3.47}$$

Therefore, since we are able to introduce an arbitrary function $f(x_c(t), p_c(t))$ into the dynamics, we have found an entire class of dynamics that conserve the ensemble and can be used within the CW expression for the time correlation function. Furthermore, the direct propagation of the (q_t, p_t) variables through the dynamics in Eq. 3.46 is not necessary due to the fact that once the dimensionless and centroid variables have been propagated according to Eq. 3.45 and 3.24, respectively, we can obtain the instantaneous quantum phase space variables through

$$\begin{aligned}
q_t &= \sqrt{\frac{\hbar\alpha_t}{m\Omega_t}} \tilde{q}(t) + x_c(t) \\
p_t &= \sqrt{m\hbar\Omega_t\alpha_t} \tilde{p}(t) + p_c(t),
\end{aligned} \tag{3.48}$$

which is the inversion of Eq. 3.33. Furthermore, the multi-dimensional generalization of this method is relatively straightforward since it amounts to propagating the dimensionless relative coordinates through the same dynamics in Eq. 3.45, only now written in terms of the mass-weighted normal mode coordinates defined in Ref. [2].

However, there does exist one drawback to this entire class of dynamics since the momentum becomes imaginary when the FK effective frequency takes on imaginary values. Explicitly, when $\Omega_t^2 < 0$ the $\Omega_t \alpha_t$ term in Eq. 3.48 becomes negative which does not allow us to transform from $\tilde{p}(t)$ to p_t . Thus, there exists a limitation in these dynamics since in order to use it for barriers one must adopt the convention to set $p_t = p_c(t)$, which is the limiting value of p_t for $\Omega_t \rightarrow 0$, as seen from Eq. 3.48. While this convention does not present a problem when used within the CW expression for the time correlation of linear operators, it would be desirable to have a similar method that conserves the ensemble and is also able to handle imaginary frequencies in a robust way. This is the motivation for an additional class of dynamics which are presented in Sec. V. However, as we show in Appendix F, this entire class of dynamics when used within the CW approximation for the Kubo-transformed time-correlation function reduces to CMD for linear operators.

3.4.1 Harmonic limit

Although a whole class of dynamics exist which conserve the initial quantum ensemble, one can easily conjecture that only a subset of these would

actually be useful and provide a reasonable approximation to the real quantum dynamics. Therefore, we now provide a way to tailor the general frequency function introduced into the dynamics such that we recover exact quantum dynamics in the harmonic limit.

For a harmonic potential, Ω_t and α_t are simply constants. Furthermore, as we alluded to in Eq. 3.40, the exact dynamics of the dimensionless variables in Eq. 3.33 in the harmonic limit takes the form

$$\begin{aligned}\dot{\tilde{q}}(t) &= \Omega\tilde{p}(t) \\ \dot{\tilde{p}}(t) &= -\Omega\tilde{q}(t),\end{aligned}\tag{3.49}$$

which is easily shown by using the fact that the exact dynamics of the centroid and quantum phase space variables are given by their corresponding classical equations. Therefore, if we choose for our arbitrary function in the dynamics of Eq. 3.45 the FK effective frequency

$$f(x_c(t)) = \Omega(x_c(t)),\tag{3.50}$$

then these dynamics will be exact in the harmonic limit, since in this limit $\Omega(x_c(t)) \rightarrow \Omega$. Furthermore, since the CW approximation is exact in this limit, the time correlation function will also be exact.

3.4.2 Classical and high temperature limits

In both the classical ($\hbar \rightarrow 0$) and high temperature ($\beta \rightarrow 0$) limits, it is easy to show from Eq. 3.48 that q_t and p_t become fixed at $x_c(t)$

and $p_c(t)$, respectively. Furthermore, the centroid equations of motion reduce to the corresponding classical equations of motion since the smearing width $a^2(x_c(t)) \rightarrow 0$ in both of these limits. Using these properties, it is straightforward to show that when the FK approximation to the density operator is used, the CW expression for the time correlation function in Eq. 3.3 reduces to the corresponding classical expression. Thus, the entire class of dynamics in Eq. 3.45 are able to recover both the classical and high temperature limits of the quantum time correlation function exactly.

3.4.3 Low temperature limit

At low temperatures the centroid distribution in Eq. 3.11 singles out $p_c = 0$ as well as the x_c value corresponding to the global minimum of the centroid potential $W_1(x_c)$, denoted x_c^m . Therefore, from Eq. 3.24 we have that $(x_c(t), p_c(t))$ will be fixed at $(x_c^m, 0)$, and the dynamics of Eq. 3.45 reduce to

$$\begin{aligned} \dot{q}_t &= \frac{p_t}{m} \\ \dot{p}_t &= -mf(x_c^m, 0)\Omega(x_c^m)(q_t - x_c^m). \end{aligned} \tag{3.51}$$

Furthermore, as discussed in Refs. [8] and [9], in the low temperature limit $\hbar\Omega(x_c^m)$ provides an approximation to the energy difference between the ground and first excited state. Thus, choosing for the dynamics the FK effective frequency $f = \Omega(x_c(t))$, then in the low temperature limit we have that $f \rightarrow \Omega(x_c^m)$ and the solution to Eq. 3.51 is

$$\begin{aligned}
q_t &= x_c^m + (q - x_c^m) \cos(\Omega(x_c^m)t) + \frac{p}{m\Omega(x_c^m)} \sin(\Omega(x_c^m)t) \\
p_t &= p \cos(\Omega(x_c^m)t) - m\Omega(x_c^m) (q - x_c^m) \sin(\Omega(x_c^m)t), \quad (3.52)
\end{aligned}$$

Therefore, since in the low temperature limit the exact dynamics are dominated by the ground and first excited states, then, similar to CMD[34], this method produces coherent quantum dynamics in this limit when the FK effective frequency is used in the dynamics.

3.5 An additional Feynman-Kleinert Quasi-Classical Wigner method: FK-QCW(2)

The imaginary frequency problem encountered in the dynamics of Sec. IV occurs because the $\Omega_t \alpha_t$ factor in Eq. 3.48 becomes negative for imaginary frequencies. Looking back at how we defined the dimensionless variables, we see that the root of this problem stems from the $\exp\{-(p_t - p_c(t))^2/m\hbar\Omega_t\alpha_t\}$ factor contained within the FK Wigner distribution function in Eq. 3.26, which in addition becomes divergent for imaginary frequencies. However, the FK Wigner distribution function is Gaussian in the centroid momentum, and after integrating this variable out takes the form

$$\begin{aligned}
[e^{-\beta\hat{H}}]_W(q, p) &= \int dx_c \rho_{FK}(x_c) \\
&\times \sqrt{\frac{8\pi m \tanh(\frac{\beta\hbar\Omega_0}{2})}{\beta\alpha_0}} \tilde{\rho}(x_c, q, p), \quad (3.53)
\end{aligned}$$

where we have defined

$$\rho_{FK}(x_c) \equiv \frac{1}{2\pi\hbar} \exp\{-\beta W_1(x_c)\} \quad (3.54)$$

and

$$\begin{aligned} \tilde{\rho}(x_c, q, p) &\equiv \exp \left\{ -\frac{m\Omega_0}{\hbar\alpha_0} (q - x_c)^2 \right\} \\ &\times \exp \left\{ -\frac{\tanh(\frac{\beta\hbar\Omega_0}{2})}{m\hbar\Omega_0} p^2 \right\}. \end{aligned} \quad (3.55)$$

One can show that this form is well defined for imaginary frequencies so long as $|\Omega_0| < \pi/\hbar\beta$.

As we now show, we are able to use this form to find another class of ensemble conserving dynamics that are well defined for this range of imaginary frequencies. This is accomplished by multiplying Eq. 3.53 by

$$1 = \sqrt{\frac{\beta}{2\pi m}} \int dp_c \exp \left\{ \frac{-\beta p_c^2}{2m} \right\}, \quad (3.56)$$

after which we obtain

$$\begin{aligned} [e^{-\beta\hat{H}}]_W(q, p) &= \int dx_c dp_c \rho_{FK}(x_c, p_c) \\ &\times \sqrt{\frac{4 \tanh(\frac{\beta\hbar\Omega_0}{2})}{\alpha_0}} \tilde{\rho}(x_c, q, p). \end{aligned} \quad (3.57)$$

Thus after making a dummy variable substitution in this expression by changing the integration variables from $(x_c, p_c) \rightarrow (x_c(t), p_c(t))$, we have that this function evaluated at a point (q_t, p_t) becomes

$$\begin{aligned} [e^{-\beta\hat{H}}]_W(q_t, p_t) &= \int dx_c(t) dp_c(t) \rho_{FK}(x_c(t), p_c(t)) \\ &\times \sqrt{\frac{4 \tanh(\frac{\beta\hbar\Omega_t}{2})}{\alpha_t}} \tilde{\rho}(x_c(t), q_t, p_t). \end{aligned} \quad (3.58)$$

Furthermore, since we have made the full centroid distribution function reappear in this expression, we can use Liouville's theorem such that

$$\begin{aligned}
[e^{-\beta\hat{H}}]_W(q_t, p_t) &= \int dx_c dp_c \rho_{FK}(x_c, p_c) \\
&\times \sqrt{\frac{4 \tanh(\frac{\beta\hbar\Omega_t}{2})}{\alpha_t}} \tilde{\rho}(x_c(t), q_t, p_t).
\end{aligned} \tag{3.59}$$

Therefore, using Eqs. 3.59 and 3.57 we have that in order for

$$dq_t dp_t [e^{-\beta\hat{H}}]_W(q_t, p_t) = dq dp [e^{-\beta\hat{H}}]_W(q, p) \tag{3.60}$$

such that the ensemble is conserved, the dynamics must fulfil

$$\begin{aligned}
&\int dx_c dp_c \rho_{FK}(x_c, p_c) \\
&\times \left(dq_t dp_t \sqrt{\frac{4 \tanh(\frac{\beta\hbar\Omega_t}{2})}{\alpha_t}} \tilde{\rho}(x_c(t), q_t, p_t) \right. \\
&\left. - dq dp \sqrt{\frac{4 \tanh(\frac{\beta\hbar\Omega_0}{2})}{\alpha_0}} \tilde{\rho}(x_c, q, p) \right) = 0
\end{aligned} \tag{3.61}$$

which, after using Eq. 3.30, can be satisfied by requiring

$$\begin{aligned}
&\det(J(t)) \sqrt{\frac{\tanh(\frac{\beta\hbar\Omega_t}{2})}{\alpha_t}} \tilde{\rho}(x_c(t), q_t, p_t) \\
&= \sqrt{\frac{\tanh(\frac{\beta\hbar\Omega_0}{2})}{\alpha_0}} \tilde{\rho}(x_c, q, p).
\end{aligned} \tag{3.62}$$

However, similar to our previous analysis in Sec. IV, this condition for the dynamics to conserve the ensemble can be greatly simplified by working in the new dimensionless coordinates defined as

$$\begin{aligned}
\tilde{q}(t) &\equiv \sqrt{\frac{m\Omega_t}{\hbar\alpha_t}} (q_t - x_c(t)) \\
\tilde{p}(t) &\equiv \sqrt{\frac{\tanh(\frac{\beta\hbar\Omega_t}{2})}{m\hbar\Omega_t}} p_t,
\end{aligned} \tag{3.63}$$

in which

$$\tilde{\rho}(x_c(t), q_t, p_t) \equiv \tilde{\rho}(\tilde{q}(t), \tilde{p}(t)) = \exp(-\tilde{q}(t)^2 - \tilde{p}(t)^2). \tag{3.64}$$

Furthermore, one can show, by using an argument similar to that in Appendix E, that the determinant of the Jacobian matrix in terms of these new dimensionless coordinates takes the form

$$\det(J(t)) = \exp\left(\int_0^t \frac{\partial \dot{\tilde{q}}(t)}{\partial \tilde{q}(t)} + \frac{\partial \dot{\tilde{p}}(t)}{\partial \tilde{p}(t)} dt\right) \sqrt{\frac{\alpha_t \tanh(\frac{\beta\hbar\Omega_0}{2})}{\alpha_0 \tanh(\frac{\beta\hbar\Omega_t}{2})}} \tag{3.65}$$

Therefore, using these relations in Eq. 3.62, we have that the ensemble will be conserved as long as these new dynamics fulfil

$$\begin{aligned}
&\exp\left(\int_0^t \frac{\partial \dot{\tilde{q}}(t)}{\partial \tilde{q}(t)} + \frac{\partial \dot{\tilde{p}}(t)}{\partial \tilde{p}(t)} dt\right) \exp(-\tilde{q}(t)^2 - \tilde{p}(t)^2) \\
&= \exp(-\tilde{q}(0)^2 - \tilde{p}(0)^2),
\end{aligned} \tag{3.66}$$

which we recognize is the same condition as Eq. 3.36, only now written in terms of these new dimensionless variables. Therefore, as long as these new dynamics simultaneously fulfil

$$\tilde{q}(t) \dot{\tilde{q}}(t) + \tilde{p}(t) \dot{\tilde{p}}(t) = 0 \tag{3.67}$$

and

$$\frac{\partial \dot{\tilde{q}}(t)}{\partial \tilde{q}(t)} + \frac{\partial \dot{\tilde{p}}(t)}{\partial \tilde{p}(t)} = 0, \tag{3.68}$$

the ensemble will be conserved.

Thus, after assuming the same harmonic like form of $\dot{\tilde{q}}(t)$ as in Sec. IV, one can show that these two conditions determine these new dynamics as

$$\begin{aligned}\dot{\tilde{q}}(t) &= f(x_c(t)) \tilde{p}(t) \\ \dot{\tilde{p}}(t) &= -f(x_c(t)) \tilde{q}(t),\end{aligned}\tag{3.69}$$

where now $\tilde{q}(t)$ and $\tilde{p}(t)$ are given by Eq. 3.63. Furthermore, by using Eq. 3.63 these new dynamics can be written explicitly in terms of the quantum phase space variables as

$$\begin{aligned}\dot{q}_t &= \dot{x}_c(t) + \frac{f\sqrt{\alpha_t \tanh(\frac{\beta\hbar\Omega_t}{2})}}{m\Omega_t} p_t - \frac{1}{2} \frac{d}{dt} \ln\left(\frac{\Omega_t}{\alpha_t}\right) (q_t - x_c(t)) \\ \dot{p}_t &= -\frac{fm\Omega_t}{\sqrt{\alpha_t \tanh(\frac{\beta\hbar\Omega_t}{2})}} (q_t - x_c(t)) \\ &\quad - \frac{1}{2} \frac{d}{dt} \ln\left(\frac{\tanh(\frac{\beta\hbar\Omega_t}{2})}{\Omega_t}\right) p_t.\end{aligned}\tag{3.70}$$

from which one can verify that the determinant of the Jacobian matrix is given by

$$\det(J(t)) = \sqrt{\frac{\alpha_t \tanh(\frac{\beta\hbar\Omega_0}{2})}{\alpha_0 \tanh(\frac{\beta\hbar\Omega_t}{2})}}.\tag{3.71}$$

Thus we have found another class of dynamics which conserve the ensemble, and can be used within the CW approximation of the quantum time correlation function. Furthermore, the direct propagation of the (q_t, p_t) variables is also not necessary for this new class of dynamics since the instantaneous quantum phase space variables can be obtained through

$$\begin{aligned}
q_t &= \sqrt{\frac{\hbar\alpha_t}{m\Omega_t}} \tilde{q}(t) + x_c(t) \\
p_t &= \sqrt{\frac{m\hbar\Omega_t}{\tanh(\frac{\beta\hbar\Omega_t}{2})}} \tilde{p}(t).
\end{aligned}
\tag{3.72}$$

In addition, one can show from this relation that p_t is real as long as $|\Omega_t| < \pi/\hbar\beta$ and we are therefore able to use these dynamics in the presence of barriers. Furthermore, by adopting the same convention as FK-LPI[2] in which we set $p_t = 0$ for frequencies outside of this range, we are able to apply this method for imaginary frequencies so long as $|\Omega_t| < 2\pi/\hbar\beta$, which is the entire range where the FK approximation to the density operator is well defined. Thus this new class of dynamics allow us to handle imaginary frequencies in a robust way. Similar to the dynamics in Sec. IV, the multi-dimensional generalization of this method is relatively straightforward since it only amounts to propagating the dimensionless coordinates written in terms of the mass-weighted normal mode coordinates defined in Ref. [2] through the dynamics in Eq. 3.69.

3.5.1 Harmonic limit

In general, there does not exist a frequency function, $f(x_c(t))$, such that we are able to recover the harmonic limit exactly for these dynamics. This hindrance can be traced back to the way we defined $\tilde{p}(t)$, in which $p_c(t)$ is absent. However, if one chooses for the frequency function the FK effective frequency $f = \Omega_t$, then one can show that in the harmonic limit these dynamics used within the CW approximation gives for the position autocorrelation

function

$$\begin{aligned} \langle \hat{x}(0)\hat{x}(t) \rangle &= \frac{\hbar}{2m\Omega} \left[\coth\left(\frac{\beta\hbar\Omega}{2}\right) \cos(\Omega t) \right. \\ &\quad \left. + i\sqrt{\alpha \tanh\left(\frac{\beta\hbar\Omega}{2}\right)} \sin(\Omega t) \right], \end{aligned} \quad (3.73)$$

while the exact expression is

$$\langle \hat{x}(0)\hat{x}(t) \rangle_{exact} = \frac{\hbar}{2m\Omega} \left[\coth\left(\frac{\beta\hbar\Omega}{2}\right) \cos(\Omega t) + i \sin(\Omega t) \right]. \quad (3.74)$$

Thus one sees that these dynamics correctly reproduce the real part of the position autocorrelation function, but not the imaginary part. In addition, one can show that

$$\lim_{T \rightarrow 0} \alpha \tanh\left(\frac{\beta\hbar\Omega}{2}\right) = 1 \quad (3.75)$$

and

$$\lim_{T \rightarrow \infty} \alpha \tanh\left(\frac{\beta\hbar\Omega}{2}\right) = 0 \quad (3.76)$$

such that Eq. 3.73 reduces to the exact expression in both the high and low temperature limits.

3.5.2 Classical and high temperature limits

Using an argument similar to that presented in Sec. IV B, one can show that this entire class of dynamics produces the correct classical and high temperature limits of the quantum time correlation function for position dependent operators when used within the CW approximation.

3.5.3 Low temperature limit

For low temperatures, the dynamics in Eq. 3.69 with $f = \Omega(x_c(t))$ reduce to the same low temperature limit of Eq. 3.52 in Sec. IV C. Thus it follows that when the FK effective frequency is used in the dynamics of Eq. 3.69, one also obtains coherent quantum dynamics in the low temperature limit that approximate the exact dynamics.

3.6 Application to model problems

As we have shown, the CW approximation in Eq. 3.3 evaluated with the dynamics of Secs. IV and V, which we term FK-QCW(1) and FK-QCW(2) respectively, is able to recover the exact classical and high temperature limits of the quantum time correlation function. In addition, the FK-QCW(1) method is able to recover the exact harmonic limit when the function $f = \Omega_t$ is used in the dynamics. To find out how well these dynamics perform outside of these limits, we compute the quantum time correlation function of two challenging systems, the quartic potential and the double-well potential, in which quantum coherence effects are very important. However, since the CW approximation in Eq. 3.3 lacks the phase information necessary to capture these effects, the main goal of studying these model problems is to see how FK-QCW(1) and FK-QCW(2) compare to exact results and other approximate methods over relatively short times. This is because ultimately we would like to apply these

dynamics to realistic condensed phase systems, in which the coupling to the many degrees of freedom quenches long time quantum coherence effects[2, 25], and the behavior of the correlation function over relatively short times is most important. To this end, we compute both linear and non-linear correlation functions for these two model systems using FK-QCW(1) and FK-QCW(2) and then provide a comparison to the exact results, as well as to those obtained by RPMD, CMD, and FK-LPI. It should be noted that the results we present here can also be compared with those previously obtained by Jang and Voth[15], Craig and Manolopoulos[26], and Liu[24].

In all of the following simulations, we have used natural units in which $m = \hbar = k_B = 1$. The quantum time correlation function was evaluated using the FK-QCW(1) and FK-QCW(2) methods by performing a molecular dynamics simulation of the centroid variables, which are propagated according to Eq. 3.24. For each centroid trajectory, 100 $(\tilde{q}(0), \tilde{p}(0))$ values were sampled according to the gaussian distribution $\exp(-\tilde{q}(0)^2 - \tilde{p}(0)^2)$. For FK-QCW(1) (FK-QCW(2)), these dimensionless coordinates were then propagated through Eq. 3.45 (Eq. 3.69) and then by using Eq. 3.48 (Eq. 3.72) the instantaneous (q_t, p_t) values were obtained. For all of the time correlation functions presented in this section, we constructed the CW approximation of $\langle \hat{A}(0)\hat{B}(t) \rangle$ in Eq. 3.3 by averaging over 50,000 consecutive centroid trajectories, in which the centroid momentum was resampled at the beginning of each trajectory and a time step of .005 was used. To illustrate the applicability of multiple sets of dynamics, we have performed the simulations using two different frequency

functions:

$$f_1 = \Omega_t \tag{3.77}$$

and

$$f_2 = \frac{\Omega_t}{\sqrt{\alpha_t \tanh(\frac{\beta \hbar \Omega_t}{2})}}, \tag{3.78}$$

where f_2 is a temperature dependent effective frequency such that $f_2 \geq \Omega_t$, and the equality is met in the limit that $T \rightarrow 0$.

The evaluation of CMD using the FK approximation of the density operator was accomplished by also performing a molecular dynamics simulation of the centroid variables in which the centroid momentum was resampled at the beginning of each trajectory and a time step of .005 was used. The Kubo transformed time correlation function was constructed by averaging over 50,000 consecutive centroid trajectories. For the implementation of RPMD, a molecular dynamics simulation in the extended ring-polymer phase space was performed in which we used $n = 48$ beads. At the beginning of each trajectory the momentum was resampled from the Boltzmann distribution at an inverse temperature of β/n , and a time step of .005 was used. The Kubo transformed time correlation function was also constructed by averaging over 50,000 consecutive trajectories. For both RPMD and CMD, the standard time correlation function was obtained from the Kubo transformed quantity by inverse Fourier transforming the relation in Eq. F.2.

3.6.1 The double-well potential

The first model system is the double-well potential in which

$$V(x) = -\frac{1}{2}x^2 + \frac{1}{10}x^4. \quad (3.79)$$

This system presents a very challenging case due to the presence of a barrier, the maximum of the barrier being located at $x = 0$. For imaginary frequencies encountered within FK-QCW(1), we used the convention to set $p_t = p_c(t)$. For imaginary frequencies $|\Omega| \geq \pi/\hbar\beta$ encountered within FK-QCW(2) we set $p_t = 0$ which is the limiting value for $|\Omega_t| \rightarrow \pi/\hbar\beta$ in Eq. 3.72.

In Fig. 3.1 we present a representative trajectory that really shows the differences between these new ensemble conserving dynamics and the classical dynamics used within the normal CW approximation. As seen, the coupling of the quantum phase space to the time evolved centroid through the dynamics in Eqs. 3.45 and 3.69 results in relative motion about the centroid. Furthermore, one sees that when the initial momentum is not enough to make it over the barrier for the classical dynamics, a particle undergoing relative motion about the centroid is essentially pulled over the barrier by the centroid, which evolves on a smeared potential.

As seen in Fig. 3.2, for $\langle \hat{x}(0)\hat{x}(t) \rangle$ at $\beta = 8$ the exact dynamics exhibit significant coherent tunneling and none of the approximate methods are able to reproduce this behavior since they all show significant dephasing. While FK-QCW(1) and FK-QCW(2) give results comparable to RPMD, FK-CMD penetrates the potential barrier the deepest. However, as we show in Appendix

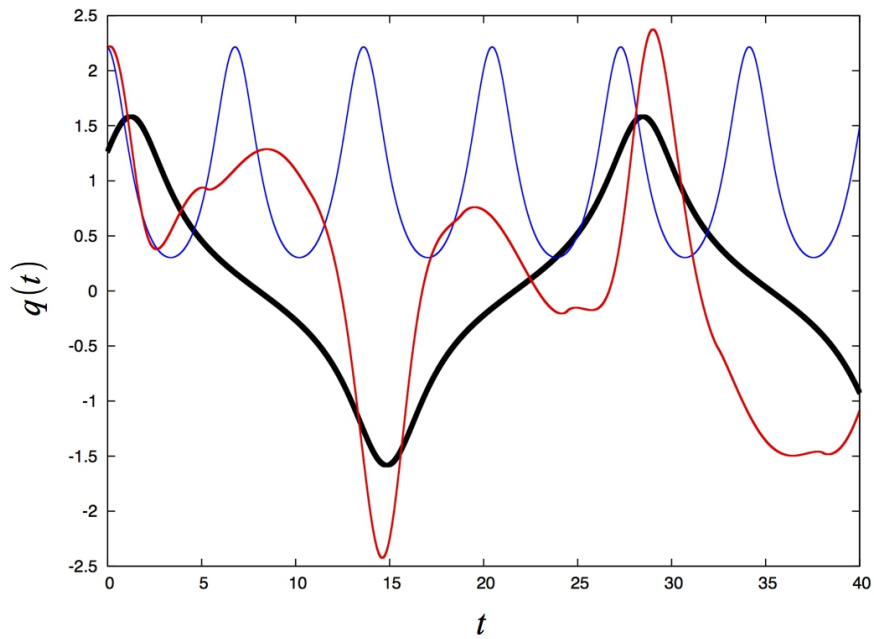


Figure 3.1: A representative trajectory for the double well potential in Eq. 3.79 for $\beta = 8$. Black line: $x_c(t)$; Blue line: q_t from FK-LPI; Red line: q_t from FK-QCW(2) ($f = \Omega_t$). Both the FK-LPI and FK-QCW(2) dynamics were propagated from the same initial conditions.

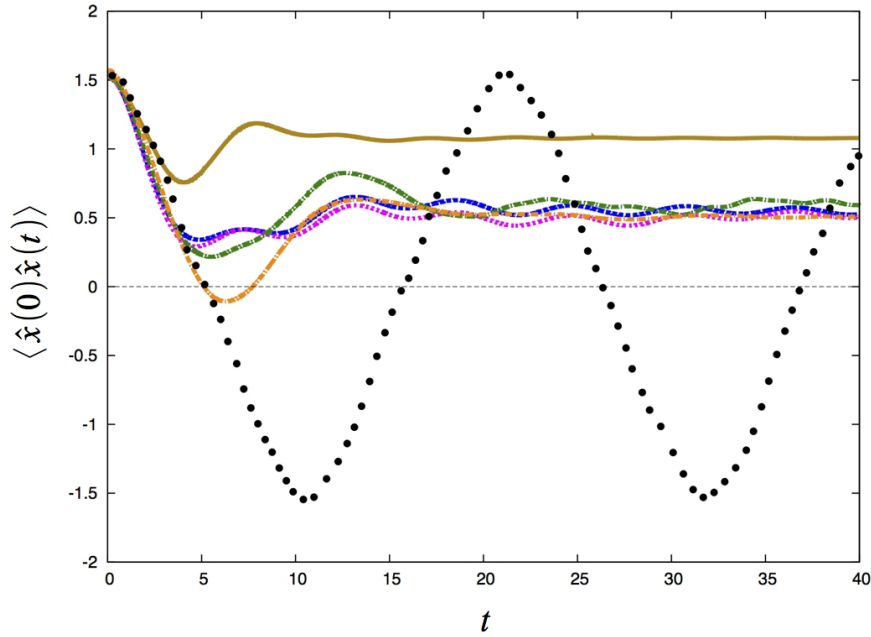


Figure 3.2: The real part of the autocorrelation function for the double well potential in Eq. 3.79 for $\beta = 8$. Black points: exact; Green dot-dashed line: RPMD; Orange dot-dashed line: FK-CMD; Gold line: FK-LPI; Blue dashed line: FK-QCW(1) ($f = \Omega_t$); Magenta dashed line: FK-QCW(2) ($f = \Omega_t$). The exact results were taken from Ref. [15].

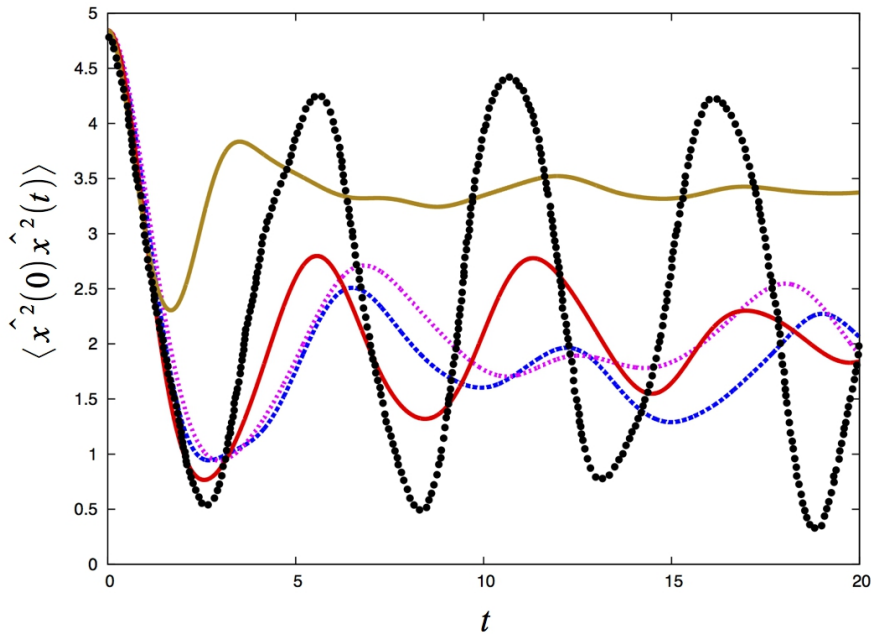


Figure 3.3: The real part of the autocorrelation function for the double well potential in Eq. 3.79 for $\beta = 8$. Black points: exact; Gold line: FK-LPI; Blue dashed line: FK-QCW(1) ($f = \Omega_t$); Magenta dashed line: FK-QCW(2) ($f = \Omega_t$); Red line: FK-QCW(2) with f given by Eq. 3.78. The exact results were taken from Ref. [24].

F, the entire class of dynamics in FK-QCW(1) reduces to FK-CMD when used in the expression for the Kubo transformed time correlation function for linear operators. This then suggests that there exist an advantage in obtaining the standard correlation function from the Kubo transformed version when possible (e.g linear operators). In comparing FK-QCW(1) and FK-QCW(2) to FK-LPI, one sees that even in this challenging case where none of the approximate methods are able to correctly produce the behavior of the exact correlation function except at very short times, the ensemble conserving dynamics used within these two new methods extends the accuracy of the CW approximation to significantly longer times.

Shown in Fig. 3.3 are the results for $\langle \hat{x}^2(0)\hat{x}^2(t) \rangle$ at $\beta = 8$. Due to the non-linear operators, we did not apply RPMD or FK-CMD for this correlation function. As seen, the use of $f_1 = \Omega_t$ is able to produce somewhat coherent oscillations which agree at least qualitatively with the exact results. However, the use of f_2 in Eq. 3.78 results in a slightly higher frequency in the correlation function that is closer to the exact. Once again, in comparison to FK-LPI, it is evident that these new dynamics extends the accuracy of the CW approximation.

3.6.2 The quartic potential

The next model system we look at is the quartic potential in which the potential energy takes the form

$$V(x) = \frac{1}{4}x^4. \tag{3.80}$$

This model system presents a challenging test case due to the lack of a harmonic term. The results for $\langle \hat{x}(0)\hat{x}(t) \rangle$ at $\beta = 8$ are shown in Fig. 3.4. As seen, both FK-QCW(1) and FK-QCW(2) give essentially the same results for the linear correlation function. Furthermore, both of these methods are able to maintain coherent oscillations longer than RPMD, which in comparison shows significant dephasing. Out of all of the approximate methods employed, FK-CMD seems to maintain coherent oscillations the longest for this correlation function. This again suggest that there is an advantage in working with the Kubo transformed correlation function, since FK-QCW(1) and FK-CMD are equivalent for this quantity. In comparison to FK-LPI, which is almost completely quenched after the first oscillation, it is evident that these new ensemble conserving dynamics extends the accuracy of the CW approximation to much longer times.

Presented in Fig. 3.5 is $\langle \hat{x}^2(0)\hat{x}^2(t) \rangle$ at $\beta = 8$. Once again, due to the failure of RPMD and CMD for non-linear operators, neither of these methods were applied for this correlation function. One notices in Fig. 3.5 that the use of $f_1 = \Omega_t$ in FK-QCW(1) and FK-QCW(2) results in a slight frequency shift as compared to the exact correlation function, while, similar to the results in Fig. 3.3, the use of f_2 in Eq. 3.78 results in a slightly higher frequency which seems to corrects this. Furthermore, while FK-QCW(1), FK-QCW(2), and FK-LPI are all very accurate for short times, once again, the ensemble conserving dynamics used in FK-QCW(1) and FK-QCW(2) maintains coherent oscillations much longer than FK-LPI, which suffers from strong dephasing.

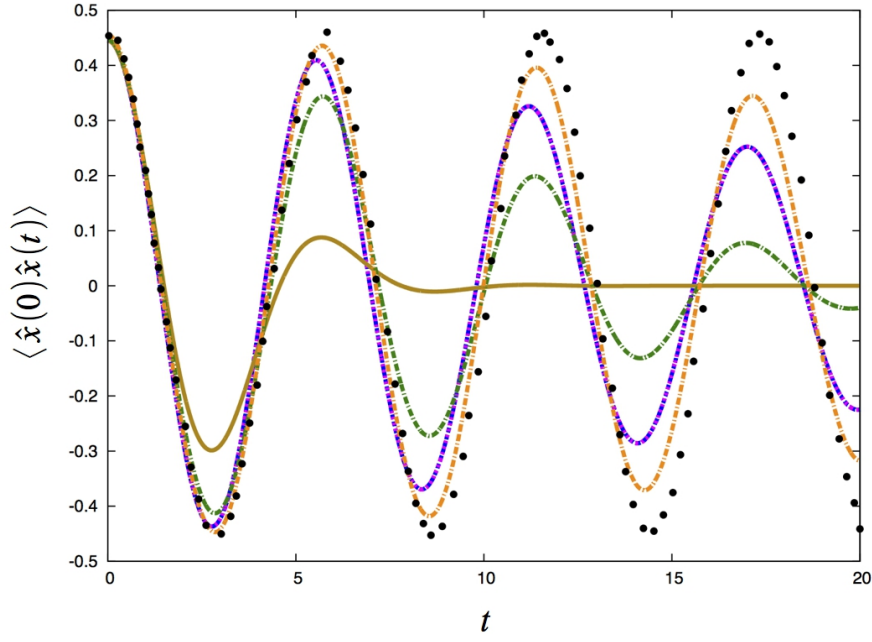


Figure 3.4: The real part of the autocorrelation function for the quartic potential in Eq. 3.80 for $\beta = 8$. Black points: exact; Green dot-dashed line: RPMD; Orange dot-dashed line: FK-CMD; Gold line: FK-LPI; Blue dashed line: FK-QCW(1) ($f = \Omega_t$); Magenta dashed line: FK-QCW(2) ($f = \Omega_t$). The exact results were taken from Ref. [15].

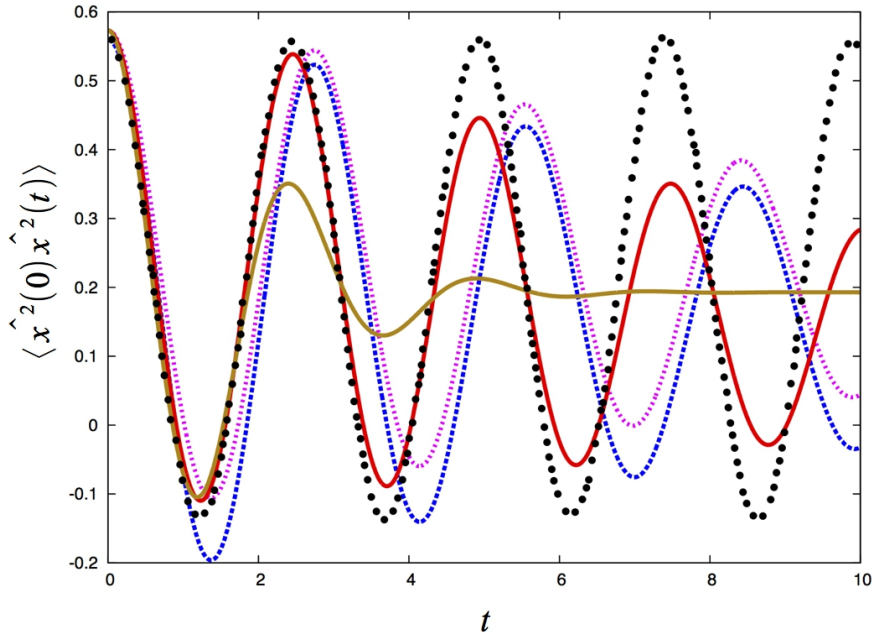


Figure 3.5: The real part of the autocorrelation function for the quartic potential in Eq. 3.80 for $\beta = 8$. Black points: exact; Gold line: FK-LPI; Blue dashed line: FK-QCW(1) ($f = \Omega_t$); Magenta dashed line: FK-QCW(2) ($f = \Omega_t$); Red line: FK-QCW(2) with f given by Eq. 3.78. The exact results were taken from Ref. [24].

3.7 Conclusions

We have developed two classes of quasi-classical dynamics that have been shown to conserve the initial quantum ensemble. When used within the CW approximation of the quantum time correlation function, both classes produce the exact classical and high temperature limits, and one set produces the exact harmonic limit (FK-QCW(1) with $f = \Omega_t$). Although FK-QCW(1) and FK-QCW(2) were shown to fail at capturing the long time quantum coherence effects for the model potentials studied, overall, these dynamics maintain coherent oscillations much longer than the classical dynamics implemented within FK-LPI and therefore significantly extend the accuracy of the CW approximation. Furthermore, the fact that these new dynamics fails in this regard is not surprising since they lack the phase information necessary to capture these effects. However, this does not in general present a problem for realistic condensed phase systems, since the coupling to the many degrees of freedom acts as a bath that quenches quantum coherence effects[2, 25].

The fact that these new dynamics were shown to be comparable to both RPMD and CMD suggests that they provide a potentially more appealing algorithm than these methods, since one is not limited to correlation functions involving linear operators. In addition, one will not encounter artificial frequencies when using FK-QCW(1) or FK-QCW(2) to simulate absorption spectra, as compared to RPMD[32]. Furthermore, the practical application of these two new methods to realistic condensed phase systems is not out of reach since they present only a minimum amount of additional computational

load as compared to FK-LPI. This potential will be realized in a forthcoming paper (chapter) in which we present the multidimensional generalization of these dynamics and apply FK-QCW(2) for the determination of the dynamic structure factor in low temperature liquid para-hydrogen and ortho-deuterium and compare the results with those presented in Ref. [1] (Ch.2).

Chapter 4

Application of a New Ensemble Conserving Quantum Dynamics Simulation Algorithm to Liquid para-Hydrogen and ortho-Deuterium

4.1 Introduction

Low-temperature liquid para-hydrogen and ortho-deuterium have become a standard benchmark in the development of approximate quantum dynamics methods[1, 3, 14, 21, 27, 29, 35] which allow for the practical evaluation of a general quantum time correlation function of the form

$$\langle \hat{A}(0)\hat{B}(t) \rangle = \frac{1}{Z} Tr \left(e^{-\beta\hat{H}} \hat{A} e^{i\hat{H}t/\hbar} \hat{B} e^{-i\hat{H}t/\hbar} \right), \quad (4.1)$$

Z being the partition function and β the inverse temperature $1/k_bT$. The reason that these systems provide such a good testing ground for the development of these methods is because pronounced nuclear quantum effects are exhibited by their dynamical properties. This is due to their low molecular mass, which in turn causes their thermal de Broglie wavelength's to be relatively large at low temperatures. However, these quantum effects are not significant enough that one must worry about the quantum statistics of molecular indistinguishability[33], and in addition there exists a relatively simple pair potential[7], which provides a very accurate description of their molecular interactions[7, 36, 37].

Hence, low-temperature liquid para-hydrogen and ortho-deuterium are quantum liquids which are relatively easy to model, thus being an ideal testing ground for the development of novel approximate quantum dynamics methods.

Presently, the most successful approximate quantum dynamics methods are the Classical Wigner approximation (CW)[2, 17, 19], Centroid Molecular Dynamics (CMD) [15], and Ring-Polymer Molecular Dynamics (RPMD)[26]. All of these methods have been shown to provide relatively accurate and practical approximations to Eq. 4.1, and, in addition, to become exact in the harmonic, high temperature and short time limits[2, 15, 19, 20, 26]. However, each of these methods have their own downfalls. For example, CMD and RPMD begin to break down for correlation functions involving non-linear operators[15, 26, 28], while the CW approximation is equally valid for non-linear operators, but, in general, it does not produce time invariant thermodynamic properties for systems at thermal equilibrium. Explicitly, for $\hat{A} = 1$ the exact quantum expression in Eq. 4.1 has the property that

$$\langle \hat{B}(t) \rangle = \langle \hat{B}(0) \rangle, \quad (4.2)$$

while the purely classical propagation of the initially quantized phase space distribution in the CW approximation does not ensure this property. As shown in Ref. [31], this downfall can have a significant impact for slow processes like diffusion due to zero point energy leakage from intramolecular to intermolecular modes as the system is propagated.

Recently, Liu and Miller[20, 22–24] have proposed a route to remedy this downfall of the CW approximation by replacing the classical propagation of the initial quantum phase space distribution with a form of dynamics that ensures the equality in Eq. 4.2. Similarly, we developed in Ch. 3 a different form of dynamics that also ensures this property by requiring the dynamics to conserve the initial quantum ensemble within the Feynman-Kleinert (FK) approximation of the density operator[2, 8, 9].

This Feynman-Kleinert Quasi-Classical Wigner (FK-QCW) method was shown to greatly extend the accuracy of the Feynman-Kleinert implementation of the CW approximation (FK-LPI)[2] in the challenging model problems of both the quartic and double well potentials, in which numerically exact solutions are obtainable. Furthermore, we were able to show that one can introduce an arbitrary frequency function into the dynamics of this method, resulting in an entire class of ensemble conserving dynamics that preserve the equality in Eq. 4.2. The FK-QCW method was shown to recover the exact classical and high temperature limits of the quantum time correlation function, and, in addition, to recover the exact harmonic limit when the FK effective frequency is used within the dynamics. Furthermore, since this method is developed within the framework of the CW approximation, no problems arise for non-linear operators.

The purpose of this work is to test how well the FK-QCW method performs when applied to the standard benchmark systems of low-temperature liquid para-hydrogen and ortho-deuterium. We accomplish this task by com-

puting the dynamic structure factor, which is experimentally accessible by inelastic X-ray scattering (IXS). We then provide a comparison between present calculations and the experimental determinations, as well as with the ones obtained by RPMD and FK-LPI previously published in Ref. [1] (Ch. 2). Specifically, it was found in Ref. [1] (Ch. 2) that for a momentum transfer of $k = 20 \text{ nm}^{-1}$, the FK-LPI method fails to correctly reproduce the IXS spectrum for the para-hydrogen system, in which quantum effects are more prevalent. In addition, due to the increased non-linearity of the correlation function at high momentum transfers, RPMD could not be applied to this specific case. Hence, a challenging test case has been established for the development of improved methods, and it would therefore be interesting to check how the FK-QCW method performs where these leading methods fail.

This chapter is organized as follows: In Section II, we provide an introduction to the classical Wigner (CW) approximation to quantum time correlation functions, as well as the multidimensional generalization of the FK-QCW method. In addition, we also give a brief introduction to the theory of inelastic scattering. In Section III we begin by discussing the computational details of our simulations, followed by a comparison of the FK-QCW method with the the experimental dynamic structure factor and that obtained by RPMD and FK-LPI previously published in Ref. [1] (Ch. 2). The conclusions are presented in Section IV.

4.2 Theory and Methodology

4.2.1 Classical Wigner

The CW[2, 17, 19] expression for a general quantum time correlation function of a many-body system is given by

$$\begin{aligned} \langle \hat{A}(0)\hat{B}(t) \rangle &\approx \frac{1}{Z (2\pi\hbar)^{3N}} \int_{-\infty}^{\infty} d\mathbf{q} d\mathbf{p} [e^{-\beta\hat{H}} \hat{A}]_W(\mathbf{q}, \mathbf{p}) \\ &\quad \times [\hat{B}]_W(\mathbf{q}(t), \mathbf{p}(t)), \end{aligned} \quad (4.3)$$

where $(\mathbf{q}(t), \mathbf{p}(t))$ are the classically evolved quantum phase space variables propagated from the initial quantum distribution (\mathbf{q}, \mathbf{p}) . Here the Wigner transform of a general operator \hat{C} is given by

$$[\hat{C}]_W(\mathbf{q}, \mathbf{p}) \equiv \int_{-\infty}^{\infty} d\boldsymbol{\eta} e^{-i\mathbf{p}\cdot\boldsymbol{\eta}/\hbar} \left\langle \mathbf{q} + \frac{\boldsymbol{\eta}}{2} \left| \hat{C} \right| \mathbf{q} - \frac{\boldsymbol{\eta}}{2} \right\rangle, \quad (4.4)$$

where $|\mathbf{q}\rangle$ is the direct product of the single particle position kets.

Although the CW approximation has been shown to perform relatively well[1–6, 19], as we previously noted, the classical evolution of the quantum phase space results in thermodynamic properties of equilibrium systems being incorrectly time dependent. Our newly developed FK-QCW method corrects this inconsistency by simply replacing the purely classical dynamics used within Eq. 4.3 with a time evolution that ensures that the initial quantum ensemble is conserved such that

$$d\mathbf{q} d\mathbf{p} [e^{-\beta\hat{H}}]_W(\mathbf{q}, \mathbf{p}) = d\mathbf{q}(t) d\mathbf{p}(t) [e^{-\beta\hat{H}}]_W(\mathbf{q}(t), \mathbf{p}(t)), \quad (4.5)$$

from which it follows that $\langle \hat{B}(t) \rangle = \langle \hat{B}(0) \rangle$, in accord with the exact quantum time correlation function. However, since these dynamics were developed within the Feynman-Kleinert (FK) approximation to the density operator[2, 8, 9], before we present their multidimensional generalization, we first provide an introduction to the FK density operator, which allows for a practical evaluation of the Wigner function $[e^{-\beta\hat{H}}\hat{A}]_W(\mathbf{q}, \mathbf{p})$ appearing in Eq. 4.3.

4.2.2 Many-body Feynman-Kleinert density operator

The most difficult part in evaluating the CW expression of Eq. 4.3 is obtaining the Wigner transform of $e^{-\beta\hat{H}}\hat{A}$, since knowledge of the many-body density matrix is required. As in the FK-LPI method, we accomplish this within the FK-QCW method by combining the effective frequency variational theory of Feynman[8] and Kleinert[9] (FK) with the quasidensity operator formalism of Jang and Voth[16]. This Feynman-Kleinert approximation to the density operator allows for an efficient evaluation of the Wigner transform of $e^{-\beta\hat{H}}\hat{A}$ and has been shown to be very accurate when applied to realistic many-body systems[1–6]. In addition, the FK approximation to the density operator gives the best local harmonic approximation to the systems free energy[8, 9] and becomes exact in the harmonic and high temperature limits[2]

For a many-body system, the FK approximation to the density operator is explicitly given by

$$e^{-\beta\hat{H}} \approx \int_{-\infty}^{\infty} d\mathbf{x}_c d\mathbf{p}_c \rho_{FK}(\mathbf{x}_c, \mathbf{p}_c) \hat{\delta}_{FK}(\mathbf{x}_c, \mathbf{p}_c), \quad (4.6)$$

where $\hat{\delta}_{FK}(\mathbf{x}_c, \mathbf{p}_c)$ is the effective frequency quasidensity operator (QDO), and the FK approximation to the centroid phase space density, for a system of N particles, is given by

$$\rho_{FK}(\mathbf{x}_c, \mathbf{p}_c) \equiv \frac{1}{(2\pi\hbar)^{3N}} \exp\left(-\frac{\beta}{2}\mathbf{M}^{-1}\mathbf{p}_c^T\mathbf{p}_c - \beta W_1(\mathbf{x}_c)\right), \quad (4.7)$$

$W_1(\mathbf{x}_c)$ being the FK approximation to the centroid potential. In Eq. 4.7, \mathbf{M} is the diagonal matrix of particle masses and $(\mathbf{x}_c, \mathbf{p}_c)$ are the $3N$ dimensional vectors of centroid positions and momenta, the x , y , and z components of the k^{th} centroid being the $3(k-1)+1$, $3(k-1)+2$, and $3(k-1)+3$ elements, respectively.

The FK variational effective frequency matrix is determined from the local curvature of the systems Gaussian smeared potential by

$$\begin{aligned} \Omega^2(\mathbf{x}_c) &= \frac{1}{\sqrt{(2\pi)^{3N} \det(\mathbf{A}(\mathbf{x}_c))}} \\ &\times \int_{-\infty}^{\infty} d\mathbf{q} \mathbf{M}^{-1/2} \mathbf{H}(\mathbf{q}) \mathbf{M}^{-1/2} \\ &\times \exp\left\{-\frac{1}{2}(\mathbf{q} - \mathbf{x}_c)^T \mathbf{A}^{-1}(\mathbf{x}_c) (\mathbf{q} - \mathbf{x}_c)\right\}, \end{aligned} \quad (4.8)$$

$\mathbf{H}(\mathbf{q})$ being the $3N \times 3N$ classical Hessian matrix and $\mathbf{A}(\mathbf{x}_c)$ the smearing width matrix which measures the importance of quantum fluctuations around the classical-like centroid positions. Defining $\mathbf{U}(\mathbf{x}_c)$ as the orthonormal matrix containing the eigenvectors of the effective frequency matrix, then

$$\mathbf{U}^\dagger(\mathbf{x}_c) \Omega^2(\mathbf{x}_c) \mathbf{U}(\mathbf{x}_c) = \mathbf{I} \boldsymbol{\omega}^2(\mathbf{x}_c) \quad (4.9)$$

where $\boldsymbol{\omega}^2(\mathbf{x}_c)$ is the $3N$ dimensional vector of eigenvalues and I is the identity matrix. Using this, one can define the mass-weighted normal modes as

$$\begin{aligned}
\boldsymbol{\eta} &\equiv \mathbf{U}^\dagger(\mathbf{x}_c) \mathbf{M}^{1/2} \mathbf{q} \\
\boldsymbol{\eta}^c &\equiv \mathbf{U}^\dagger(\mathbf{x}_c) \mathbf{M}^{1/2} \mathbf{x}_c \\
\boldsymbol{\nu} &\equiv \mathbf{U}^\dagger(\mathbf{x}_c) \mathbf{M}^{-1/2} \mathbf{p} \\
\boldsymbol{\nu}^c &\equiv \mathbf{U}^\dagger(\mathbf{x}_c) \mathbf{M}^{-1/2} \mathbf{p}_c,
\end{aligned} \tag{4.10}$$

and the smearing width matrix can be diagonalized through

$$\mathbf{U}^\dagger(\mathbf{x}_c) \mathbf{M}^{1/2} \mathbf{A}(\mathbf{x}_c) \mathbf{M}^{1/2} \mathbf{U}(\mathbf{x}_c) = \boldsymbol{\Lambda}(\mathbf{x}_c), \tag{4.11}$$

where

$$[\boldsymbol{\Lambda}(\mathbf{x}_c)]_{ij} = \delta_{ij} \frac{1}{\beta \omega_i^2(\mathbf{x}_c)} \left[\frac{\beta \hbar \omega_i(\mathbf{x}_c)}{2} \coth \left(\frac{\beta \hbar \omega_i(\mathbf{x}_c)}{2} \right) - 1 \right]. \tag{4.12}$$

In terms of the eigenvalues of the effective frequency matrix, the centroid potential in Eq. 4.7 is explicitly written as

$$\begin{aligned}
W_1(\mathbf{x}_c) &= \frac{1}{\beta} \sum_{i=1}^{3N} \ln \left[\frac{2 \sinh \left(\frac{\beta \hbar \omega_i(\mathbf{x}_c)}{2} \right)}{\beta \hbar \omega_i(\mathbf{x}_c)} \right] + V_{\mathbf{A}}(\mathbf{x}_c) \\
&\quad - \frac{1}{2} \sum_{i=1}^{3N} \Lambda_{ii}(\mathbf{x}_c) \omega_i^2(\mathbf{x}_c),
\end{aligned} \tag{4.13}$$

where

$$\begin{aligned}
V_{\mathbf{A}}(\mathbf{x}_c) &= \frac{1}{\sqrt{(2\pi)^{3N} \det(\mathbf{A}(\mathbf{x}_c))}} \int_{-\infty}^{\infty} d\mathbf{q} V(\mathbf{q}) \\
&\quad \times \exp \left\{ -\frac{1}{2} (\mathbf{q} - \mathbf{x}_c)^T \mathbf{A}^{-1}(\mathbf{x}_c) (\mathbf{q} - \mathbf{x}_c) \right\}
\end{aligned} \tag{4.14}$$

is the FK smeared potential. In $3N$ dimensions, the effective frequency QDO written in terms of the mass-weighted normal modes is simply a direct product of 1-dimensional QDOs and is given by

$$\begin{aligned} \hat{\delta}_{FK}(\mathbf{x}_c, \mathbf{p}_c) &= \prod_{k=1}^{3N} \sqrt{\frac{\omega_k(\mathbf{x}_c)}{\pi \hbar \alpha_k(\mathbf{x}_c)}} \int_{-\infty}^{\infty} d\eta_k d\eta'_k |\eta'_k\rangle \langle \eta_k| \\ &\times \exp \left\{ i \frac{\nu_k^c}{\hbar} (\eta'_k - \eta_k) - \frac{\omega_k(\mathbf{x}_c)}{\hbar \alpha_k(\mathbf{x}_c)} \left(\frac{\eta'_k + \eta_k}{2} - \eta_k^c \right)^2 \right\} \\ &\times \exp \left\{ -\frac{\omega_k(\mathbf{x}_c) \alpha_k(\mathbf{x}_c)}{4\hbar} (\eta'_k - \eta_k)^2 \right\}, \end{aligned} \quad (4.15)$$

with

$$\alpha_k(\mathbf{x}_c) \equiv \coth \left(\frac{\beta \hbar \omega_k(\mathbf{x}_c)}{2} \right) - \frac{2}{\beta \hbar \omega_k(\mathbf{x}_c)}. \quad (4.16)$$

For all but the simplest potentials, determination of the FK effective frequency matrix is the main computational load in applying the FK approximation to the density operator since Eqs. 4.8 and 4.11 must be solved iteratively. For a discussion of efficient ways to determine the FK effective frequency matrix using different numerical schemes, the interested reader is referred to Ref. [5].

Using the FK approximation to the density operator, the Wigner transform of $e^{-\beta \hat{H}} \hat{A}$ becomes

$$\begin{aligned} [e^{-\beta \hat{H}} \hat{A}]_W(\mathbf{q}, \mathbf{p}) &\approx \int_{-\infty}^{\infty} d\mathbf{x}_c d\mathbf{p}_c \rho_{FK}(\mathbf{x}_c, \mathbf{p}_c) \\ &\times [\hat{\delta}_{FK}(\mathbf{x}_c, \mathbf{p}_c) \hat{A}]_W(\mathbf{q}, \mathbf{p}). \end{aligned} \quad (4.17)$$

Due to the Gaussian form of the QDO in Eq. 4.15, an analytical expression for the Wigner transform of $\hat{\delta}_{FK}(\mathbf{x}_c, \mathbf{p}_c)\hat{A}$ is readily obtained for any operator \hat{A} depending only on position or momentum.

4.2.3 FK-QCW in many dimensions

The multi-dimensional generalization of the FK-QCW dynamics derived in Eq. 69 of Ch. 3 simply become

$$\begin{aligned}\dot{\tilde{q}}_k(t) &= f_k(\mathbf{x}_c(t))\tilde{p}_k(t) \\ \dot{\tilde{p}}_k(t) &= -f_k(\mathbf{x}_c(t))\tilde{q}_k(t),\end{aligned}\tag{4.18}$$

where

$$\begin{aligned}\tilde{q}_k(t) &\equiv \sqrt{\frac{\omega_k(\mathbf{x}_c(t))}{\hbar\alpha_k(\mathbf{x}_c(t))}}(\eta_k(t) - \eta_k^c(t)) \\ \tilde{p}_k(t) &\equiv \sqrt{\frac{\tanh\left(\frac{\beta\hbar\omega_k(\mathbf{x}_c(t))}{2}\right)}{\hbar\omega_k(\mathbf{x}_c(t))}}\nu_k(t)\end{aligned}\tag{4.19}$$

are the k^{th} elements of the dimensionless normal mode coordinates $(\tilde{\mathbf{q}}(t), \tilde{\mathbf{p}}(t))$, and $f_k(\mathbf{x}_c(t))$ is an arbitrary frequency function. As shown in Ch. 3, the 1-dimensional version of these dynamics gives the exact real part of the position autocorrelation function in the harmonic limit if the FK effective frequency is chosen for the frequency function. Similarly, one can show that this exact limit is also obtained in the multi-dimensional case if we choose

$$f_k(\mathbf{x}_c(t)) = \omega_k(\mathbf{x}_c(t)).\tag{4.20}$$

In Eq. 4.19, the time evolved normal modes are given by

$$\begin{aligned}
\boldsymbol{\eta}(t) &= \mathbf{U}^\dagger(\mathbf{x}_c(t))\mathbf{M}^{1/2}\mathbf{q}(t) \\
\boldsymbol{\eta}^c(t) &= \mathbf{U}^\dagger(\mathbf{x}_c(t))\mathbf{M}^{1/2}\mathbf{x}_c(t) \\
\boldsymbol{\nu}(t) &= \mathbf{U}^\dagger(\mathbf{x}_c(t))\mathbf{M}^{-1/2}\mathbf{p}(t) \\
\boldsymbol{\nu}^c(t) &= \mathbf{U}^\dagger(\mathbf{x}_c(t))\mathbf{M}^{-1/2}\mathbf{p}_c(t), \tag{4.21}
\end{aligned}$$

where $\mathbf{U}(\mathbf{x}_c(t))$ diagonalizes the the effective frequency matrix evaluated at $\mathbf{x}_c(t)$, and the centroid dynamics are governed by the classical-like equations

$$\dot{\mathbf{x}}_c(t) = \mathbf{M}^{-1}\mathbf{p}_c(t)$$

$$\dot{\mathbf{p}}_c(t) = -\nabla_c[V_{\mathbf{A}}(\mathbf{x}_c(t))]_{\mathbf{A}=\mathbf{A}(\mathbf{x}_c(t))}, \tag{4.22}$$

the gradient with respect to $\mathbf{x}_c(t)$ being taken while holding the smearing width matrix constant.

Once the centroid and dimensionless normal mode coordinates have been propagated through Eqs. 4.18 and 4.22, the instantaneous quantum phase space variables can be obtained from

$$\begin{aligned}
\mathbf{q}(t) &= \mathbf{x}_c(t) + \mathbf{M}^{-1/2}\mathbf{U}(\mathbf{x}_c(t))\tilde{\boldsymbol{\eta}}(t) \\
\mathbf{p}(t) &= \mathbf{M}^{1/2}\mathbf{U}(\mathbf{x}_c(t))\tilde{\boldsymbol{\nu}}(t), \tag{4.23}
\end{aligned}$$

where

$$\begin{aligned}
\tilde{\boldsymbol{\eta}}(t) &\equiv \boldsymbol{\eta}(t) - \boldsymbol{\eta}^c(t) \\
\tilde{\boldsymbol{\nu}}(t) &\equiv \boldsymbol{\nu}(t), \tag{4.24}
\end{aligned}$$

and in terms of the dimensionless normal mode coordinates have the elements

$$\begin{aligned}\tilde{\eta}_k(t) &= \sqrt{\frac{\hbar\alpha_k(\mathbf{x}_c(t))}{\omega_k(\mathbf{x}_c(t))}} \tilde{q}_k(t) \\ \tilde{v}_k(t) &= \sqrt{\frac{\hbar\omega_k(\mathbf{x}_c(t))}{\tanh\left(\frac{\beta\hbar\omega_k(\mathbf{x}_c(t))}{2}\right)}} \tilde{p}_k(t).\end{aligned}\quad (4.25)$$

The FK-QCW approximation to the quantum time correlation function takes the same form as the CW expression in Eq. 4.3

$$\begin{aligned}\langle \hat{A}(0)\hat{B}(t) \rangle &\approx \frac{1}{Z(2\pi\hbar)^{3N}} \int_{-\infty}^{\infty} d\mathbf{q} d\mathbf{p} [e^{-\beta\hat{H}}\hat{A}]_W(\mathbf{q}, \mathbf{p}) \\ &\quad \times [\hat{B}]_W(\mathbf{q}(t), \mathbf{p}(t)).\end{aligned}\quad (4.26)$$

However, within FK-QCW $[e^{-\beta\hat{H}}\hat{A}]_W(\mathbf{q}, \mathbf{p})$ is obtained through Eq. 4.17, and $(\mathbf{q}(t), \mathbf{p}(t))$ are propagated from the initial quantum distribution (\mathbf{q}, \mathbf{p}) using the ensemble conserving dynamics in Eq. 4.18. It should be noted that the Wigner transform of \hat{B} in this expression is easily obtainable when \hat{B} is a function of only position or momentum operators, since in this case one obtains the corresponding classical expression

$$[B(\hat{\mathbf{x}})]_W(\mathbf{q}(t), \mathbf{p}(t)) = B(\mathbf{q}(t)) \quad (4.27)$$

or

$$[B(\hat{\mathbf{p}})]_W(\mathbf{q}(t), \mathbf{p}(t)) = B(\mathbf{p}(t)). \quad (4.28)$$

For completeness, we note that the the multi-dimensional generalization of the dynamics within the FK-QCW method that was derived in Eq. 45 of

Ch. 3 are very similar to Eq. 4.18, the only difference is that $\tilde{p}_k(t)$ in Eq. 4.19 takes the form

$$\tilde{p}_k(t) \equiv \sqrt{\frac{1}{\hbar\omega_k(\mathbf{x}_c(t))\alpha_k(\mathbf{x}_c(t))}} (\nu_k(t) - \nu_k^c(t)), \quad (4.29)$$

and Eq. 4.23 is changed accordingly. As shown in Appendix F, these dynamics reduce to CMD when used within the expression for the Kubo transformed time correlation function and also become exact in the harmonic limit, if one uses Eq. 4.20 for the frequency function. However, they are not very practical when used within Eq. 4.26 for non-linear operators since they are ill-defined when $\omega_k(\mathbf{x}_c(t))$ becomes imaginary. This then makes the FK-QCW dynamics in Eq. 4.18 preferable for condensed phase systems since one can show that these dynamics are well defined in this case so long as $|\omega_k(\mathbf{x}_c(t))| < \pi/\beta\hbar$. In addition, by adopting the same convention as FK-LPI[2] in which we set $\nu_k(t) = 0$ for frequencies outside of this range, we are then able to apply these FK-QCW dynamics for imaginary frequencies so long as $|\omega_k(\mathbf{x}_c(t))| < 2\pi/\hbar\beta$, which is the entire range that the FK approximation to the density operator is well defined.

4.2.4 Inelastic Scattering

The quantum time correlation function we apply the FK-QCW method to in this chapter is the intermediate scattering function given by

$$F(\mathbf{k}, t) = \frac{1}{N} \sum_{i,j=1}^N \langle e^{-i\mathbf{k}\cdot\hat{\mathbf{x}}_i(0)} e^{i\mathbf{k}\cdot\hat{\mathbf{x}}_j(t)} \rangle, \quad (4.30)$$

where $\langle \dots \rangle$ denotes a canonical ensemble average, and $\hat{\mathbf{x}}_i(t)$ is the time-dependent position operator of the i^{th} particle, given in the Heisenberg picture by $\hat{\mathbf{x}}_i(t) = e^{i\hat{H}t/\hbar} \hat{\mathbf{x}}_i e^{-i\hat{H}t/\hbar}$. This correlation function is related to the dynamic structure factor, $S(\mathbf{k}, \omega)$, through

$$S(\mathbf{k}, \omega) = \frac{1}{2\pi} \int_{-\infty}^{\infty} dt e^{-i\omega t} F(\mathbf{k}, t). \quad (4.31)$$

The dynamic structure factor gives the spectrum of density fluctuations and Van Hove[13] showed that within the first Born approximation this quantity is proportional to the inelastic scattering cross-section. Measured by either inelastic neutron or X-ray scattering, the inelastic scattering cross-section measures the probability that a neutron or photon transfers momentum $\hbar\mathbf{k} = \hbar(\mathbf{k}_f - \mathbf{k}_i)$ and energy $\hbar\omega = \hbar(\omega_f - \omega_i)$ to the sample.

The shape of the dynamic structure factor is defined by its n -order spectral moments

$$\langle \omega^n \rangle \equiv \int_{-\infty}^{\infty} d\omega \omega^n S(\mathbf{k}, \omega) = i^{-n} \left[\frac{\partial^n F(\mathbf{k}, t)}{\partial t^n} \right]_{t=0}. \quad (4.32)$$

The comparison between measured and computed values of the spectral moments can be used as a metric to judge the quality of a theoretical simulation. The zeroth moment of the dynamic structure factor is referred to as the static structure factor[11], $S(\mathbf{k})$, which is related to the spatial Fourier transform of the pair distribution function by

$$S(\mathbf{k}) \equiv \langle \omega^0 \rangle = 1 + \int_{-\infty}^{\infty} d^3\mathbf{r} e^{i\mathbf{k}\cdot\mathbf{r}} g(\mathbf{r}). \quad (4.33)$$

The first moment of $S(\mathbf{k}, \omega)$ is of special interest since for a system which interacts through a momentum-independent potential [12], this quantity is exactly given by

$$\langle \omega \rangle \equiv \int_{-\infty}^{\infty} d\omega \omega S(\mathbf{k}, \omega) = \frac{\hbar k^2}{2m}, \quad (4.34)$$

where m is the molecular mass. This relation, in principal valid for monatomic systems, can be extended to molecular ones provided the rotational and vibrational motions of the molecule can be neglected in the probed dynamic range.

Since the dynamic structure factor is related to the temporal Fourier transform of a quantum time correlation function, it obeys the principle of detailed balance

$$S(\mathbf{k}, \omega) = e^{\beta \hbar \omega} S(\mathbf{k}, -\omega), \quad (4.35)$$

which is straightforward to show by working in the basis of energy eigenstates. Using this principle of detailed balance along with the symmetry of Eq. 4.30, $F(\mathbf{k}, t) = F(\mathbf{k}, -t)^*$, one can show that the dynamic structure factor can be equivalently written using only the real part of the intermediate scattering function as

$$S(\mathbf{k}, \omega) = \frac{2}{1 + e^{-\beta \hbar \omega}} \frac{1}{2\pi} \int_{-\infty}^{\infty} dt e^{-i\omega t} \text{Re}[F(\mathbf{k}, t)]. \quad (4.36)$$

For an isotropic system such as a liquid, the intermediate scattering function depends only on the magnitude of \mathbf{k} , such that $F(\mathbf{k}, t) = F(k, t)$. Hence when computing the intermediate scattering function of an isotropic system, we are free to choose the direction of \mathbf{k} .

The FK-QCW approximation to the intermediate scattering function takes the form

$$F(\mathbf{k}, t) \approx \frac{1}{Z(2\pi\hbar)^{3N}} \frac{1}{N} \sum_{i,j=1}^N \int_{-\infty}^{\infty} d\mathbf{q} d\mathbf{p} \times [e^{-\beta\hat{H}} e^{-i\mathbf{k}\cdot\hat{\mathbf{x}}_i}]_W(\mathbf{q}, \mathbf{p}) [e^{i\mathbf{k}\cdot\hat{\mathbf{x}}_j}]_W(\mathbf{q}(t), \mathbf{p}(t)), \quad (4.37)$$

where, after choosing \mathbf{k} to be parallel to the x-axis,

$$[e^{i\mathbf{k}\cdot\hat{\mathbf{x}}_j}]_W(\mathbf{q}(t), \mathbf{p}(t)) = \exp\left(i k q_{3(j-1)+1}^{(t)}\right), \quad (4.38)$$

and in terms of the FK approximation to the density operator,

$$\begin{aligned} [e^{-\beta\hat{H}} e^{-i\mathbf{k}\cdot\hat{\mathbf{x}}_i}]_W(\mathbf{q}, \mathbf{p}) &= \int_{-\infty}^{\infty} d\mathbf{x}_c \rho_{FK}(\mathbf{x}_c) \\ &\times \exp(-i k q_{3(i-1)+1}) \prod_{n=1}^{3N} \sqrt{\frac{8\pi m_n \tanh\left(\frac{\beta\hbar\omega_n(\mathbf{x}_c)}{2}\right)}{\beta\alpha_n(\mathbf{x}_c)}} \\ &\times \exp\{-\tilde{q}_n^2 - \tilde{p}_n^2\} \\ &\times \exp\left\{\frac{\tanh\left(\frac{\beta\hbar\omega_n(\mathbf{x}_c)}{2}\right)}{\omega_n(\mathbf{x}_c)} k m_j^{-1/2} U(\mathbf{x}_c)_{3(j-1)+1,n} \nu_n\right\} \\ &\times \exp\left\{-\frac{\hbar \tanh\left(\frac{\beta\hbar\omega_n(\mathbf{x}_c)}{2}\right)}{4\omega_n(\mathbf{x}_c)} \left(k m_j^{-1/2} U(\mathbf{x}_c)_{3(j-1)+1,n}\right)^2\right\}, \end{aligned} \quad (4.39)$$

where

$$\rho_{FK}(\mathbf{x}_c) \equiv \frac{1}{(2\pi\hbar)^{3N}} \exp(-\beta W_1(\mathbf{x}_c)). \quad (4.40)$$

We note that the derivation of Eq. 4.39 is shown in Ref. [4] (see Appendix A therein), where it was derived for FK-LPI, which uses the same FK approximation to the density operator in Eq. 4.6.

4.3 Results

4.3.1 Computational Details

To obtain the dynamic structure factor for liquid para-hydrogen and ortho-deuterium at the state points ($T = 20.0\text{ K}, n = 21.24\text{ nm}^{-3}$) and ($T = 23.0\text{ K}, n = 24.61\text{ nm}^{-3}$) respectively, the FK-QCW approximation to the intermediate scattering function in Eq. 4.37 was evaluated by using the Silver-Goldman (SG) potential[7]. The SG potential has been used in a number of previous studies[14, 20, 21, 27, 29, 35] and has been shown to provide very accurate descriptions of the fluid and solid thermodynamics, except at extremely high pressure[36, 37]. This semi-empirical isotropic pair potential, applicable to both para-hydrogen and ortho-deuterium, treats each molecule as a spherical particle which is justifiable at low temperatures since only the $J=0$ rotational state is populated in each isotope. To expedite the determination of the FK centroid potential we represented the SG potential as a sum over four Gaussian functions whose parameters can be found in Table II of Ref. [3].

Starting from an equilibrated centroid configuration, the real part of the intermediate scattering function was evaluated using the FK-QCW approximation by performing a molecular dynamics simulation of the centroid variables, which are propagated according to Eq. 4.22. For each centroid trajectory, 100 sets of initial dimensionless normal mode coordinates ($\tilde{\mathbf{q}}(0), \tilde{\mathbf{p}}(0)$) were sampled according to their Gaussian distribution

$$\exp(-\tilde{\mathbf{q}}^T(0)\tilde{\mathbf{q}}(0) - \tilde{\mathbf{p}}^T(0)\tilde{\mathbf{p}}(0)) = \prod_{n=1}^{3N} \exp\{-\tilde{q}_n^2 - \tilde{p}_n^2\}, \quad (4.41)$$

which appears in the FK approximation of $[e^{-\beta\hat{H}}\hat{A}]_W(\mathbf{q}, \mathbf{p})$ (see for example Eq. 4.39). Using the the frequency function in Eq. 4.20, the dimensionless normal mode coordinates were then propagated through Eq. 4.18 and the instantaneous $(\mathbf{q}(t), \mathbf{p}(t))$ values were obtained from the relations in Eq. 4.23. The real part of the intermediate scattering function was constructed by averaging over 1,000 consecutive 3 *ps* centroid trajectories, in which the centroid momentum was resampled at the beginning of each trajectory and a time step of 1 *fs* was used. In order to obtain statistical uncertainties, this entire process was repeated six times. For an exact outline of the algorithm used for the integration of the centroid and dimensionless normal mode coordinates over one time step Δt , which allows for the propagation of $(\mathbf{q}(t), \mathbf{p}(t)) \rightarrow (\mathbf{q}(t + \Delta t), \mathbf{p}(t + \Delta t))$, the interested reader is referred to Appendix G.

Within the simulation, we employed cubic periodic boundary conditions with the minimum image convention and a spherical cutoff at half box length. Furthermore, due to the isotropic nature of the SG potential, the momentum transfer \mathbf{k} was chosen, without loss of generality, to be in the x -direction. In order to fulfill the Laue condition [10] $k = 2\pi n/l$, where l is the length of the simulation cell and n is an integer, the number of particles N treated in the simulation had to be varied for each momentum transfer. These, as well as the simulation box size used, for each k are listed in Table. I.

The dynamic structure factor was obtained from the real part of the FK-QCW approximation to the intermediate scattering function using the relation in Eq. 4.36, which ensures that this quantity fulfills the detailed balance

Table 4.1: The simulation parameters used for the FK-QCW calculation of Eq. 4.37.

$k (nm^{-1})$	D_2			H_2		
	N	$l (bohr)$	$n (nm^{-3})$	N	$l (bohr)$	$\rho (nm^{-3})$
5.5	37	21.65	24.61	32	21.66	21.24
12.8	78	27.76	24.61	68	27.85	21.24
15.3	109	31.03	24.61	94	31.03	21.24
20.0	95	29.64	24.61	82	29.65	21.24

condition. The imaginary part of the intermediate scattering function was then obtained from the inverse Fourier transform of this quantity. By processing the data in this manner, we are ensuring that the approximate quantum time correlation function fulfils the detailed balance condition. Furthermore, since the detailed balance condition in Eq. 4.35 holds for the spectrum of any quantum time correlation function, this procedure could be applied to any correlation function involving hermitian operators[49], since in this case the general relation

$$C_{AB}(\omega) = \frac{2}{1 + e^{-\beta\hbar\omega}} \frac{1}{2\pi} \int_{-\infty}^{\infty} dt e^{-i\omega t} Re[C_{AB}(t)] \quad (4.42)$$

will always hold due to the symmetry[26] relation $C_{AB}(t) = C_{AB}(-t)^*$, where $C_{AB}(t)$ is given by Eq. 4.1 and $C_{AB}(\omega)$ is its Fourier transform.

4.3.2 The Experimental Dynamic Structure Factor

In an IXS experiment on a liquid, one must cope with the spurious scattering from the container which must be carefully subtracted from the raw intensity. Due to random temperature drifts in the analyzer crystal[1, 39]

which introduce an uncertainty in the zero of energy transfer ($\hbar\omega = 0$) between the sample+container and empty container scattering measurements, such a subtraction was not completely straightforward for the experimental data used in our previous study[1]. In order to deal with these spurious experimental effects, we developed in Ref. [1] (Ch. 2) a method that enables one to use the dynamic structure factor obtained from a simulation as an input to fix this unknown spectral shift.

Denoting $I_{raw}(\mathbf{k}, \omega)$ and $I_{EC}(\mathbf{k}, \omega)$ as the measured intensities scattered by the sample+container system and by the empty container, respectively, the unknown shift in the zero of energy transfer, $|\delta - \theta|$, can be taken into account within the experimental dynamic structure factor by writing this quantity as

$$S_{exp}(\mathbf{k}, \omega) = \alpha(\mathbf{k}) (I_{raw}(\mathbf{k}, \omega - \delta) - T(\mathbf{k})I_{EC}(\mathbf{k}, \omega - \theta)), \quad (4.43)$$

where $\alpha(\mathbf{k})$ is the proportionality factor that relates the dynamic structure factor to the inelastic scattering cross-section, and $T(\mathbf{k})$ is the transmission coefficient of the sample[1]. Due to the finite resolution of the experiment, the experimental dynamic structure factor, $S_{exp}(\mathbf{k}, \omega)$, in Eq. 4.43 is related to the sample's true dynamic structure factor, $S(\mathbf{k}, \omega)$, through a convolution with the instrument resolution function, $R(\omega)$, such that

$$S_{exp}(\mathbf{k}, \omega) \equiv S(\mathbf{k}, \omega) \otimes R(\omega) = \int_{-\infty}^{\infty} d\omega' S(\mathbf{k}, \omega') R(\omega - \omega'). \quad (4.44)$$

Using the procedure developed in Ref. [1] (Ch. 2), the refined experimental dynamic structure factor is obtained by performing a least squares fit

Table 4.2: The fitting parameters used in Eq. 4.43 to refine the experimental dynamic structure factor using the FK-QCW results. Here the R^2 values are the coefficients of determination for the various fits.

D_2						
$k (nm^{-1})$	$\alpha(\mathbf{k})$	$T(\mathbf{k})$	$\delta (meV)$	$\theta (meV)$	$ \delta - \theta (meV)$	R^2
5.5	7.51×10^4	0.897	-0.616	-0.545	0.070	0.97
12.8	1.41×10^5	0.896	-0.090	0.143	0.233	0.99
15.3	2.12×10^5	0.895	-0.391	-0.205	0.186	0.99
20.0	3.78×10^5	0.893	-0.678	0.228	0.906	0.99
H_2						
$k (nm^{-1})$	$\alpha(\mathbf{k})$	$T(\mathbf{k})$	$\delta (meV)$	$\theta (meV)$	$ \delta - \theta (meV)$	R^2
5.5	5.27×10^4	0.731	-0.134	0.233	0.367	0.97
12.8	1.79×10^5	0.954	0.183	0.531	0.348	0.93
15.3	1.57×10^5	0.740	0.188	0.929	0.742	0.97
20.0	4.05×10^5	0.952	-0.734	-0.703	0.032	1.00

of Eq. 4.43 to the results of a theoretical simulation which have been convoluted with the instrument resolution function, $R(\omega)$, for the determination of the unknown spectral shifts (δ, θ) . Within this fitting procedure, $\alpha(\mathbf{k})$ is determined for each (δ, θ) through

$$\alpha(\mathbf{k}) = \frac{\frac{\hbar k^2}{2m} \int_{-\infty}^{\infty} d\omega R(\omega) + S(\mathbf{k}) \int_{-\infty}^{\infty} d\omega R(\omega) \omega}{\int_{-\infty}^{\infty} d\omega \omega (I_{raw}(\mathbf{k}, \omega - \delta) - T(\mathbf{k}) I_{EC}(\mathbf{k}, \omega - \theta))}, \quad (4.45)$$

which ensures that the refined experimental quantity fulfills the first moment sum rule in Eq. 4.34. We note that $S(\mathbf{k})$ in Eq. 4.45 is the static structure factor, which in the present work has been obtained from the theoretical simulation. However, if the experimental measurement of this quantity was available, one could in principal use it within the fitting procedure.

Within this study we have reperformed this refinement process of the experimental quantity using the FK-QCW method as an input, and the result-

ing fitting parameters are shown in Table II. In the next section, we provide a comparison of the new experimental dynamic structure factors obtained using the FK-QCW method, and compare this with the experimental quantities previously published in Ref. [1] (Ch. 2), which were obtained using FK-LPI as an input. In addition, we also compare the theoretical dynamic structure factors obtained using the FK-QCW method with the results of FK-LPI and RPMD, also published in Ref. [1] (Ch. 2).

4.3.3 Dynamic Structure Factor

The FK-QCW results for the intermediate scattering function are shown in Fig. 4.1. Also included in Fig. 4.1 are the results obtained by FK-LPI and RPMD previously published in Ref. [1] (Ch. 2). Interestingly, for low momentum transfers where RPMD is applicable, due to the approximate linearity of Eq. 4.30, the FK-QCW method predicts nearly the same results as RPMD. This suggests that FK-QCW provides a method with an accuracy comparable to RPMD that does not suffer from the non-linear operator problem, since FK-QCW was developed within the framework of the CW approximation and therefore is able to access correlation functions involving non-linear operators.

When comparing the intermediate scattering functions of FK-QCW and FK-LPI in Fig. 4.1, one notices a significantly longer decay time predicted by FK-QCW for both para-hydrogen and ortho-deuterium at $k = 20.0 \text{ nm}^{-1}$. Due to the fact that in Ref. [1] (Ch. 2) we attributed the failure of FK-LPI for para-hydrogen at this momentum transfer to the purely classical propagation within

this method not being able to correctly account for the long-time behavior of the correlation function, the fact that the dynamics within FK-QCW predicts a significantly longer decay time suggests that this method may be able to stand up to this challenging test case where FK-LPI failed and RPMD was not applicable.

This hypothesis is confirmed in Fig. 4.2, where for the case of para-hydrogen at $k = 20.0 \text{ nm}^{-1}$ FK-QCW is in almost exact agreement with the experimental dynamic structure factor obtained using this method as an input. This then shows that the ensemble conserving dynamics of FK-QCW extends the accuracy of the FK-LPI method to longer times, where the classical propagation within the CW approximation fails. In addition, one sees that the experimental quantities obtained using FK-QCW and FK-LPI as an input are in relatively good agreement for all of the momentum transfers considered. The fact that this is true for para-hydrogen at $k = 20.0 \text{ nm}^{-1}$, where FK-LPI fails, shows that the process we developed in Ref. [1] (Ch. 2) to refine the experimental dynamic structure factor provides a robust method that allows one to correct for spurious experimental effects, even when the theoretical input is relatively inaccurate.

For the case of ortho-deuterium at $k = 20.0 \text{ nm}^{-1}$, one sees in Fig. 4.3 that, similar to the case of para-hydrogen, the FK-QCW method reproduces the experimental quantity almost exactly. While FK-LPI is in relatively good agreement with the experimental quantity for this momentum transfer, the fact that FK-QCW is more accurate shows that the longer decay time predicted in

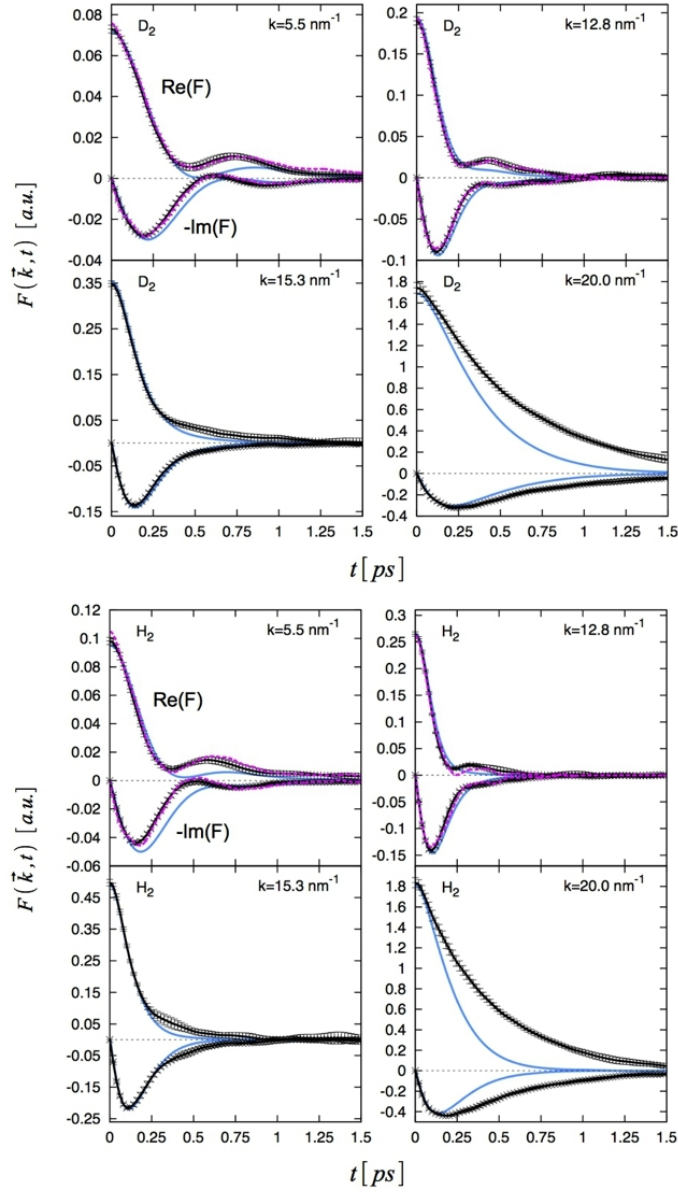


Figure 4.1: The FK-QCW (black line with error bars), FK-LPI (blue line), and RPMD (magenta dashed line at low k 's) approximation to the intermediate scattering function for both ortho-deuterium (upper four panels) and para-hydrogen (lower four panels) for the different momentum transfers considered (as labeled). The real part of the correlation function is the upper curve while the negative imaginary part is the lower curve in each figure. Both the FK-LPI and RPMD results were taken from Ref. [1] (Ch. 2).

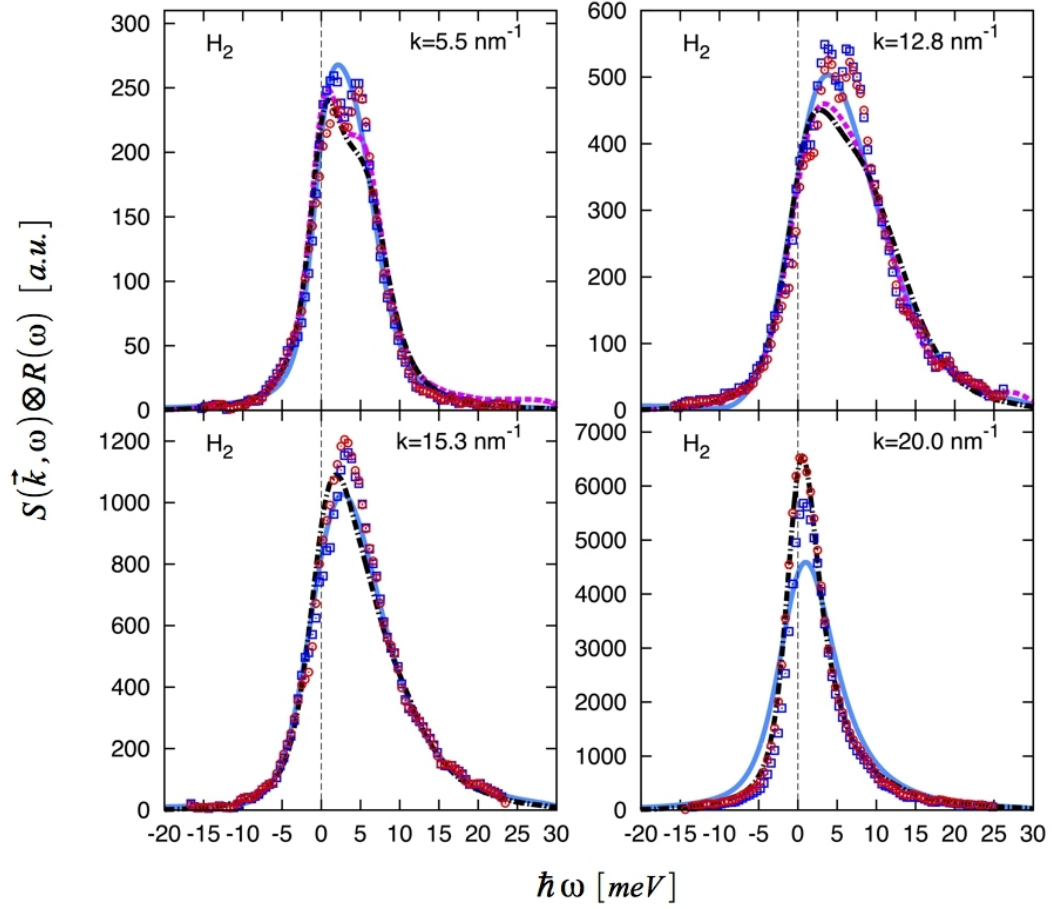


Figure 4.2: The refined experimental dynamic structure factors for para-hydrogen, as obtained using either FK-QCW (red dots) or FK-LPI (blue squares) as the input (see text). The FK-QCW (black dashed dot line), FK-LPI (blue line), and RPMD (magenta dashed line) dynamic structure factors are convoluted with the instrumental resolution function. The FK-LPI and RPMD results, as well as the experimental quantity obtained using FK-LPI as an input were taken from Ref. [1] (Ch. 2).

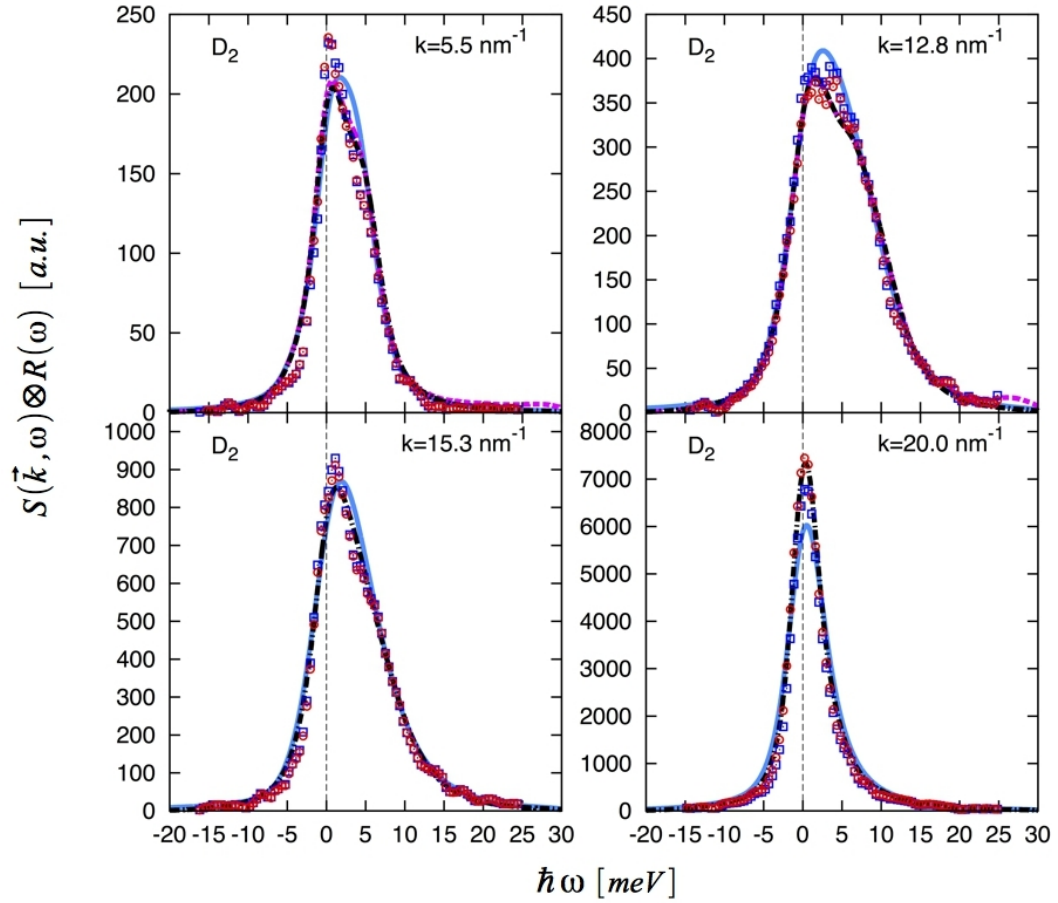


Figure 4.3: The refined experimental dynamic structure factors for ortho-deuterium, as obtained using either FK-QCW (red dots) or FK-LPI (blue squares) as the input (see text). The FK-QCW (black dashed dot line), FK-LPI (blue line), and RPMD (magenta dashed line) dynamic structure factors are convoluted with the instrumental resolution function. The FK-LPI and RPMD results, as well as the experimental quantity obtained using FK-LPI as an input were taken from Ref. [1] (Ch. 2).

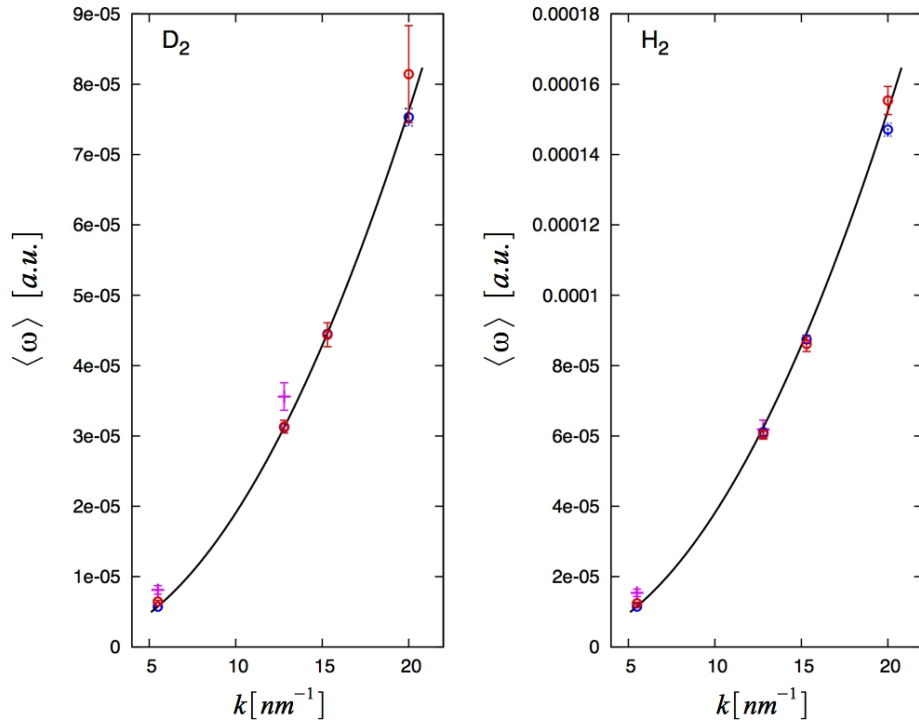


Figure 4.4: The first moment of the dynamic structure factors obtained from the the intermediate scattering function using the relation in Eq. 4.34 for both ortho-deuterium (left panel) and para-hydrogen (right panel) using FK-QCW (red circle), FK-LPI (blue circle), and RPMD (magenta cross). These results are compared with the exact relation of Eq. 4.34 (black line).

the correlation function by the ensemble conserving dynamics of this method, once again, better reflects the true dynamics of the system.

As seen in Figs. 2 and 3, the similarity of the FK-QCW and RPMD intermediate scattering functions for both para-hydrogen and ortho-deuterium at low momentum transfers translates to similar predictions for their corresponding dynamic structure factors. While not completely systematic due to the case of para-hydrogen at $k = 12.8 \text{ nm}^{-1}$, overall one sees a better agreement between the predictions of these two methods and the experimental quantity for both systems, as compared to FK-LPI. This then suggests that the more pronounced oscillations in the intermediate scattering functions of FK-QCW and RPMD more accurately describes the large wavelength density fluctuations of both the para-hydrogen and ortho-deuterium systems, consistent with the ensemble conserving dynamics used within FK-QCW being comparable to RPMD and more accurate than the purely classical dynamics of FK-LPI.

We note that for para-hydrogen, particularly at $k = 12.8 \text{ nm}^{-1}$, the disagreement of FK-QCW with the experimental quantity appears, at first glance, to be due to this method somewhat underestimating the area underneath the experimental dynamic structure factor. However, this area is precisely the static structure factor $S(\mathbf{k}) = F(\mathbf{k}, t = 0)$, for which FK-QCW and FK-LPI are equivalent, to within statistical accuracy. The FK-LPI static structure factor was published in Ref. [1] (Ch. 2), where it was found to be in agreement with the experimental measurements of Ref. [38]. It is reasonable, then, to turn to alternative explanations. One possibility is an uncertainty in

the normalization of the empty container scattering contribution; this was the case for para-hydrogen at $k = 5.5 \text{ nm}^{-1}$ and $k = 15.3 \text{ nm}^{-1}$.

The first moment of the dynamic structure factor obtained by FK-QCW, FK-LPI, and RPMD are shown in Fig. 4.4. The different dynamics of these three methods becomes relevant for the first moment since this quantity depends on the time derivative of the intermediate scattering function through Eq. 4.32. However, as seen in Fig. 4.4, FK-QCW exactly reproduces the first moment of the dynamic structure factor to within the uncertainty of the simulation for all of the momentum transfers considered. While FK-LPI is also able to exactly reproduce this quantity for all of the momentum transfers considered, this is not true for RPMD. The fact that these new ensemble conserving dynamics are shown to obey this exact quantum mechanical sum rule testifies even more to the accuracy of this new method.

4.4 Conclusions

We have shown that the ensemble conserving dynamics of the FK-QCW method can be easily applied to realistic condensed phase systems, such as low temperature para-hydrogen and ortho-deuterium. Furthermore, it was found that the dynamics of the FK-QCW method greatly extend the accuracy of the FK-LPI approximation when the long-time behavior of the quantum time correlation function becomes important. This was evidenced by the FK-QCW method nearly exactly reproducing the experimental dynamic structure factor of para-hydrogen at $k = 20.0 \text{ nm}^{-1}$, where the purely classical dynamics used

within the FK-LPI approximation fail and RPMD is not applicable.

In addition, where RPMD was applicable due to the approximate linearity of Eq. 4.30, we found that FK-QCW provides an accuracy comparable to RPMD. This then suggests that FK-QCW may be a top contender in the realm of approximate quantum dynamics methods since, unlike RPMD, FK-QCW is not only able to access correlation functions involving non-linear operators, but will also not encounter artificial frequencies in the simulated absorption spectra arising from unphysical high frequency oscillations within the dynamics[30–32].

Appendices

Appendix A

Overview of the FK-LPI method

To illustrate the main idea of the *FK – LPI* method and for simplicity, we present it here for a single particle in one dimension (the generalization to a system of N particles in three dimensions is relatively straight forward, see for example Ref. [5]). The *FK – LPI* approximation for $e^{-\beta\hat{H}}$ in one dimension is given by

$$e^{-\beta\hat{H}} \approx \int_{-\infty}^{\infty} dx_c dp_c \rho_{FK}(x_c, p_c) \hat{\delta}_{FK}(x_c, p_c) \quad (\text{A.1})$$

where (x_c, p_c) are the classical centroid phase-space variables describing the average position and momentum of a particle during thermal time $\beta\hbar$ and are defined as

$$x_c \equiv \frac{1}{\beta\hbar} \int_0^{\beta\hbar} d\tau x(\tau) \quad p_c \equiv \frac{1}{\beta\hbar} \int_0^{\beta\hbar} d\tau p(\tau). \quad (\text{A.2})$$

The FK approximation to the centroid phase-space density $\rho_{FK}(x_c, p_c)$ is given by

$$\rho_{FK}(x_c, p_c) \equiv \frac{1}{2\pi\hbar} \exp \left\{ -\beta \left(\frac{p_c^2}{2m} + W_1(x_c) \right) \right\}, \quad (\text{A.3})$$

$W_1(x_c)$ being the FK approximation to the centroid potential. The effective frequency quasidensity operator $\hat{\delta}_{FK}(x_c, p_c)$ is defined as

$$\begin{aligned}
\hat{\delta}_{FK}(x_c, p_c) &\equiv \sqrt{\frac{m\Omega(x_c)}{\pi\hbar\alpha}} \int_{-\infty}^{\infty} dx dx' |x'\rangle \langle x| \\
&\quad \times \exp\left\{i\frac{p_c}{\hbar}(x' - x)\right\} \\
&\quad \times \exp\left\{-\frac{m\Omega(x_c)}{\hbar\alpha} \left(\frac{x' + x}{2} - x_c\right)^2 - \frac{m\Omega(x_c)\alpha}{4\hbar} (x' - x)^2\right\}, \quad (\text{A.4})
\end{aligned}$$

where the centroid dependent variational effective frequency $\Omega(x_c)$ is determined from the local curvature of the systems Gaussian smeared potential, and is given by

$$\Omega^2(x_c) = \frac{1}{m} \left[\frac{\partial^2 V_{a^2}(x_c)}{\partial x_c^2} \right]_{a^2=a^2(x_c)}. \quad (\text{A.5})$$

The smeared potential, $V_{a^2}(x_c)$, which accounts for quantum-statistical path fluctuations is defined as

$$V_{a^2}(x_c) \equiv \sqrt{\frac{1}{2\pi a^2}} \int_{-\infty}^{\infty} dy V(y) \exp\left\{-\frac{(y - x_c)^2}{2a^2}\right\}, \quad (\text{A.6})$$

the smearing width $a^2(x_c)$ being

$$a^2(x_c) = \frac{1}{m\beta\Omega^2(x_c)} \left(\frac{\beta\hbar\Omega(x_c)}{2} \coth\left(\frac{\beta\hbar\Omega(x_c)}{2}\right) - 1 \right) \quad (\text{A.7})$$

which measures the importance of quantum fluctuations around the classical-like position x_c . In Eq. A.4, α is related to the smearing width $a^2(x_c)$ by

$$\alpha = \frac{2m\Omega(x_c)a^2(x_c)}{\hbar} = \coth\left(\frac{\beta\hbar\Omega(x_c)}{2}\right) - \frac{2}{\beta\hbar\Omega(x_c)}. \quad (\text{A.8})$$

Note that when using Eq. A.5 to determine the effective frequency $\Omega(x_c)$, the derivative is taken while treating $a^2(x_c)$ as a constant. Furthermore, by using

Eq. A.5 and A.6 one can write the explicit form that $\Omega^2(x_c)$ takes in terms of $a^2(x_c)$, and it is given by

$$\Omega^2(x_c) = \frac{1}{m} \sqrt{\frac{1}{2\pi a^2(x_c)}} \int_{-\infty}^{\infty} dy \frac{\partial^2 V(y + x_c)}{\partial x_c^2} \times \exp \left\{ -\frac{y^2}{2a^2(x_c)} \right\}. \quad (\text{A.9})$$

For all but the simplest potentials, determination of $\Omega(x_c)$ is the main computational load in applying the *FK – LPI* methodology since Eq. A.7 and A.9 must be solved iteratively (see Ref. [5] for a discussion of efficient ways to determine $\Omega(x_c)$ using different numerical schemes). Once $\Omega(x_c)$ is determined, the FK approximation to the centroid potential $W_1(x_c)$ is given by

$$W_1(x_c) = \frac{1}{\beta} \ln \left\{ \frac{\sinh \left(\frac{\beta \hbar \Omega(x_c)}{2} \right)}{\frac{\beta \hbar \Omega(x_c)}{2}} \right\} + V_{a^2}(x_c) - \frac{1}{2} m \Omega^2(x_c) a^2(x_c). \quad (\text{A.10})$$

The main advantage of the *FK – LPI* prescription is that due to the harmonic form of $e^{-\beta \hat{H}}$ an analytical expression for the Wigner transform of $e^{-\beta \hat{H}} \hat{A}$ is readily obtained for an operator \hat{A} depending only on position or momentum since for example $\hat{A} = \hat{A}(\hat{x})$, $[e^{-\beta \hat{H}} \hat{A}(\hat{x})]_W(q_0, p_0)$ becomes

$$\begin{aligned}
[e^{-\beta\hat{H}}\hat{A}(\hat{x})]_W(q_0, p_0) &= \int_{-\infty}^{\infty} dx_c dp_c \sqrt{\frac{m\Omega(x_c)}{\pi\hbar\alpha}} \rho_{FK}(x_c, p_c) \\
&\quad \times \exp\left\{-\frac{m\Omega(x_c)}{\hbar\alpha}(q_0 - x_c)^2\right\} \\
&\quad \times \int_{-\infty}^{\infty} d\eta A(q_0 - \frac{\eta}{2}) \exp\left\{-\frac{m\Omega(x_c)\alpha}{4\hbar}\eta^2 - \frac{i}{\hbar}(p - p_c)\eta\right\}. \quad (\text{A.11})
\end{aligned}$$

Hence, under the *FK-LPI* approximation an analytical expression of $[e^{-\beta\hat{H}}\hat{A}(\hat{x})]_W(q_0, p_0)$ in terms of the centroid phase-space density $\rho_{FK}(x_c, p_c)$ is easily obtained for any operator in which the gaussian integral in Eq. A.11 can be performed. Furthermore, due to the dependence of Eq. A.11 on the centroid density, the evaluation of quantum time correlation functions using the *FK-LPI* method can be performed by using a combination of Monte Carlo and molecular dynamics methods, with the general computational procedure being given by the following:

(1) an analytical expression for $[\hat{B}]_W(q_t, p_t)$ is computed using Eq. 2.13, and an analytical expression for $[e^{-\beta\hat{H}}\hat{A}]_W(q_0, p_0)$ in terms of an integral over the centroid phase-space density $\rho_{FK}(x_c, p_c)$ is obtained by using Eq. A.11.

(2) a centroid position and momentum (x_c, p_c) is sampled from $\rho_{FK}(x_c, p_c)$.

(3) for each (x_c, p_c) , one then samples (q_0, p_0) and these are then propagated classically to (q_t, p_t) using Hamilton's equations of motion and the explicit evaluation of $[\hat{B}]_W(q_t, p_t)$ as a function of time is performed.

Appendix B

Time invariance of thermodynamic properties within the CW expression

The classical Wigner (CW) expression for $\langle \hat{B}(t) \rangle$ is given by

$$\langle \hat{B}(t) \rangle = \frac{1}{Z} \frac{1}{2\pi\hbar} \int_{-\infty}^{\infty} dpdq [e^{-\beta\hat{H}}]_W(q, p) [\hat{B}]_W(q_t, p_t), \quad (\text{B.1})$$

while $\langle \hat{B}(0) \rangle$ is

$$\langle \hat{B}(0) \rangle = \frac{1}{Z} \frac{1}{2\pi\hbar} \int_{-\infty}^{\infty} dpdq [e^{-\beta\hat{H}}]_W(q, p) [\hat{B}]_W(q, p). \quad (\text{B.2})$$

After making a making a dummy variable substitution of the integration variables from $(q, p) \rightarrow (q_t, p_t)$ in Eq. B.2 we have that

$$\langle \hat{B}(0) \rangle = \frac{1}{Z} \frac{1}{2\pi\hbar} \int_{-\infty}^{\infty} dp_t dq_t [e^{-\beta\hat{H}}]_W(q_t, p_t) [\hat{B}]_W(q_t, p_t), \quad (\text{B.3})$$

which we see is equivalent to $\langle \hat{B}(t) \rangle$ in Eq. B.1 if

$$dpdq [e^{-\beta\hat{H}}]_W(q, p) = dp_t dq_t [e^{-\beta\hat{H}}]_W(q_t, p_t). \quad (\text{B.4})$$

Therefore, the CW expression can be made to preserve the time invariance of thermal equilibrium properties as long as the dynamics are chosen to conserve the phase space probability within the infinitesimal phase space volume along the trajectory, which is equivalent to the initial quantum ensemble being conserved.

Appendix C

Time-dependent dummy variable substitution

Suppose we have some set of dynamics such that we are able to propagate a phase space point (x_c, p_c) to $(x_c(t), p_c(t))$. By the property of the delta function we can write the operator $\rho_{FK}(x_c, p_c) \hat{\delta}_{FK}(x_c, p_c)$ evaluated at any point in phase space (x'_c, p'_c) as

$$\begin{aligned} \rho_{FK}(x'_c, p'_c) \hat{\delta}_{FK}(x'_c, p'_c) &= \int dx_c(t) dp_c(t) \rho_{FK}(x_c(t), p_c(t)) \\ &\quad \times \hat{\delta}_{FK}(x_c(t), p_c(t)) \delta(x_c(t) - x'_c) \delta(p_c(t) - p'_c) \end{aligned} \quad (\text{C.1})$$

Furthermore, by integrating both sides of this equation over (x'_c, p'_c) we have

$$\begin{aligned} &\int dx'_c dp'_c \rho_{FK}(x'_c, p'_c) \hat{\delta}_{FK}(x'_c, p'_c) \\ &= \int dx_c(t) dp_c(t) \rho_{FK}(x_c(t), p_c(t)) \hat{\delta}_{FK}(x_c(t), p_c(t)) \\ &\quad \times \int dx'_c dp'_c \delta(x_c(t) - x'_c) \delta(p_c(t) - p'_c) \\ &= \int dx_c(t) dp_c(t) \rho_{FK}(x_c(t), p_c(t)) \hat{\delta}_{FK}(x_c(t), p_c(t)). \end{aligned} \quad (\text{C.2})$$

Thus we have that

$$\begin{aligned}
& \int dx'_c dp'_c \rho_{FK}(x'_c, p'_c) \hat{\delta}_{FK}(x'_c, p'_c) \\
&= \int dx_c(t) dp_c(t) \rho_{FK}(x_c(t), p_c(t)) \hat{\delta}_{FK}(x_c(t), p_c(t)). \tag{C.3}
\end{aligned}$$

Therefore, after making a change of variables from (x'_c, p'_c) to (x_c, p_c) in the LHS of Eq. C.3 this expression becomes

$$\begin{aligned}
& \int dx_c dp_c \rho_{FK}(x_c, p_c) \hat{\delta}_{FK}(x_c, p_c) \\
&= \int dx_c(t) dp_c(t) \rho_{FK}(x_c(t), p_c(t)) \hat{\delta}_{FK}(x_c(t), p_c(t)) \tag{C.4}
\end{aligned}$$

for a given set of dynamics. Next, by taking the Wigner transform of both sides of Eq. C.4 and evaluating it at a point (q_t, p_t) we arrive at

$$\begin{aligned}
& \int dx_c dp_c \rho_{FK}(x_c, p_c) [\hat{\delta}_{FK}(x_c, p_c)]_W(q_t, p_t) \\
&= \int dx_c(t) dp_c(t) \rho_{FK}(x_c(t), p_c(t)) \\
&\quad \times [\hat{\delta}_{FK}(x_c(t), p_c(t))]_W(q_t, p_t), \tag{C.5}
\end{aligned}$$

which is equivalent to making a dummy variable substitution of the integration variables in Eq. 3.23 from $(x_c, p_c) \rightarrow (x_c(t), p_c(t))$. In addition, one can form a similar argument to rigorously justify the dummy variable substitution of the integration variables in Eq. 3.58.

Appendix D

Liouville's theorem for the centroid distribution function

Liouville's theorem in classical mechanics states that the phase space distribution function, $\rho(x, p)$, is time-invariant such that

$$\rho(x(t), p(t)) = \rho(x, p) \quad (\text{D.1})$$

or equivalently

$$\frac{d}{dt}\rho(x(t), p(t)) = 0. \quad (\text{D.2})$$

The FK approximation to the exact centroid distribution function is defined as

$$\rho_{FK}(x_c, p_c) \equiv \frac{1}{2\pi\hbar} \exp \left\{ -\beta \left(\frac{p_c^2}{2m} + W_1(x_c) \right) \right\}, \quad (\text{D.3})$$

where the FK approximation to the centroid potential is given by

$$W_1(x_c) = \frac{1}{\beta} \ln \left\{ \frac{\sinh \left(\frac{\beta\hbar\Omega(x_c)}{2} \right)}{\frac{\beta\hbar\Omega(x_c)}{2}} \right\} + V_{a^2}(x_c) - \frac{1}{2}m\Omega^2(x_c)a^2(x_c). \quad (\text{D.4})$$

The centroid variables evolve according to the classical like dynamics given by

$$\begin{aligned}\dot{x}_c(t) &= \frac{p_c(t)}{m} \\ \dot{p}_c(t) &= -\frac{\partial W_1(x_c(t))}{\partial x_c(t)},\end{aligned}\tag{D.5}$$

such that the time derivative of the centroid distribution function is given by

$$\begin{aligned}\frac{d}{dt}\rho_{FK}(x_c(t), p_c(t)) &= -\beta \rho_{FK}(x_c(t), p_c(t)) \\ &\times \left[-\frac{p_c(t)}{m} \frac{\partial W_1(x_c(t))}{\partial x_c(t)} + \frac{\partial W_1(x_c(t))}{\partial x_c(t)} \frac{p_c(t)}{m} \right] = 0,\end{aligned}\tag{D.6}$$

and therefore

$$\rho_{FK}(x_c(t), p_c(t)) = \rho_{FK}(x_c, p_c).\tag{D.7}$$

Next, we evaluate $\det(J(t))$ in order to show that the volume element is conserved. Therefore, using Eq. D.5 we have that

$$\frac{\partial \dot{x}_c(t)}{\partial x_c(t)} + \frac{\partial \dot{p}_c(t)}{\partial p_c(t)} = \frac{\partial}{\partial x_c(t)} \frac{p_c(t)}{m} - \frac{\partial}{\partial p_c(t)} \frac{\partial W_1(x_c(t))}{\partial x_c(t)} = 0\tag{D.8}$$

such that

$$\det(J(t)) = \exp\left(\int_0^t \frac{\partial \dot{x}_c(t)}{\partial x_c(t)} + \frac{\partial \dot{p}_c(t)}{\partial p_c(t)} dt\right) = 1,\tag{D.9}$$

and therefore

$$dx_c(t)dp_c(t) = dx_c dp_c.\tag{D.10}$$

Thus combining Eq. D.7 and D.10 we have that

$$dx_c(t)dp_c(t)\rho_{FK}(x_c(t), p_c(t)) = dx_c dp_c \rho_{FK}(x_c, p_c)\tag{D.11}$$

We now show that for FK approximation to the centroid distribution function, the centroid evolves on the FK smeared potential. This can be shown

by explicitly taking the derivative of $W_1(x_c(t))$ in Eq. D.4, which is given by

$$\begin{aligned} \frac{\partial W_1(x_c(t))}{\partial x_c(t)} &= \frac{1}{\beta} \frac{\partial}{\partial \Omega_t} \ln \left\{ \frac{\sinh\left(\frac{\beta \hbar \Omega_t}{2}\right)}{\frac{\beta \hbar \Omega_t}{2}} \right\} \frac{\partial \Omega_t}{\partial x_c(t)} \\ &\quad - m \Omega_t a^2(x_c(t)) \frac{\partial \Omega_t}{\partial x_c(t)} - \frac{1}{2} m \Omega_t^2 \frac{\partial a^2(x_c(t))}{\partial x_c(t)} \\ &+ \left[\frac{\partial V_{a^2}(x_c(t))}{\partial x_c(t)} \right]_{a^2=a^2(x_c(t))} + \frac{\partial V_{a^2}(x_c(t))}{\partial a^2(x_c(t))} \frac{\partial a^2(x_c(t))}{\partial x_c(t)}. \end{aligned} \quad (\text{D.12})$$

However, using the definition of $a^2(x_c(t))$ one can easily show that

$$\frac{1}{\beta} \frac{\partial}{\partial \Omega_t} \ln \left\{ \frac{\sinh\left(\frac{\beta \hbar \Omega_t}{2}\right)}{\frac{\beta \hbar \Omega_t}{2}} \right\} = m \Omega_t a^2(x_c(t)), \quad (\text{D.13})$$

such that

$$\begin{aligned} \frac{\partial W_1(x_c(t))}{\partial x_c(t)} &= -\frac{1}{2} m \Omega_t^2 \frac{\partial a^2(x_c(t))}{\partial x_c(t)} \\ &+ \left[\frac{\partial V_{a^2}(x_c(t))}{\partial x_c(t)} \right]_{a^2=a^2(x_c(t))} + \frac{\partial V_{a^2}(x_c(t))}{\partial a^2(x_c(t))} \frac{\partial a^2(x_c(t))}{\partial x_c(t)}. \end{aligned} \quad (\text{D.14})$$

Furthermore, an equivalent definition of Ω_t^2 is[9]

$$\Omega_t^2 = \frac{2}{m} \frac{\partial V_{a^2}(x_c(t))}{\partial a^2(x_c(t))}. \quad (\text{D.15})$$

Hence we have that

$$\frac{1}{2} m \Omega_t^2 = \frac{\partial V_{a^2}(x_c(t))}{\partial a^2(x_c(t))} \quad (\text{D.16})$$

such that the derivative of $W_1(x_c(t))$ now becomes

$$\frac{\partial W_1(x_c(t))}{\partial x_c(t)} = \left[\frac{\partial V_{a^2}(x_c(t))}{\partial x_c(t)} \right]_{a^2=a^2(x_c(t))}, \quad (\text{D.17})$$

where the derivative is taken while holding $a^2(x_c(t))$ constant. Thus the centroid dynamics can be equivalently written as

$$\begin{aligned} \dot{x}_c(t) &= \frac{p_c(t)}{m} \\ \dot{p}_c(t) &= - \left[\frac{\partial V_{a^2}(x_c(t))}{\partial x_c(t)} \right]_{a^2=a^2(x_c(t))}. \end{aligned} \tag{D.18}$$

Appendix E

Determinant of the Jacobian matrix in terms of the dimensionless coordinates

The dimensionless coordinates in Eq. 3.33 can be written as

$$\begin{aligned}\tilde{q}(t) &\equiv \gamma_t (q_t - x_c(t)) \\ \tilde{p}(t) &\equiv \zeta_t (p_t - p_c(t))\end{aligned}\tag{E.1}$$

where

$$\begin{aligned}\gamma_t &\equiv \sqrt{\frac{m\Omega_t}{\hbar\alpha_t}} \\ \zeta_t &\equiv \sqrt{\frac{1}{m\hbar\Omega_t\alpha_t}}.\end{aligned}\tag{E.2}$$

Furthermore, by taking the time derivative of Eq. E.1 and rearranging terms one can show that in terms of these coordinates

$$\begin{aligned}\dot{q}_t &= \dot{x}_c(t) + \frac{\dot{\tilde{q}}(t)}{\gamma_t} - \frac{\dot{\gamma}_t}{\gamma_t^2} \tilde{q}(t) \\ \dot{p}_t &= \dot{p}_c(t) + \frac{\dot{\tilde{p}}(t)}{\zeta_t} - \frac{\dot{\zeta}_t}{\zeta_t^2} \tilde{p}(t).\end{aligned}\tag{E.3}$$

In addition, by using the fact that $(x_c(t), p_c(t))$ is independent of (q_t, p_t) , since the centroid variables evolve according to the classical like dynamics in Eq.

3.24, then from Eq. E.1 we have that

$$\begin{aligned}\frac{\partial}{\partial q_t} &= \gamma_t \frac{\partial}{\partial \tilde{q}(t)} \\ \frac{\partial}{\partial p_t} &= \zeta_t \frac{\partial}{\partial \tilde{p}(t)}.\end{aligned}\tag{E.4}$$

Therefore, using Eqs. E.3 and E.4, one has that

$$\frac{\partial \dot{q}_t}{\partial q_t} + \frac{\partial \dot{p}_t}{\partial p_t} = \frac{\partial \dot{\tilde{q}}(t)}{\partial \tilde{q}(t)} + \frac{\partial \dot{\tilde{p}}(t)}{\partial \tilde{p}(t)} - \frac{\dot{\gamma}_t}{\gamma_t} - \frac{\dot{\zeta}_t}{\zeta_t},\tag{E.5}$$

such that $\det(J(t))$ in terms of these coordinates takes the form

$$\begin{aligned}\det(J(t)) &= \exp\left(\int_0^t \frac{\partial \dot{q}_t}{\partial q_t} + \frac{\partial \dot{p}_t}{\partial p_t} dt\right) \\ &= \exp\left(\int_0^t \frac{\partial \dot{\tilde{q}}(t)}{\partial \tilde{q}(t)} + \frac{\partial \dot{\tilde{p}}(t)}{\partial \tilde{p}(t)} - \frac{\dot{\gamma}_t}{\gamma_t} - \frac{\dot{\zeta}_t}{\zeta_t} dt\right).\end{aligned}\tag{E.6}$$

Part of this expression can be explicitly integrated to give

$$\det(J(t)) = \exp\left(\int_0^t \frac{\partial \dot{\tilde{q}}(t)}{\partial \tilde{q}(t)} + \frac{\partial \dot{\tilde{p}}(t)}{\partial \tilde{p}(t)} dt\right) \frac{\gamma_0 \zeta_0}{\gamma_t \zeta_t},\tag{E.7}$$

which after using Eq. E.2 becomes

$$\det(J(t)) = \exp\left(\int_0^t \frac{\partial \dot{\tilde{q}}(t)}{\partial \tilde{q}(t)} + \frac{\partial \dot{\tilde{p}}(t)}{\partial \tilde{p}(t)} dt\right) \frac{\alpha_t}{\alpha_0}.\tag{E.8}$$

Appendix F

Equivalence of FK-QCW and CMD for the Kubo-transformed time-correlation function of linear operators

The Kubo transformed time-correlation function

$$\langle \hat{A}(0)\hat{B}(t) \rangle_K \equiv \frac{1}{\beta Z} \int_0^\beta d\lambda \text{Tr} \left(e^{-(\beta-\lambda)\hat{H}} \hat{A}(0) e^{-\lambda\hat{H}} \hat{B}(t) \right) \quad (\text{F.1})$$

is related to the standard quantum time correlation function in Eq. 3.1 through

$$C_{AB}(\omega) = \frac{\beta\hbar\omega}{1 - e^{-\beta\hbar\omega}} \tilde{C}_{AB}(\omega), \quad (\text{F.2})$$

where $C_{AB}(\omega)$ and $\tilde{C}_{AB}(\omega)$ are the Fourier transforms of the standard and Kubo transformed time correlation functions, respectively. This quantity can be expressed in terms of the exact centroid distribution and QDO in which it takes the form[16]

$$\begin{aligned} \langle \hat{A}(0)\hat{B}(t) \rangle_K &= \frac{1}{Z 2\pi\hbar} \int dx_c dp_c \rho_c(x_c, p_c) A_c(x_c, p_c) \\ &\quad \times \text{Tr} \left(\hat{\delta}(x_c, p_c) \hat{B}(t) \right), \end{aligned} \quad (\text{F.3})$$

where $A_c(x_c, p_c) \equiv \text{Tr}(\hat{\delta}(x_c, p_c)\hat{A})$. This expression is exact so long as \hat{A} is linear in position and/or momentum[16].

Using the Wigner representation for the trace of two general operators

$$\text{Tr}(\hat{A}\hat{C}) = \frac{1}{2\pi\hbar} \int dqdp [\hat{A}]_W(q, p) [\hat{C}]_W(q, p), \quad (\text{F.4})$$

we can rewrite Eq. F.3 as

$$\begin{aligned} \langle \hat{A}(0)\hat{B}(t) \rangle_K &= \frac{1}{Z(2\pi\hbar)^2} \int dx_c dp_c \rho_c(x_c, p_c) A_c(x_c, p_c) \\ &\times \int dqdp [\hat{\delta}(x_c, p_c)]_W(q, p) [\hat{B}(t)]_W(q, p). \end{aligned} \quad (\text{F.5})$$

Invoking the CW approximation, $[\hat{B}(t)]_W(q, p) \rightarrow [\hat{B}]_W(q_t, p_t)$, along with the FK approximation to the density operator, Eq. F.5 becomes

$$\begin{aligned} \langle \hat{A}(0)\hat{B}(t) \rangle_K &\approx \frac{1}{Z2\pi\hbar} \int dx_c dp_c \rho_{FK}(x_c, p_c) A_c(x_c, p_c) \\ &\times \int dqdp [\hat{\delta}_{FK}(x_c, p_c)]_W(q, p) [\hat{B}]_W(q_t, p_t), \end{aligned} \quad (\text{F.6})$$

where a factor of $2\pi\hbar$ has been absorbed into the definition of ρ_{FK} . However, for the entire class of dynamics in Sec. IV the following equality holds

$$\begin{aligned} &dqdp [\hat{\delta}_{FK}(x_c, p_c)]_W(q, p) \\ &= dq_t dp_t [\hat{\delta}_{FK}(x_c(t), p_c(t))]_W(q_t, p_t). \end{aligned} \quad (\text{F.7})$$

Thus using this equality and then making a dummy variable substitution of the integration variables from $(q_t, p_t) \rightarrow (q, p)$, Eq. F.6 can be equivalently expressed as

$$\begin{aligned} \langle \hat{A}(0)\hat{B}(t) \rangle_K &\approx \frac{1}{Z2\pi\hbar} \int dx_c dp_c \rho_{FK}(x_c, p_c) A_c(x_c, p_c) \\ &\times \int dq dp [\hat{\delta}_{FK}(x_c(t), p_c(t))]_W(q, p) [\hat{B}]_W(q, p). \end{aligned} \quad (\text{F.8})$$

Furthermore, switching back from the Wigner representation to the trace, we have that

$$\begin{aligned} \langle \hat{A}(0)\hat{B}(t) \rangle_K &\approx \frac{1}{Z} \int dx_c dp_c \rho_{FK}(x_c, p_c) A_c(x_c, p_c) \\ &\times B_c(x_c(t), p_c(t)), \end{aligned} \quad (\text{F.9})$$

where we have defined $B_c(x_c(t), p_c(t)) \equiv \text{Tr} \left(\hat{\delta}_{FK}(x_c(t), p_c(t)) \hat{B} \right)$. Recognizing this expression as being equivalent to using the FK approximation of the density operator within the framework of CMD, we see that the entire class of quasi-classical dynamics in Sec. IV reduces to CMD when used to evaluate the Kubo transformed correlation function of linear operators. Furthermore, the fact that one can alternatively arrive at the expression in Eq. F.9 by only invoking the CMD approximation[16]

$$e^{-i\hat{H}t/\hbar} \hat{\delta}_{FK}(x_c, p_c) e^{i\hat{H}t/\hbar} \approx \hat{\delta}_{FK}(x_c(t), p_c(t)) \quad (\text{F.10})$$

shows that the CW approximation is equivalent to making the CMD approximation for the Kubo transformed correlation function, so long as the dynamics retain the property in Eq. F.7.

Appendix G

FK-QCW Molecular Dynamics Algorithm

Defining the $3N$ dimensional vector that contains the FK smeared force as

$$\mathbf{F}_c(t) \equiv -\nabla_c [V_A(\mathbf{x}_c(t))]_{\mathbf{A}=\mathbf{A}(\mathbf{x}_c(t))}, \quad (\text{G.1})$$

where the gradient is taken with respect to $\mathbf{x}_c(t)$, the algorithm for integrating the FK-QCW method dynamics one time step Δt using the velocity Verlet algorithm goes as follows:

$$\tilde{q}_k(t + \Delta t) \leftarrow \tilde{q}_k(t) + f_k(\mathbf{x}_c(t))\tilde{p}_k(t)\Delta t \quad (\text{G.2})$$

$$\tilde{p}_k(t + \Delta t) \leftarrow \tilde{p}_k(t) - f_k(\mathbf{x}_c(t))\tilde{q}_k(t)\Delta t \quad (\text{G.3})$$

$$\mathbf{x}_c(t + \Delta t) \leftarrow \mathbf{x}_c(t) + \mathbf{M}^{-1}\mathbf{p}_c(t)\Delta t + \frac{\Delta t^2}{2}\mathbf{M}^{-1}\mathbf{F}_c(t) \quad (\text{G.4})$$

$$\mathbf{p}_c(t + \Delta t) \leftarrow \mathbf{p}_c(t) + \frac{\Delta t}{2} [\mathbf{F}_c(t) + \mathbf{F}_c(t + \Delta t)] \quad (\text{G.5})$$

$$\tilde{\mathbf{q}}(t + \Delta t) \leftarrow \mathbf{U}^\dagger(\mathbf{x}_c(t + \Delta t))\mathbf{U}(\mathbf{x}_c(t))\tilde{\mathbf{q}}(t + \Delta t) \quad (\text{G.6})$$

$$\tilde{\mathbf{p}}(t + \Delta t) \leftarrow \mathbf{U}^\dagger(\mathbf{x}_c(t + \Delta t))\mathbf{U}(\mathbf{x}_c(t))\tilde{\mathbf{p}}(t + \Delta t). \quad (\text{G.7})$$

$$\tilde{\eta}_k(t + \Delta t) \leftarrow \sqrt{\frac{\hbar\alpha_k(\mathbf{x}_c(t + \Delta t))}{\omega_k(\mathbf{x}_c(t + \Delta t))}}\tilde{q}_k(t + \Delta t) \quad (\text{G.8})$$

$$\tilde{\nu}_k(t + \Delta t) \leftarrow \sqrt{\frac{\hbar\omega_k(\mathbf{x}_c(t + \Delta t))}{\tanh\left(\frac{\beta\hbar\omega_k(\mathbf{x}_c(t + \Delta t))}{2}\right)}}\tilde{p}_k(t + \Delta t) \quad (\text{G.9})$$

$$\mathbf{q}(t + \Delta t) \leftarrow \mathbf{x}_c(t + \Delta t) + \mathbf{M}^{-1/2}\mathbf{U}(\mathbf{x}_c(t + \Delta t))\tilde{\boldsymbol{\eta}}(t + \Delta t) \quad (\text{G.10})$$

$$\mathbf{p}(t + \Delta t) \leftarrow \mathbf{M}^{1/2}\mathbf{U}(\mathbf{x}_c(t + \Delta t))\tilde{\boldsymbol{\nu}}(t + \Delta t). \quad (\text{G.11})$$

It is important to note the intermediate steps G.6 and G.7. These are performed to ensure that the dimensionless normal modes $\tilde{\mathbf{q}}(t + \Delta t)$ and $\tilde{\mathbf{p}}(t + \Delta t)$ are formed properly for the use in steps G.8 and G.9 since the eigenvector within the j^{th} column of the orthonormal matrices $\mathbf{U}(\mathbf{x}_c(t))$ and $\mathbf{U}(\mathbf{x}_c(t + \Delta t))$ will typically not correspond to the same normal mode due to the numerical method used for the diagonalization of $\boldsymbol{\Omega}^2(\mathbf{x}_c(t))$ and $\boldsymbol{\Omega}^2(\mathbf{x}_c(t + \Delta t))$.

Bibliography

References and Notes

- [1] K. K. G. Smith, J. A. Poulsen, A. Cunsolo, and P. J. Rossky, *J. Chem. Phys.* 140, 034501 (2014).
- [2] J. A. Poulsen, G. Nyman, and P. J. Rossky, *J. Chem. Phys.* 119, 12179 (2003).
- [3] J. A. Poulsen, G. Nyman, and P. J. Rossky, *J. Phys. Chem. B* 108, 19799 (2004).
- [4] J. A. Poulsen, G. Nyman, and P. J. Rossky, *J. Phys. Chem. A* 108, 8743 (2004).
- [5] J. A. Poulsen, G. Nyman, and P. J. Rossky, *J. Chem. Theory Comput.* 2, 1482 (2006).
- [6] J. A. Poulsen, J. Scheers, G. Nyman, and P. J. Rossky, *Phys. Rev. B* 75, 224505 (2007).
- [7] I. F. Silvera and V. V. Goldman, *J. Chem. Phys.* 69, 9 (1978).
- [8] R. P. Feynman and H. Kleinert, *Phys. Rev. A* 34, 5080 (1986).
- [9] H. Kleinert, *Path Integrals in Quantum Mechanics, Statistics, and Polymer Physics* (World Scientific, Singapore, 1995).

- [10] C. Kittel, Introduction to Solid State Physics, 7th ed. (Wiley, New York, 1996).
- [11] G. L. Squires, Introduction to the Theory of Thermal Neutron Scattering (Cambridge University Press, Cambridge, 1978).
- [12] D. Pines and P. Nozieres, The Theory of Quantum Liquids (Benjamin, New York, 1966), Vol. I.
- [13] L. Van Hove, Phys. Rev. 95, 249 (1954).
- [14] T. D. Hone and G. A. Voth, J. Chem. Phys. 121, 6412 (2004).
- [15] S. Jang and G. A. Voth, J. Chem. Phys. 111, 2371 (1999).
- [16] S. Jang and G. A. Voth, J. Chem. Phys. 111, 2357 (1999).
- [17] E. J. Heller, J. Chem. Phys. 65, 1289 (1976).
- [18] Q. Shi and E. Geva, J. Chem. Phys. 118, 8173 (2003).
- [19] H. Wang, X. Sun, W. H. Miller, J. Chem. Phys. 108, 9726 (1998).
- [20] J. Liu and W. H. Miller, J. Chem. Phys. 126, 234110 (2007).
- [21] J. Liu and W. H. Miller, J. Chem. Phys. 128, 144511 (2008).
- [22] J. Liu and W. H. Miller, J. Chem. Phys. 134, 104101 (2011).
- [23] J. Liu and W. H. Miller, J. Chem. Phys. 134, 104102 (2011).
- [24] J. Liu, J. Chem. Phys. 134, 194110 (2011).

- [25] W. H. Miller, *J. Chem. Phys.* 136, 210901 (2012).
- [26] I. R. Craig and D. E. Manolopoulos, *J. Chem. Phys.* 121, 3368 (2004).
- [27] I. R. Craig, and D. E. Manolopoulos, *Chem. Phys.* 322, 236 (2006).
- [28] S. Habershon, D. E. Manolopoulos, T. E. Markland, and T. F. Miller III, *Annu. Rev. Phys. Chem.* 64, 387 (2013).
- [29] T. F. Miller III and D. E. Manolopoulos, *J. Chem. Phys.* 122, 184503 (2005).
- [30] S. Habershon, G. S. Fanourgakis, and D. E. Manolopoulos, *J. Chem. Phys.* 129, 074501 (2008).
- [31] S. Habershon and D. E. Manolopoulos, *J. Chem. Phys.* 131, 244518 (2009).
- [32] A. Witt, S. D. Ivanov, M. Shiga, H. Forbert, and D. Marx, *J. Chem. Phys.* 130, 194510 (2009).
- [33] D. Scharf, G. J. Martyna, and M. L. Klein, *Low Temp. Phys.* 19, 364 (1993).
- [34] G. Krilov and B. J. Berne, *J. Chem. Phys.* 111, 9140 (1999).
- [35] D. R. Reichman and E. Rabani, *J. Chem. Phys.* 116, 6279 (2002).
- [36] T. Omiyinka and M. Boninsegni, *Phys. Rev. B* 88, 024112 (2013).

- [37] Q. Wang, J. K. Johnson, and J. Q. Broughton, *Mol. Phys.* 89, 1105 (1996).
- [38] A. Cunsolo, G. Pratesi, D. Colognesi, R. Verbeni, M. Sampoli, F. Sette, G. Ruocco, R. Senesi, M. H. Krisch, and M. Nardone, *J. Low Temp. Phys.* 129, 117 (2002).
- [39] A. Cunsolo, private communication
- [40] F. J. Mompean, M. Garcia-Hernandez, F. J. Bermejo, and S. M. Bennington, *Phys. Rev. B* 54, 970 (1996).
- [41] A. Cunsolo, D. Colognesi, M. Sampoli, R. Senesi, and R. Verbeni, *J. Chem. Phys.* 123, 114509 (2005).
- [42] A. Cunsolo, G. Pratesi, D. Colognesi, R. Verbeni, M. Sampoli, F. Sette, G. Ruocco, R. Senesi, M. H. Krisch, and M. Nardone, *Journal of Low Temperature Physics*, 129, 314 (2002).
- [43] T. F. Miller III, D. E. Manolopoulos, P. A. Madden, M. Konieczny, H. Oberhofer, *J. Chem. Phys.* 122, 057101 (2005).
- [44] P. H. Berens, S. R. White, and K. R. Wilson, *J. Chem. Phys.* 75, 515 (1981).
- [45] M. Ceriotti, M. Parrinello, T. E. Markland, and D. E. Manolopoulos, *J. Chem. Phys.* 133, 124104 (2010).
- [46] [http : //henke.lbl.gov/optical_constants/atten2.html](http://henke.lbl.gov/optical_constants/atten2.html)

[47] When referring to quantum effects it is customary to distinguish between those related to the non-commutative character of the operators describing dynamical variables and those connected with the quantum character of particle statistics (Bose-Einstein or Fermi-Dirac). While the latter are relevant in strongly quantum fluids (as e.g. superfluid ^4He , degenerate fluid ^3He and jellium), these seem to play no significant role for the semi-quantum fluids considered in the present work, whose properties can be consistently described using Maxwell-Boltzmann statistics.

[48] Due to a normalization issue associated with the empty container scattering contribution for $H_2(k = 5.5 \text{ nm}^{-1})$ and $H_2(k = 15.3 \text{ nm}^{-1})$, the use of Eq. 2.36 for the transmission coefficient resulted in unphysical results for the refined dynamic structure factor for these two cases. To avoid this, we treated the transmission coefficient as a free parameter for these two cases and the values used in the refinement process are shown in Table III.

[49] We note that even though the operators in Eq. 4.30 are not hermitian, the relation $F(\mathbf{k}, t) = F(\mathbf{k}, -t)^*$ still holds since in this case $A^* = B$, and for non hermitian operators one can show that $C_{AB}(-t)^* = C_{B^*A^*}(t)$.

Vita

Kyle Kurt Gabriel Smith was born in Springfield, Ohio on 18 December 1987, the son of Kurt Smith and Maria Ballard. He grew up in Marietta, Georgia and received a Bachelor of Science degree in Physics from the Georgia Institute of Technology in May of 2011. Quickly after, he married his wife Megan, and they then packed up everything they could into their car, including their little chihuahua Tinkerbelle, and headed out west for Texas. Kyle began his PhD studies in June of 2011 at the University of Texas at Austin in theoretical chemistry.

Permanent address: 1452 Alison Jane Lane
Kennesaw, Georgia 30144

This dissertation was typeset with \LaTeX^\dagger by the author.

[†] \LaTeX is a document preparation system developed by Leslie Lamport as a special version of Donald Knuth's \TeX Program.